Coal Occurrence and Quality at Mushithe Area, Soutpansberg Coalfield, South Africa

By

Mphanama Thangeni

Student Number: 15001079

Dissertation Submitted to the Department of Earth Sciences, Faculty of Science, Engineering and Agriculture, in Fulfilment of the Requirements for the Degree of Master of Earth Sciences in Mining and Environmental Geology

Supervisor : Dr. H.R. Mundalamo

Co-supervisors : Emeritus Professor J.S. Ogola

: Dr. L.R. Kone

AUGUST 2023

DECLARATION

I, Mphanama Thangeni, declare that this research dissertation titled “Coal Occurrence and Quality at Mushithe Area, Soutpansberg Coalfield, South Africa” is my own work and it has never been submitted for a degree at this or any other university and all reference materials contained therein have been duly acknowledged.

Signature  Date: 16/08/2023

……

ACKNOWLEDGEMENT

Firstly, I would like to express my sincere gratitude to God Almighty for His guidance, protection, and blessings throughout this research. His grace and provision have been instrumental in making this work possible.

I would like to express my sincerest gratitude to my supervisor Dr. H.R. Mundalamo and co-supervisors, Emeritus Professor J.S. Ogola and Dr. L.R. Kone for their unwavering support, guidance, and encouragement throughout my research. Their invaluable insights, expertise, and feedback have been instrumental in shaping this work.

I would also like to extend my sincere appreciation to DSI-NRF CIMERA for funding this research project. Their support has been crucial in enabling the successful completion of this work.

I express my heartfelt gratitude to Dr. M.O. Kataka and the rest of the Earth Science Department staff members at the University of Venda for their support and motivation. Additionally, I am grateful for the laboratory assistance provided by Mrs. N. Lilimu and Mr. N. Nemapate. Their contributions have been invaluable to my progress and success.

I am deeply grateful to Professor Wagner and the staff members of the University of Johannesburg Geology department for their invaluable assistance and support during the coal petrography training and analysis. Their expertise, guidance and support have greatly enhanced the quality of this project.

I would also like to acknowledge the Council for Geoscience for providing valuable borehole data for my research project. Their support has been crucial in enabling the successful completion of this work.

I would like to acknowledge my colleagues, Ramphabana Tom, Munyai Phumudzo, and Maponya Julia for their unwavering encouragement, motivation, advice, and support throughout the research, whose contributions and support have been invaluable and greatly appreciated. Additionally, I extend my sincere gratitude to Vhuma Trust, Tshifularo Vuledzani, and Tshamano Given for their invaluable assistance and support with the fieldwork, whose help and dedication were crucial in collecting the data and making this research possible.

ABSTACT

South Africa is the 7th largest coal producer in the world and continues to rely on coal as its primary energy source, owing to its abundant availability and low cost. The Mushithe coal occurrence, located within the Pafuri basin of the Soutpansberg Coalfield, has been overlooked compared to other coal occurrences in the Tshikondeni area. The coal occurrence at Mushithe outcrops at Mbodi River. The study aims at establishing the geological setting, mode of occurrence, coal quality and economic value of the Mushithe coal occurrence. Geological mapping and sampling, petrography, and geochemical analysis were done on 14 host rock and 6 coal samples.

Coal bearing rocks at Mushithe are occurring as a valley isolated from the Pafuri Basin. The outcropping seam at Mushithe is exposed along the Tshamatsha Fault. The coal measures contain four to seven seams, ranging from 0.35 m to 11.38 m in thickness. Pink and red quartzite, mudstone, basalt, quartz vein, sandstone, shale, carbonaceous shale, and calcrete were identified as associated rock types. The general strike is northeast, and the dip direction is northwest, with an average dip angle of 23°.

Mushithe coal is dominated by vitrinite (65.77%) and inertinite (34.23%), with no liptinite detected. The high presence of vitrinite suggests that the coal is formed in a wet swamp environment. Additionally, signs of weathering such as cracks, fissures, and oxidation rims were observed in the coal. Coal quality belongs to bituminous C on UNECE 1998 classification, being characterised by low sulphur content (0.23 to 0.38 wt %) and high moisture (6.07 to 10.94 wt %), ash yield (16.7 to 41.9 wt %), volatile matter (29.7 to 35.8 wt %), fixed carbon (25.25 to 50.49 wt %) and calorific value (12.97 MJ/kg to 23.35 MJ/kg). Mineral matter constitutes approximately 5.7 to 35.8 wt %, predominantly quartz with varying proportions of clay (kaolinite), as well as minor carbonates (siderite) and sulphides (pyrite). The geochemistry is characterised by high values of Al_2O_3 from 7.56 to 15.83 wt %, SiO_2 (9.76 to 20.04 wt %), and MgO (0.26 to 2.80 wt %).

The outcropping seam was found to be of economic value and suitable for use as thermal coal for electricity generation.

***Keywords**: Mushithe coal occurrence, coal stratigraphy, geological mapping, coal quality*

TABLE OF CONTENTS

LIST OF FIGURES

LIST OF TABLES

LIST OF ACRONYMS AND ABBREVIATIONS

%	Percentage
<	Less Than
>	Greater Than
±	Plus–minus
≤	Less Than or Equal
≥	Greater Than or Equal
°	Degree
°C	Degree Celsius
µm	Micrometre
ad	Air Dried
Ag	Silver
Al_2O_3	Alumina
As	Arsenic
ASTM	American Society for Testing and Materials
Ba	Barium
Bi	Bismuth
CaO	Calcium Oxide
Cd	Cadmium
Cdt	Collodetrinite
Ce	Cerium
Cl	Clay
cm	Centimetre
Co	Cobalt
Cr	Chromium
Cr_2O_3	Chromium Oxide

Cs	Caesium
Ct	Collotelinite
Cu	Copper
CuO	Cupric Oxide
Db	Dry Basis
Dy	Dysprosium
Er	Erbium
Eu	Europium
Fe_2O_3	Ferric oxide
Fs	Fusinite
g	Gram
Ga	Gallium
Gd	Gadolinium
Ge	Germanium
Hf	Hafnium
ICSD	Inorganic Crystal Structure Database
inc. mm	Including Mineral Matter
ISCOR	Iron and Steel Industrial Corporation
ISO	International Organization for Standardization
K_2O	Potassium oxide
kcal/kg	Calories per Kilogram
Kg	Kilogram
km	Kilometre
km^2	Square Kilometre
La	Lanthanum
LOI	Loss on Ignition

M	Metre
MgO	Magnesium Oxide
MJ/kg	Megajoules per Kilogram
MKB	Main Karoo Basin
ml	Millilitre
mm	Millimetre
mmf	Mineral Matter Free basis
MnO	Manganese oxide
Mo	Molybdenum
Na_2O	Sodium oxide
Nb	Niobium
Ni	Nickel
NiO	Nickel oxide
P_2O_5	Phosphorus Pentoxide
Pb	Lead
PPL	Plane polarized light
Ppm	Parts per million
Qtz	Quartz
Rb	Rubidium
RoV %	Vitrinite Reflectance measurement
S	Sulphur
SABS	South African Bureau of Standards
Sc	Secretinite
SACS	South African Committee for Stratigraphy
Sb	Antimony
Sf	Semifusinite

Sid	Siderite
SiO_2	Silicon Dioxide
Sm	Samarium
Sn	Tin
Sr	Strontium
SrO	Strontium Oxide
Ta	Tantalum
Tb	Terbium
Th	Thorium
TiO2	Titanium Dioxide
Tl	Titanium
U	Uranium
UCC	Upper Continental Crust
UNECE	United Nations Economic Commission for Europe
V	Vanadium
V_2O_5	Vanadium Pentoxide
vol. %	Volume Percentage
W	Tungsten
wt %	Weight Percentage
Y	Yttrium
Y_2O_3	Yttria
Yb	Ytterbium
Zn	Zinc
ZnO	Zinc oxide
Zr	Zirconium
ZrO_2	Zirconium dioxide

θ	Theta
λ	Wavelength

CHAPTER 1 : INTRODUCTION

1.1 Background

According to the Word Coal Association (2019), South Africa ranks as the 7th largest coal producer. About 77% of the country's primary energy needs are provided by coal resources. South Africa's coal production is mostly for domestic consumption and export. Domestic use is mostly by Eskom power stations for electricity generation, Sasol for coal-derived synthetic fuels and petrochemical products, and general industry for various applications (Hancox and Götz, 2014). Despite environmental concerns, coal will continue to dominate South Africa's energy supply for the next decade, while renewable energy sources are set to grow rapidly alongside natural gas and nuclear power (International Trade Administration, 2023). The dominance of coal as a major energy source is driven by its low cost and abundant availability (Jeffrey, 2005).

Coal resources in Southern Africa are hosted within sedimentary rocks of the Karoo Supergroup and their temporal equivalents (Hancox, 2016). Based on geographic considerations, origin, variation in sedimentation, distribution, and coal quality, 19 coalfields are generally recognised in South Africa (Hancox and Götz, 2014). Coal resources in South Africa are located mainly in Mpumalanga, KwaZulu-Natal, Limpopo, and Free State provinces, with lesser amounts in Gauteng, Eastern Cape, and North West Provinces (Jeffrey, 2005). Many coalfields in South Africa have been extensively explored and exploited, but coalfields located in the north of the country including the Soutpansberg Coalfield have until recently received less attention from researchers. Prominent coalfields in South Africa are the Witbank, Highveld, Ermelo, and Waterberg coalfields. The Witbank and Highveld coalfields are nearing depletion and other additional sources for coal supply must soon be identified if the South African coal industry is to continue in the 21st Century (Jeffrey, 2005).

The Mushithe coal occurrence which is located within the Soutpansberg Coalfield had received less attention from researchers as compared to other coal occurrences within the Tshikondeni area which previously hosted the Tshikondeni colliery. According to Hancox and Götz (2014), four coalfields located within the Limpopo Province contain as much as 70% of South Africa's remaining coal resources. Fragile environments, severe water scarcities, inadequately developed infrastructure, and poor roof

conditions due to complex geology and depth are major challenges for exploiting some of the coalfields within Limpopo Province (Jeffrey, 2005).

In the past, coal quality was only evaluated based on two factors: its ability to remain intact during transportation and its capacity to generate the desired amount of heat energy while producing minimal ash (Rubiera *et al*.,1995). Currently, concerns about the environment, human health and energy demands have broadened the concept of coal quality and have increased the need to know more about all aspects of the coal origin, depositional environments, and composition to understand their effects on coal quality (Schweinfurth, 2009). Better knowledge of coal quality characteristics may help reduce some health and environmental impacts. Coal quality characterisation and the distribution of potentially toxic elements in coal may help to delineate areas to be avoided during mining (Finkelman, 1999).

During the 1970s and 1980s, the Iron and Steel Industrial Corporation (ISCOR) undertook an extensive survey of the Soutpansberg Coalfield, which involved the drilling of over two thousand boreholes. During 1978 and 1979, ISCOR developed the Fripp Box to assess coking coal resources in the Tshipise Sub-basin, however, the Fripp project and other projects were eventually abandoned in favour of the Tshikondeni project, which was the sole location where mining had occurred in the Soutpansberg Coalfield previously (Hancox and Götz, 2014). At present, there is insufficient data available about the geological characteristics and quality of the Mushithe coal occurrence. Consequently, this study focused on the Mushithe coal occurrence, specifically on the geological setting, mode of occurrence and coal quality.

1.2 Study Area

The Mushithe coal occurrence is located within the Musina Local Municipality, Vhembe District, Limpopo Province of South Africa (Fig. 1.1). The Limpopo Province is the northern-most province in South Africa and borders Botswana, Zimbabwe, and Mozambique. The nearest town is Thohoyandou, situated approximately 90 km to the southwest of the study area. The town of Musina is located approximately 135 km northwest of the study area. The study area lies within latitudes 22°30'00" S and 22°31'45" S and longitudes 30°46'00" E and 30°49'00" E.

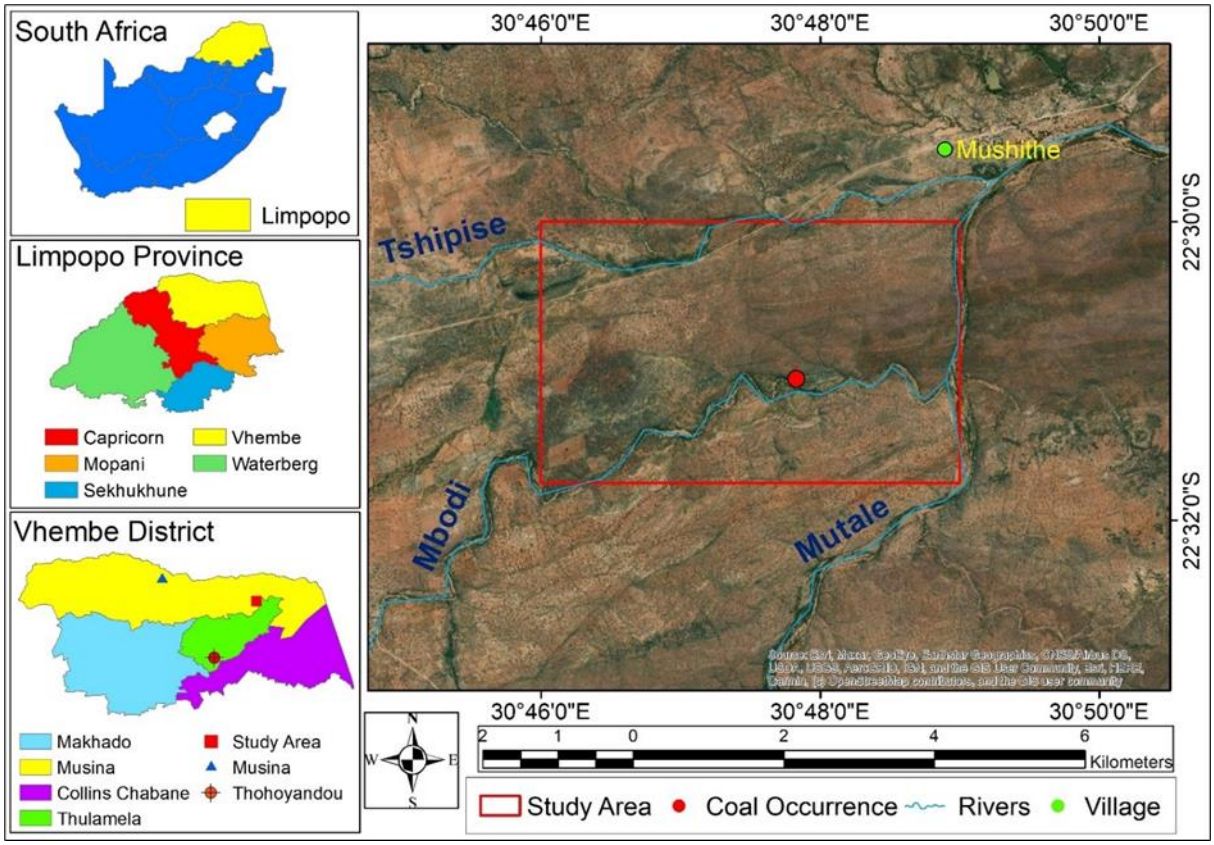

Figure 1.1: Location map of the study area (Environmental Systems Research Institute, 2019).

1.2.2 Climate

The study area features a subtropical climate, which is characterised by mild and moist winters and warm and wet summers. There is a single rainfall cycle that occurs from October to March, while the dry season spans from April to October. The rainfall pattern is heavily influenced by the orographic rain effect created by the intersection of the Drakensberg and Soutpansberg mountains. The region can experience up to 2,000 mm of annual rainfall (Phokele and Sylvester, 2015). The daily temperatures during summer can range from 16°C to 40°C, whereas during the winter season, the temperature typically falls between 12°C and 22°C (Kabanda, 2004).

1.2.3 Topography and Drainage

The geology underlying the Mushithe area has a significant influence on its topography. This region is distinguished by a pattern of low hills and open hills, which run east-west throughout the area. The surface water in Mushithe drains into the Tshipise and Mbodi Rivers, both of which are tributaries of the Mutale River.

Ultimately, the Mutale River feeds into the Luvuvhu River, which is itself a tributary of the Limpopo River.

1.2.4 Soil and Vegetation

The study area is generally dominated by sandy loam soils as well as rocky soils. The area is composed of low to medium potential arable land. The vegetation of the study area is categorised as Tropical Bush and Savannah, with Musina Mopane Bushveld and Soutpansberg Mountain Bushveld as the primary vegetation types. The representative vegetation is dominated by medium to high shrub savannah with dispersed trees.

1.3 Problem Statement

There are limited studies and information on the Soutpansberg Coalfield. The majority of the research conducted on the Soutpansberg Coalfield applies to the Coalfield as a whole, or it pertains specifically to the Tshikondeni deposit. Furthermore, a published geological map of the area by the Council for Geoscience (2020) is on a small scale of 1: 250 000. Areas such as the Mushithe coal occurrence have not been documented.

1.4 Justification

Studying the geology of the area will be useful in determining the distribution of lithologies, coalbed sequence as well as structures that may affect future mining. Furthermore, coal characterisation will be useful in understanding the intrinsic characteristics of coal and its quality. Results of the study could, therefore, be used in making decisions on whether to mine or not and will determine the mining methods to be adopted, thus serving as a guide for the exploitation of coal in the Soutpansberg coalfield with a direct implication on the Mushithe Coal Occurrence.

The proposed study will also contribute knowledge on the geology of Mushithe Coal Occurrence and will guide future studies on coal quality and coal use in the area.

1.5 Research Questions

- What is the coal geology at the Mushithe coal occurrence?
- How did the geological setting of the area influence coal occurrence and its morphology?
- Is there any structural control on coal distribution?
- What is the coal quality and suitability for exploitation?

1.6 Objectives

The main objective of the study was to establish the geological setting, mode of occurrence, coal quality and economic value of the Mushithe Coal Occurrence.

Specific objectives were to:

- Determine coalbed stratigraphy through geological field mapping and correlation of exploration core logs;
- Determine coal rank and maceral composition using coal petrography;
- Investigate coal quality through proximate and ultimate analysis;
- Characterise the mineralogy of both coal and host rocks using X-Ray Diffraction and microscopic studies; and
- Carry out geochemical analysis of coal and host rocks, using X-Ray Fluorescence Spectrometry.

CHAPTER 2 : LITERATURE REVIEW

2.1 Overview of Notable South African Coalfields

In South Africa, there are 19 recognised coalfields (Fig. 2.1), which are determined by factors such as sedimentation, quality, origin, formation, and distribution of coal (Hancox, 2016). These coalfields are all located within the rocks of the Main Karoo Basin and can be found across 5 provinces (Van der Walt, 2012). The age of South African coal varies from early Permian to late Triassic, with the majority being of Permian age. This is consistent with the coal found in other Gondwanan regions such as Sub-Saharan Africa, Australia, and South America (Hancox and Götz, 2014).

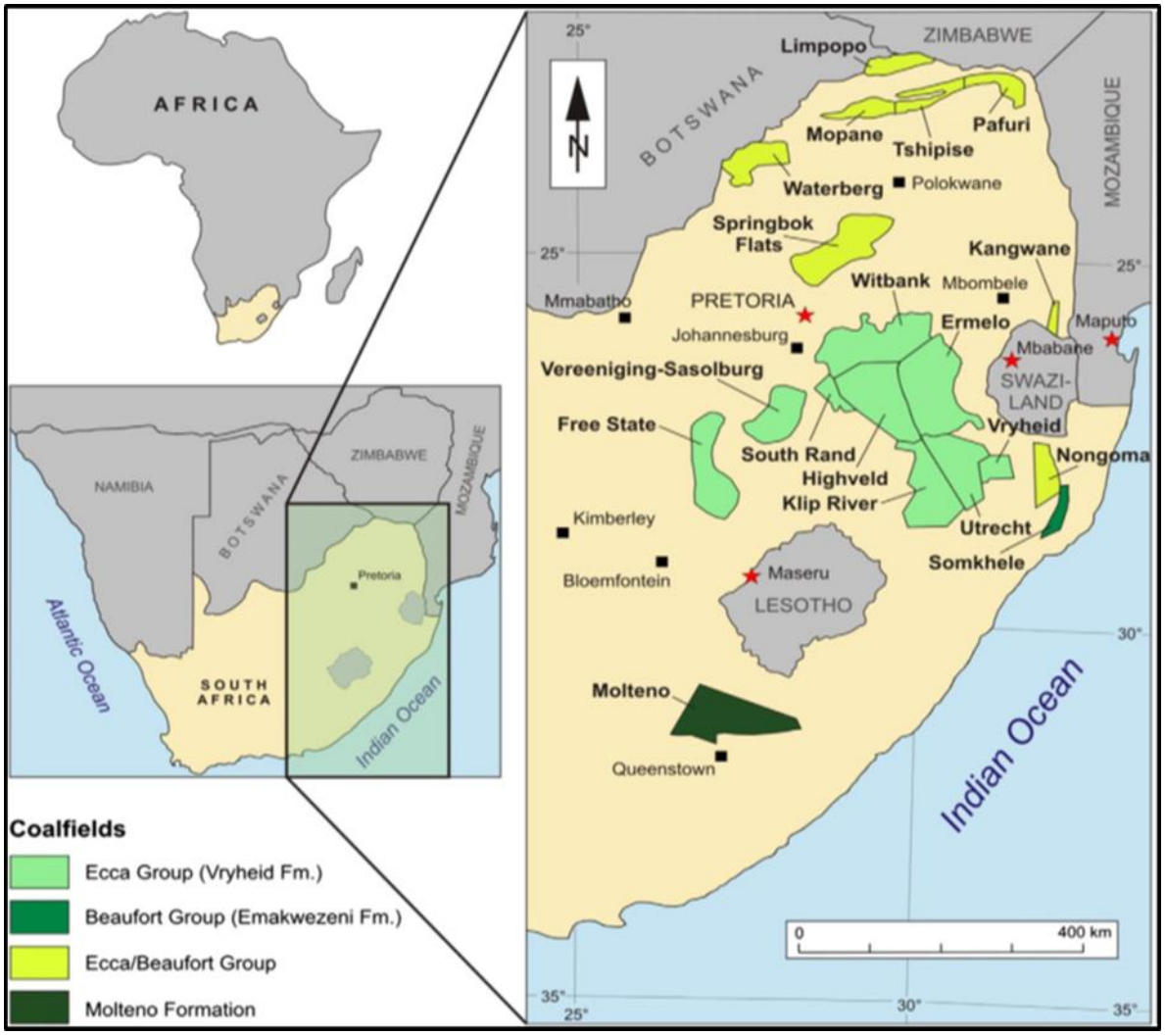

Figure 2.1: Map showing 19 South African coalfields (Hancox, 2016).

2.1.1 Witbank Coalfield

The Witbank Coalfield is located in the Mpumalanga Province to the east of Johannesburg, spanning an area of approximately 568,000 hectares between 25°30′ S to 26°30′ S by 28°30′ E to 30°00′ E (Hancox and Götz, 2014). With a history of more than 125 years of commercial exploration, this coalfield is a significant contributor to South Africa's coal supply, accounting for over 50% of the country's saleable coal according to Hancox (2016). The coal seams in this region are predominantly flat lying, with a regional dip ranging from 1° to 3°, and the No. 2, 4, and 5 seams are the most economically important (Hancox, 2016). The Witbank Coalfield produces both thermal and metallurgical coal for local and international markets, and it is home to major coal-fired power stations such as Arnot, Komati, Kendal, and Duvha (Hancox and Götz, 2014).

2.1.2 Waterberg Coalfield

The Waterberg Coalfield is situated about 400 km northwest of Johannesburg in the Limpopo Province, immediately north of the Waterberg Mountain ranges (Hancox and Götz, 2014). Coal seams in the Waterberg Coalfield are confined within the Ecca Group, Vryheid Formation and Volksrust Formation which is known as the Grootegeluk Formation in the Waterberg region (Cairncross, 2001). The coalfield has eleven coal zones, four of which are found in the Vryheid Formation, and the remaining seven are found in the Grootegeluk Formation. Waterberg Coalfield is considered to be South Africa’s last major coalfield as it contains 40% to 50% of the country’s remaining coal resources. The coalfield hosts the Eskom 3.990 Megawatts Matimba Power Station which is the world's largest direct dry cooling power station (Hancox, 2016).

2.1.3 Highveld Coalfield

The Highveld coalfield is located in the Mpumalanga Province, approximately 200 km south-east of Pretoria, and to the south of the Witbank Coalfield, covering an area of around 7000 km^2 (Wagner and Hlatshwayo, 2005). The Highveld coalfield shares similarities in term of general stratigraphy with the Witbank Coalfield and is separated by the Smithfield Ridge (Hancox and Götz, 2014). The coal deposits in the Highveld Coalfield are hosted within the Vryheid Formation of the Mid-Permian Ecca Group (Wagner and Hlatshwayo, 2005), and all five coal seams present in the Witbank

Coalfield are also found in the Highveld Coalfield, with the No. 4 seam being the most economically viable (Chabedi, 2013). The reserves of the Highveld coalfield are crucial to the long-term viability of projects such as Sasol's Chemical Industries and Sasol Synthetic Fuels, which require approximately 40 million tons of coal per year, as noted by Jeffrey (2005).

2.1.4 Soutpansberg Coalfield

The Soutpansberg Coalfield is located north of the Soutpansberg Mountain Range in the Limpopo Province, extending for about 190 km from the Kruger National Park in the east, to Waterpoort in the west. The coalfield lies between latitudes 22°S and 23°S and longitudes 28°E and 32°E. The location and shape of the Soutpansberg Coalfield are controlled by ENE-WSW faults that follow the trend of the Limpopo Mobile Belt. Bosbokpoort, Tshipise and Klein Tshipise Faults are three major faults recognised within the Soutpansberg Coalfield. The faults delineate major horst and graben structures. All faults that affect the basin appear to be normal and possibly of post-Karoo age. Karoo-aged strata of the Soutpansberg Basin generally dip to the north and vary between 5° and 15° (Malaza, 2014).

The Soutpansberg Coalfield may be divided into three separate smaller sub-basins (sometimes referred to as coalfields) namely the Pafuri, (Eastern Soutpansberg), Tshipise (Central Soutpansberg) and Mopane sub-basins (Western Soutpansberg) (Hancox and Götz, 2014). Coal rank within the Soutpansberg Coalfield tends to increase with increasing depth. Tshipise Coalfield has a similar stratigraphy to the Pafuri Coalfield, except that the coal-bearing sequences are thinner and coal resources are more intimately interlaminated with mudrocks. The main seam is a composite seam with a thickness of up to 3.5 m and comprises several coal bands interbedded with carbonaceous mudstone (Hancox, 2016).

2.2 Soutpansberg Group

The Karoo sedimentary succession of the Soutpansberg Coalfield overly the Soutpansberg Group and rocks of the Beit Bridge Complex (Hancox and Götz, 2014). The Soutpansberg Group is a volcano-sedimentary suite that is developed and preserved above the Palala Shear belt which separates the Kaapvaal Craton in the South and the Central Zone of the Limpopo Mobile Belt in the north (Geng *et al*., 2014).

The ±1850 Ma. group outcrops mainly in the Soutpansberg Mountains, which form a long, continuous south-facing escarpment from Vivo in the West to Punda Maria in the east (Bumby *et al*., 2002). Gently north-tilted strata of the Soutpansberg Group are cut by numerous extensional faults (Fig. 2.2). Two fault systems are recognised, the east-northeast trending (parallel to the regional strike direction) is the most dominant followed by the northwest to west-northwest trending fault system. Most faults are believed to have been initiated in pre-Karoo or even during Soutpansberg times, with most structures having been reactivated in post-Karoo times (Brandl, 2002). Soutpansberg Group may be sub-divided into six formations, namely Tshifhefhe Formation, Sibasa Basalt Formation, Fundudzi Formation, Wyllie's Poort Formation, Musekwa Formation and Nzhelele Formation (Geng *at al*., 2014).

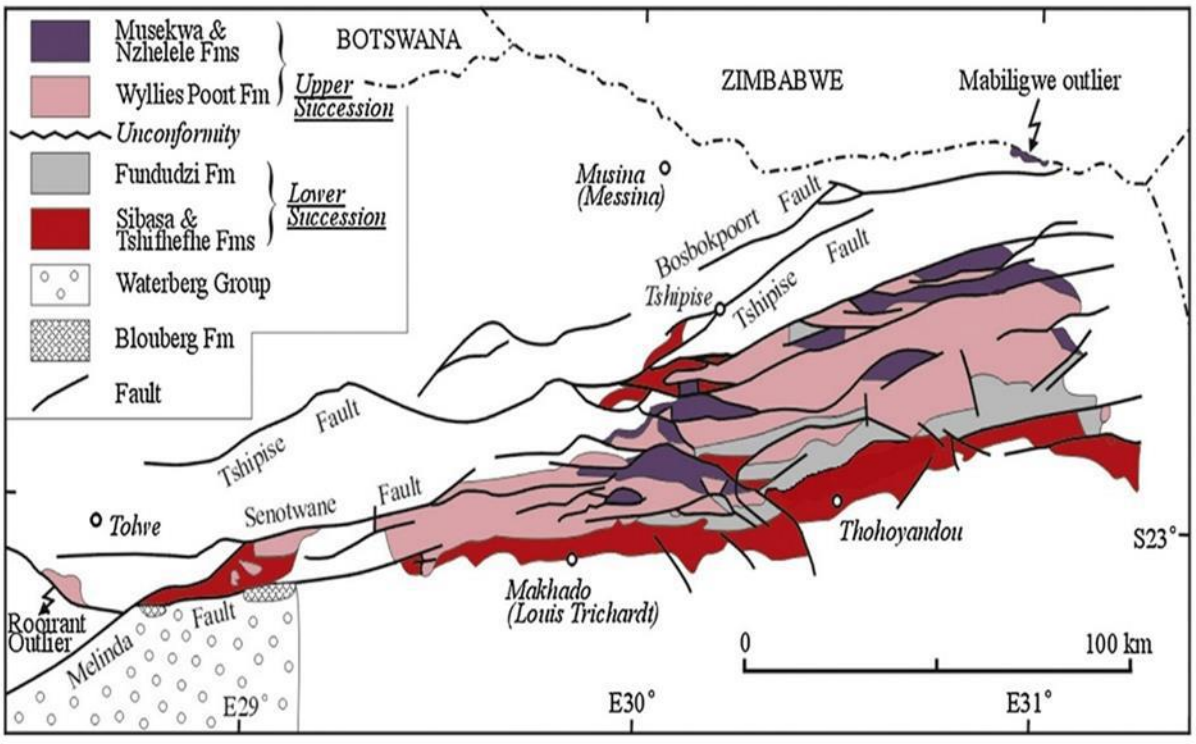

Figure 2:2: Distribution of geological formations within the Soutpansberg Group (Geng *et al*., 2014).

2.2.1 Tshifhefhe Formation

The basal Tshifhefhe Formation is only locally developed in the eastern half of the Soutpansberg Basin (Bumby *et al*., 2002). The formation consists entirely of clastic sediments that are frequently epidotised and chloritized. Conglomerate clasts often

comprise granitoid gneiss and quartz vein which are round to angular indicating local derivation (Geng *et al*., 2014). The formation is only a few metres thick (10 m) and attains thicknesses of up to 20 m in the Kruger National Park (Bristow, 1986; Geng *et al*., 2014). According to Geng *et al*. (2014), volcanic rocks overlying the Tshifhefhe basal unit were extruded on an almost featureless landscape due to its uniform thickness as seen across the Soutpansberg Group.

2.2.2 Sibasa Basalt Formation

Sibasa Formation overlies the Tshifhefhe Formation. This sequence is dominantly a volcanic succession with a minor and often discontinuous intercalations of clastic sediments. The interbedded clastic sediments include quartzite, sandstone, shale, and rare conglomerate which often form persistent markers with a thickness of up to 50 m. The volcanic rocks include cyclically erupted tholeiitic basalt and lenticular horizons of pyroclastic rocks. The basalts often exhibit narrow zones of frequently epidotised amygdales. Pyroclastic rocks are found mainly in the upper half of the sequence and form lenticular horizons within both the basalt and clastic sediments (Geng *et al*., 2014). The formation is mainly developed along the southern edge of the Soutpansberg where it forms flat to undulating topography. The formation can reach a thickness of up to 3 300 m in the Sibasa area (Bristow, 1986).

2.2.3 Fundudzi Formation

The Fundudzi formation conformably overlies the Sibasa Formation. The predominantly siliciclastic formation is only developed in the eastern half of the basin. (Bumby *et al*., 2002). The formation comprises a thinly bedded shale/siltstone lithic greywacke succession which vertically grades into a thick succession of conglomerates and orthoquartzites. The formation attains a maximum thickness of 2 800 m in the vicinity of Lake Fundudzi (Bristow, 1986). Mixed load deposits represented by the presence of immature sandstone, siltstone, and shale indicate fluviatile deposition in a braided, alluvial flood plain environment (Geng *et al*., 2014).

2.2.4 Wyllie’s Poort Formation

The Wyllie’s Poort Formation forms the base of the Soutpansberg Group’s upper succession and extends over the entire length and width of Soutpansberg Mountain

(Geng *et al*., 2014). The unit underlies a major part of the more mountainous region in the Soutpansberg and has a conformable contact with the underlying Fundudzi Formation (Bristow, 1986). The succession is mainly arenaceous and attains a thickness of approximately 4 000 m in Thengwe and Makuya areas (Bumby *et al*., 2002). The succession is dominated by mineralogical and texturally mature resistant pink quartzite with occasional pebble washes. Pebble washes encompass vein quartz, chert, jasper, agate, and rare pink quartzite (Geng *et al*., 2014).

2.2.5 Musekwa Formation

The succession has an almost constant thickness of approximately 400 – 500 m and represents the most prominent marker horizon in the Soutpansberg Group. The formation encompasses basaltic lava with minor intercalated pyroclastic rocks and clastic sediments. Syngenetic copper mineralisation is locally developed (Geng *et al*., 2014).

2.2.6 Nzhelele Formation

The uppermost unit of the Soutpansberg Group is represented by the Nzhelele Formation and comprises clastic sediments with few thin pyroclastic rock intercalations (Geng *et al*., 2014). The formation comprises primarily dark red argillaceous sandstone, however, quarzitic sandstone may be developed towards the top. A 2 m thick copper-mineralised purple tuff layer occurs about 60 m from the base (Geng *et al*., 2014).

2.3 Main Karoo Basin

The Main Karoo Basin (MKB) forms part of a major series of Gondwanan foreland basins that developed between the late Carboniferous and Middle Jurassic through subduction, compression, collision, and terrane accretion along the southern margin of Gondwana. These basins include the Bowen Basin in Australia, the Beacon Basin in Antarctica, and the Paraná Basin in South America (Hancox and Götz, 2014). The sedimentary fill of these basins hosts economically significant energy resources such as coal, coal bed methane, shale gas, uranium, and geothermal energy (Campbell *et al*., 2016). The equivalently aged coal-bearing successions which are situated north of the MKB are preserved in isolated extensional intercratonic and intracratonic

grabens or half-grabens. These basins are collectively referred to as the Northern Basins. The Karoo aged depositories in South Africa were formed in two different, yet linked, tectonic settings (Fig. 2.3). These are transtension or extension-related northern basins and compression-related MKB (Hancox and Götz, 2014).

The Karoo Basin is underlain by a stable basement including the Kaapvaal Craton in the north, the Namaqua-Natal Metamorphic Belt in the south and the Cape Fold Belt along its southern margin (Campbell *et al*., 2016). The basin is notable for containing a succession, formally named the Karoo Supergroup, which represents a geological history of about 120 million years in duration (Bordy and Paiva, 2021).

The Karoo Supergroup consists of four units, which are arranged in the following order from bottom to top: the Dwyka, Ecca, Beaufort, and Stormberg groups. These siliciclastic deposits reach a thickness of more than 5 km in the southern part of the basin and are capped by some 1.4 km of basaltic lavas of the Drakensberg Group (Hancox and Götz, 2014; Campbell *et al*., 2016). Karoo-aged depositional environments broadly range from glacial (Dwyka Group) to marine and coastal plain (Ecca Group), and to non-marine fluvial and aeolian (Beaufort and Stormberg groups) (Campbell *et al*., 2016).

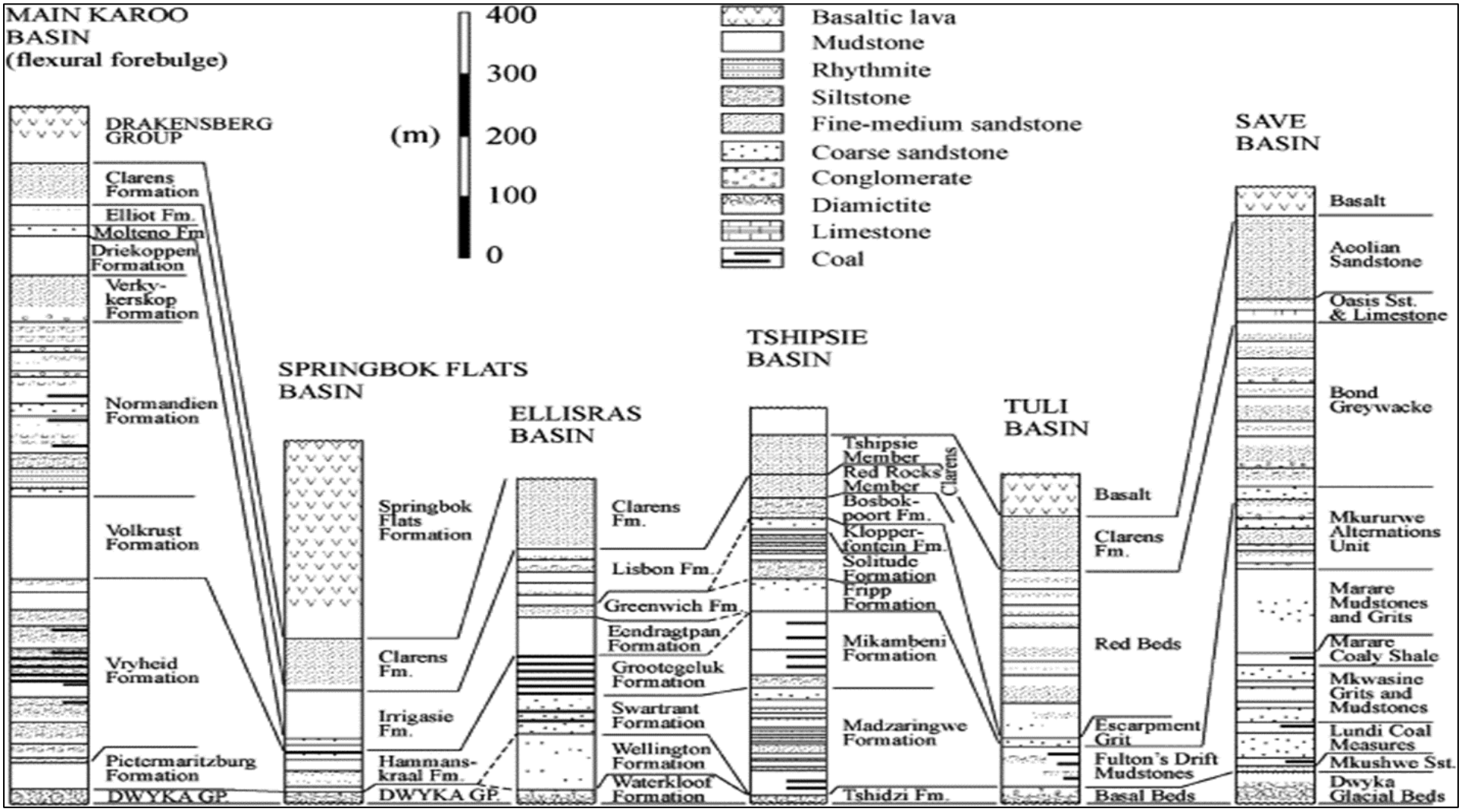

Figure 2:3: Correlation of the Karoo lithostratigraphic units of the Main Karoo Basin with the Tshipise, Ellisras, Tuli and Save Basins (Catuneanu *et al*., 2005).

2.3.1 Dwyka Group

The Dwyka Group forms the basal succession of the Karoo Supergroup. The sequence was named after exposures located along the Dwyka River east of Laingsburg (Hancox and Götz, 2014). The Dwyka Group and its equivalents comprise glacially influenced deposits that accumulated approximately during the 300–290 Ma interval. The deposition of the Dwyka glacially influenced deposits took place in different tectonic settings across South-Central Africa. Tectonic basin types range from retroarc foreland system of the MKB to extensional in northern basins (Catuneanu *et al*., 2005). Lithologies of Dwyka Group in the areas underlying South African coalfields consist of a heterolithic arrangement of massive and stratified polymictic diamictites, conglomerates, sandstones, and dropstone-bearing varved mudstones (Hancox and Götz, 2014).

2.3.2 Ecca Group

The Ecca Group strata were named after the argillaceous sedimentary strata exposed in the Ecca Pass, north of Grahamstown in the Eastern Cape Province. The clastic sequence of the Ecca Group comprises mudstone, siltstone, sandstone, minor conglomerates, and coal (in places). Rocks of the Ecca Group outcrop extensively in the MKB and Southern African Karoo Supergroup localities (Catuneanu *et al*., 2005). In the type-Karoo Basin of South Africa, The Ecca Group sequence was deposited between the Late Carboniferous Dwyka Group and the Late Permian-Middle Triassic Beaufort Group, occupying a majority of the Karoo Supergroup's Permian time slot (Catuneanu *et al*., 2005). Based on the cyclic nature of the sedimentary fills, the South African Committee for Stratigraphy (1980) divided the group into the Pietermaritzburg Shale Formation, the Vryheid Formation, and the Volksrust Shale Formation (Hancox and Götz, 2014).

The Pietermaritzburg Formation consists almost entirely of dark grey laminated siltstone and mudstone, with subordinate sandstone, and reaches a maximum thickness of over 400 m. No coal seams occur in the Pietermaritzburg Formation. The Vryheid Formation hosts the majority of the economically extracted coal in South Africa. The thickness of the Vryheid Formation ranges from less than 70 m to over 500 m, it is thickest to the south of the towns of Vryheid and Newcastle, where maximum

subsidence took place and where the basin was the deepest (Hancox and Götz, 2014). The Volksrust Formation is dominated by dark grey-green siltstones and mudstones, with phosphatic/carbonate/sideritic concretions. The general thickness of the unit is between 150 and 250 m. Coal occurs interbedded with the mudstones in places. The Volksrust Formation shows an overall coarsening-upward trend and is postulated to have formed in shallow to deep-water basinal conditions (Hancox and Götz, 2014).

2.3.3 Beaufort Group

The Beaufort Group represents the Middle Permian to Middle Triassic part of the Karoo Supergroup. These rocks cover a surface area of approximately 200 000 km^2, making up about 20% of South Africa's total surface area (Catuneanu *et al*., 2005). The succession is >2500 m thick and consists of alternating fine-grained lithofeldspathic mudstones and sandstones which preserve a rich and diverse succession of Permo-Triassic vertebrate fossils (Bordy and Paiva, 2021). The contact between the Beaufort Group and the underlying Ecca Group records a gradual change from a fluvial to a deltaic depositional environment system (Catuneanu *et al*., 2005). Two subgroups of the Beaufort Group are recognised, namely the lower Adelaide and upper Tarkastad subgroups. Coal resources are restricted to the Adelaide Subgroup and its equivalents (Hancox and Götz, 2014).

2.3.4 Stormberg Group

The Molteno, Elliot and Clarens formations are collectively referred to as the Stormberg Group. The Molteno Formation forms the basal succession of the Stormberg Group and comprises a northward thinning wedge of dominantly clastic sedimentary rocks. Molteno Formation was previously divided into lower Bamboesberg and Indwe Sandstone members, with economic coal seams occurring only in the Bamboesberg Member. No coal deposits are documented within the Elliot and Clarens formation. The Clarens Formation is the uppermost sedimentary succession of the Karoo Supergroup. The Clarens Formation is interpreted as an aeolian depositional system, with minor fluvial input (Hancox and Götz, 2014).

2.4 Tshipise Basin

The Tshipise Basin, together with the Tuli, Ellisras and Springbok Flats Basins represent the Limpopo area of Karoo-aged basins (Bordy, 2018). These equivalently aged coal-bearing successions which are situated north of the MKB are preserved in isolated extensional intercratonic and intracratonic grabens or half-grabens. These basins are collectively referred to as the Northern Basins (Hancox and Götz, 2014).

Rocks of the Karoo Tshipise Basin are divided into three tectonic periods, Permian, Triassic and Jurassic. The Permian Period comprises the Tshidzi, Madzaringwe, Mikambeni, and Fripp Formations. Additionally, the Solitude, Klopperfontein, Bosbokpoort, and Clarens Formations constitute the Triassic stratigraphy within the Soutpansberg Coalfield. Lastly, the Jurassic Period is represented by the Letaba and Jozini Formations (Malaza, 2014). Coal resources are hosted within the sandstone-rich Madzaringwe and overlying Mikambeni Formations (Hancox, 2016).

2.4.1 Tshidzi Formation

The Permo-Carboniferous Tshidzi Formation represents the Dwyka Group (Karoo Supergroup) north of the MKB and forms the basal succession in the Karoo-aged Tshipise, Tuli, Springbok Flats and Ellisras Basins in South Africa. The formation unconformably overlies the Pre-Karoo rocks of the Palaeoproterozoic Soutpansberg Group and is conformably overlain by the Permian coal-bearing Madzaringwe Formation (Bordy, 2018). The Tshidzi Formation was named after the Tshidzi Hill near Tshipise Town in Limpopo Province (South African Committee for Stratigraphy, 1980). The 5-20 m unit is composed of diamictite and coarse-grained sandstone reflecting glacial and fluvioglacial depositional environments. The upper contact of the formation is currently defined as being gradational into the overlying Madzaringwe Formation, which represents the Ecca Group equivalents in the coalfield (Hancox and Götz, 2014).

2.4.2 Madzaringwe Formation

The Madzaringwe Formation comprises up to 220 m of alternating feldspathic, often cross-bedded conglomerates, sandstone, siltstone, and shale containing coal seams (Malaza *et al*., 2013). The basal part of the succession comprises a 30 m thick unit of

carbonaceous siltstone and mudstone, shaly coal, and thin coal seams. This unit is overlain by a succession of alternating layers of coal, grey-black siltstone, carbonaceous mudstone, and very fine- to medium-grained sandstone. Prominent coal seams interlayered with carbonaceous mudstone occur in the upper third of the formation (Hancox and Götz, 2014). In areas where the Tshidzi Formation diamictites are absent, Madzaringwe sandstones rest directly on the quartzites of the Soutpansberg Group (Malaza *et al*., 2013). Due to non-deposition or pinch-out, the arenaceous Madzaringwe Formation is not present within the Mopani Coalfield (Hancox, 2016). The succession reflects a fluvial depositional system. The unit is interpreted as being laid down by meandering rivers flowing from the northwest. The sandstone possibly represents point bar, levee, and crevasse splay deposits. Coal seams formed through plant material that accumulated in flood basins under cool, reducing conditions (Malaza *et al*., 2013).

2.4.3 Mikambeni Formation

The Mikambeni Formation overlies The Madzaringwe Formation. The succession attains a thickness of between 20 and 150 m and comprises mainly medium to dark grey siltstone, minor carbonaceous mudstone and khaki-red to grey sandstone. Coal seams occur scattered throughout the unit (Hancox and Götz, 2014). The formation consists of the lower unit, middle and upper units. The lower unit comprises a 15-20 m thick alternating black shale and grey, feldspathic sandstone, the 50 m middle unit consists of black carbonaceous shale with occasional bright coal seams and the upper unit comprises dark grey mudstone with plant fragments and occasional bright coal. The overall fine-grained character of the formation reflects deposition on the distal floodplains of meandering rivers (Malaza, 2014).

2.4.4 Fripp Formation

The Fripp Formation is made up of feldspathic sandstones with a texture ranging from medium to coarse grains, and with intermittent thin layers of pebbles. These sandstones are intermixed with narrow layers of siltstone and mudstone, and display trough cross-stratification. The deposition of the sandstones in the Fripp Formation is believed to have been the result of braided river systems flowing towards the northwest and west. The formation can be linked to the Beaufort Group, which is part

of the Karoo Supergroup located in the MKB, as noted by Malaza (2014). The formation attains a thickness of up to 110 m (Hancox and Götz, 2014). The Fripp formation is overlain by Triassic and Jurassic-aged sequences (Malaza, 2014).

2.5 Coal Origin and Formation

Coal is a combustible brownish-black or black sedimentary rock with a high carbon content and varied physical, chemical, and technological properties depending on the rank reached throughout its geological history. Although most rocks are inorganic, coal consists predominantly of organic matter, mostly derived from a variety of plant remains (higher plants, ferns, fungi, and algae) and different tissues (leaves, stalks, woody trunks, bark, pollen, spores, sclerotia, and resins) with associated mineral matter content corresponding to an ash yield of less than, or equal to, 50% on a dry mass basis (Suárez-Ruiz *et al*., 2019).

Based on the coal-forming plants, coal can be classified into two main groups, humic coal and sapropelic coal (Thomas, 2012). Humic coals are composed of a diversified mixture of macroscopic plant debris, and they typically have a banded appearance. Humic coal is the most widespread coal type in nature, with the largest reserves. Sapropelic coals are composed of a restricted variety of microscopic plant debris and have a homogeneous appearance. Sapropelic coal comprises boghead coal and saprocollite. Boghead coal is mainly formed from algae, and saprocollite is a type of structureless sapropelic coal consisting almost completely of matrix materials, because the plants are thoroughly decomposed (Thomas, 2012; Xie, 2015). The character and composition of coal are controlled by the nature of the make-up of the original organic and inorganic accumulation; and by the degree of diagenesis it has undergone (Thomas, 2012).

2.5.1 Peat Formation

Two main theories for the accumulation of vegetal matter giving rise to coal seams were discussed by Miller (2005). The first and most widely accepted theory, which explains the origin of most coals, is that the coal originated in situ, and such a deposit is considered to be autochthonous. Most coal deposits started with thick peat bogs where water was nearly stagnant and plant debris accumulated. Vegetation tended to grow for many generations, with plant debris settling on the swamp bottom and microbial action converting it into peat. New future coal seams were formed when the

swamps became submerged and covered by sedimentary deposits. New additional coal seams were formed when the cycle was repeated, over hundreds of thousands of years. These cycles of accumulation and deposition were followed by diagenetic and tectonic actions and, depending on the extent of temperature, time and forces exerted, different ranks of coal are observed in the present day.

Although the formation of most coal can be explained by the autochthonous process, some coal deposits are not easily explained by this model. According to the second theory of allochthonous origin, plant debris has been carried by streams and deposited in the bottom of the lake or sea where they build up strata, which later become compressed into solid rock.

2.5.2 Coalification

Coalification refers to the process by which vegetable matter undergoes alteration to produce peat, which subsequently undergoes a transformation through various stages of coal formation, including lignite, sub-bituminous, bituminous, semi-anthracite, anthracite, and meta-anthracite coal. The level of transformation or coalification achieved is known as coal rank. Identifying the rank of a coal deposit early in the investigation is crucial as it determines the deposit's potential and interest in the future. (Thomas, 2012). Heat is generally considered to be the most important controlling factor of coalification. Increased heat corresponding with greater depths of burial has been regarded as the primary factor in coalification (O'Keefe *et al*., 2013). Coalification is characterised by loss of moisture and volatile matter, and subsequent concentration of carbon (Wagner, 2021).

2.6 Coal Petrography

2.6.1 Macerals

According to Scott (2002), Stopes (1935) is credited with introducing the concept of maceral. Macerals were defined by Spackman (1958), as “organic substances, or optically homogenous aggregates of organic substances, having distinctive chemical and physical properties, and occurring naturally in the sedimentary, metamorphic, and igneous materials of the earth’’. Macerals affect the type of coal seen macroscopically, namely the dull, bright, and banded layers (Falcon, 2013). Macerals are grouped into three main subdivisions (Table 2.1) based on major characteristics relating to each group. These groups are the vitrinite maceral group, the liptinite maceral group and

the inertinite maceral group. Each maceral group is subdivided into further macerals and sub-macerals (Falcon, 2013; Thomas, 2012). According to Suárez-Ruiz and Ward (2008), maceral groups are subdivided into a variety of macerals, sub-macerals and maceral varieties based on their reflectance, degree of destruction and preservation of original material, presence of cellular structure, gelification, and morphological features.

Vitrinite Group

Vitrinite macerals are formed from woody fibrous plant tissues such as stems and leaves (Xie, 2015). Compared to other maceral groups, vitrinite macerals contains more oxygen at any given level of rank (Speight, 2013). Due to their sensitivity to heat, vitrinite macerals become denser, tougher, and more vitreous when subjected to higher heat levels with depth in the earth or proximity to an external heat source such as an igneous intrusion or a volcano. An index of intensity of vitrinite reflectance is used to determine the level of heat, or maturity, to which coal has been subjected (Schweinfurth, 2009). Over the range of rank in which the three respective maceral groups can be readily recognised, vitrinite macerals are generally grey with reflectance mostly between that of darker liptinites and lighter inertinites (Falcon, 2013).

Based on cell structures, colour under a microscope and different degrees of gelification, Vitrinite macerals are subdivided into seven sub-macerals, namely telinite 1, telinite 2, telocollinite, gelocollinite, desmocollinite, corpocollinite, and vitrodetrinite (Xie, 2015). Telinite macerals are formed from different tree branches, trunks, stems, leaves, and roots. Collinite macerals are formed from gel precipitated in humic solutions obtained from humic particles that were degraded during the early stages of coalification. Vitrodetrinite macerals are also obtained and formed from degraded plants during the early stages of coalification but earlier than the stages of obtaining Collinite (Speight, 2013).

Table 2.1: Characteristics of different macerals in coal (Thomas, 2012)

Maceral Group	Maceral	Morphology	Origin
Vitrinite (huminite)	Telinite	Cellular structure	Cells walls of trunks, branches roots, leaves
	Collinite	Structureless	Reprecipitation of Dissolved organic matter in a gel form
	Vitrodetrinite	Fragments of vitrinite	Very early degradation of plant and humic peat particles
	Sporinite	Fossil form	Mega-microspores
	Cutinite	Bands which may have appendages	Cuticles – the outer layer of leaves, shoots and thin stems
Exinite (liptinite)	Resinite	Cell-filling layers or dispersed	Plant resins, waxes and other Secretions
	Alginite	Fossil form	Algae
	Liptodetrinite	Fragments of Exinite	Degradation residues
	Fusinite	Empty or mineral-filled cellular structure; cell structure is usually well preserved	Oxidized plant material – mostly charcoal from the burning of vegetation
	Semifusinite	Cellular structure	Partly oxidized plant Material
	Macrinite	Amorphous 'cement'	Oxidized gel material
Inertinite	Inertodetrinite	Small patches of fusinite, semi-fusinite or macrinite	Redeposited inertinites
	Micrinite	Granular, rounded Grains ~1 µm in diameter	Degradation of macerals during Coalification
	Sclerotinite	Fossil form	Mainly fungal remains

Liptinite Group

Liptinite (previously the exinite group) is a maceral group which is derived from non-humifiable plant matter, relatively hydrogen-rich remains such as sporopollenin, resins, waxes, and fats and at a given rank among the other macerals, liptinite comprises the macerals of the lowest reflectance (Pickel *et al*., 2017). Liptinite

macerals resemble plant fossils and are characterised by high reactivity, and volatility and are more aliphatic (Speight, 2013). Fluorescence properties are used as a distinguishing feature to identify different macerals; Liptinite macerals are distinguished from other maceral groups by their lower reflectance (Pickel *et al*., 2017). Liptinite macerals develop similar optical properties to those of vitrinite or disappear during coalification due to thermal transformation at the bituminous stage (Suárez-Ruiz *et al*., 2019). Compared to other maceral groups, Liptinite content is the least recognised maceral group as they rarely exceed 7 vol. % in many international coals (Speight, 2013). Liptinite macerals are classified based on their respective fossil plant nature as they appear to resist major changes during coalification. These maceral groups are subdivided into sporinite, cutinite, suberinite, resinite, alginite, and liptodetrinite (Speight, 2013).

Inertinite Group

Inertinite maceral groups are considered to be equivalent to charcoal and degraded plant materials and are derived from plant material, generally woody tissues, degradation products, or fungal remains (Speight, 2013). Chemically, they are aromatic with comparatively high amounts of carbon and low amounts of hydrogen and volatile matter (Suárez-Ruiz *et al*., 2019). Under the petrographic microscope, inertinite macerals have a well-preserved cellular structure and appear hard (high relief) and very bright white to brassy yellow (Falcon, 2013). Inertinite macerals are characterised by a distinct cell texture as well as high reflectance and are extremely oxidised in nature with high inherent carbon content resulting from biological or thermal oxidation. The inertinite group macerals are subdivided into fusinite, semi-fusinite, macrinite, micrinite, inertodetrinite, and scleronite (Speight, 2013).

2.6.2 Minerals

The mineral content represents the non-combustible inorganic fraction that is introduced into coal during coalification. The Inorganic fraction is sometimes erroneously referred to as ‘ash’ when in fact ash is the mineral residue remaining after the combustion of the coal. Mineral matter can be classified into detrital or authigenic in origin. Detrital minerals are introduced into a swamp or bog by water or air.

Authigenic minerals are introduced into peat during or after deposition, or into coal during coalification (Thomas, 2012).

Knowledge of mineral matter in coal is essential in understanding the inorganic chemistry associated with coal formation and when evaluating coal for utilization as they have profound environmental, economic, technological, and human health impacts (Ward *et al*., 2001). With a few exceptions, most elements are hosted in minerals within coal (Finkelman *et al*., 2019). As many as 50 to 60 minerals are reported in various coals, most fall into five groups: Aluminosilicates, sulphides, sulphates, carbonates, silicates, and other minerals that include minerals that may occur in trace amounts or may be specific to coal having originated because of the localized deposition (Speight, 2005). Elements associated with sulphides (e.g., S, As, Hg, Tl, Se, and Pb) are toxic to the environment and human health while those associated with silicate minerals are largely not harmful (Finkelman *et al*., 2019).

Silicate Minerals

Silicates are the largest, most complex, and generally the most abundant mineral group in coal. Silicate minerals host many elements found in coal, particularly major elements including Si and Al, and to a lesser extent, K, Ca, Na, Mg, and Fe (Finkelman *et al*., 2019). Clay is the most abundant and widespread mineral group in coal. The most common clay minerals are kaolinite and mixed-layer illite–montmorillonite (Speight, 2005). Silicates often comprise up to 80% of all present minerals in Gondwana coals (Falcon, 2013). Depending on their provenance and sedimentary history, quartz grain form and shape range from rounded to angular (Falcon, 2013). Quartz is also a major constituent of clay and siltstone partings in coal that are detrital in origin (Speight, 2005).

Carbonate Minerals

Carbonates are present in many, but not all, coals. When present, carbonates minerals could be major hosts for Ca, Mg, Fe, Mn, and Sr, and to a lesser extent, rare earth elements (REE) and F, and in a few cases Zn. Calcite, siderite, and ankerite-dolomite series are the common carbonate minerals (Finkelman *et al*., 2019). Calcite or aragonite in coal may represent remnants of shell fragments (or similar detrital

particles) organic components or admix from intra-seam bands or floor and roof strata during mining (Ward, 2016).

Sulphide Minerals

The most dominant sulphide minerals in coal are dimorphs pyrite and marcasite (Speight, 2005). Much of the pyrite present in coal occurs in close association with organic matter and was perhaps formed during or shortly after peat accumulation (Ward, 2016). In most coals, sulphide minerals are likely the primary host of S, Sb, As, Cd, Co, Cu, Fe, Pb, Hg, Mo, Ni, Se, W and Zn. Pyrite has the greatest impact on any mineral in coal. Pyrite gives rise to a range of issues, including the oxidation of pyrite, leading to the expensive challenge of acid mine drainage problems. Pyrite's oxidation also contributes to acid rain and smog. The iron and sulphur components of pyrite play significant roles in the formation of boiler slags. Moreover, pyrite is a recognised major factor in the development of Coal Workers Pneumoconiosis. Notably, the core aim of coal cleaning revolves around eliminating pyrite. Additionally, the appropriate disposal of pyrite and its resultant byproducts (coal cleaning wastes, boiler slags, fly ash, bottom ash, and fouling deposits) imposes additional costs on coal utilisation (Finkelman *et al*., 2019).

2.7 Coal Classifications Standards

Coal can be categorized based on its chemical properties for industrial purposes. There are several widely used classification systems that take into account factors such as calorific value, fixed carbon, volatile matter, and caking and coking properties, both for humic and brown coal. Some of the main commercially recognized classifications of coal include those developed by the American Society for Testing and Materials (ASTM), the United Nations Economic Commission for Europe (UNECE), and Eskom Domestic coal specifications (Flores, 2014; Steyn and Minnitt, 2010).

2.7.1 American Society for Testing and Materials classification

The ASTM classification (D 388) is used on a worldwide basis. Classification is based on two coal properties, the fixed carbon values, and the calorific values. Higher-rank coals are classified based on fixed carbon on a dry basis and lower-rank coals are classified according to gross calorific value on a moist basis (Table 2.2). Coals having

gross calorific values less than 32.557 MJ/kg can be classified according to gross calorific value on the moist, mineral-matter-free basis, provided the fixed carbon on the dry, mineral-matter-free basis is less than 69 wt %.

Table 2.2: ASTM Classification of Coals by Rank (Flores, 2014)

Class/Group	Fixed Carbon Limits (Dry, Mineral-Matter-Free Basis), %		Volatile Matter Limits (Dry, Mineral-Matter-Free Basis), %		Gross Calorific Value Limits (Moist, Mineral-Matter-Free Basis)				Agglomerating Character
					Btu/lb		Mj/kg		
	Equal or Greater Than	Less Than	Greater Than	Equal or Less Than	Equal or Greater Than	Less Than	Equal or Greater Than	Less Than	
Anthracitic:									
Meta-anthracite	98	...	...	2	...	...	...	...	nonagglomerating
Anthracite	92	98	2	8	...	...	...	...	
Semianthracite	86	92	8	14	...	...	...	...	
Bituminous:									
Low volatile bituminous coal	78	86	14	22	...	...	...	...	commonly agglomerating
Medium volatile bituminous coal	69	78	22	31	...	...	...	...	
High volatile *A* bituminous coal	...	69	31	...	14 000	...	32.557	...	
High volatile *B* bituminous coal	...	...	...	...	13 000	14 000	30.232	32.557	
High volatile *C* bituminous coal	...	...	...	...	11 500	13 000	26.743	30.232	
					10 500	11 500	24.418	26.743	agglomerating
Subbituminous:									
Subbituminous *A* coal	...	...	...	...	10 500	11 500	24.418	26.743	nonagglomerating
Subbituminous *B* coal	...	...	...	...	9 500	10 500	22.09	24.418	
Subbituminous *C* coal	...	...	...	...	8 300	9 500	19.30	22.09	
Lignitic:									
Lignite *A*	...	...	...	...	6 300[G]	8 300	14.65	19.30	
Lignite *B*	...	...	...	...	...	6 300	...	14.65	

2.7.2 United Nations Economic Commission for Europe classification

In 1987, the United Nations established an international classification scheme for medium and high-rank coals, which was accepted by the Economic Commission for Europe. The classification scheme was developed as an instrument to permit the classification of coals to contribute to the characterisation of coal deposits. The classification was based on three fundamental characteristics, namely the degree of coalification (rank), petrographic composition and impurities (grade). Since other schemes classify coal based on gross chemical properties only, the UNECE classification is more effective (Flores, 2014).

The first step taken when classifying coal based on rank is to distinguish between low-rank coals and higher-rank coals. Low-rank coals have a gross calorific value of <24 MJ/kg and (vitrinite reflectance) RoV % <0.6. Coals with a gross calorific value of ≥24 MJ/kg or gross calorific value of <24 MJ/kg are termed higher rank coals, provided that RoV % ≥0.6. To avoid misinterpretations, coal with RoV % ≥0.6 must be classified based on vitrinite mean random reflectance per cent and coals with RoV % <0.6 should

be classified based on gross calorific value. Petrographic composition is expressed in terms of the major maceral group analysis (vitrinite, liptinite and inertinite on a mineral matter-free basis) carried out according to ISO standard 7404-part 3, supplemented, where possible by visual characterisation of lithotypes (bright, intermediate, or dull). The boundary limits for grade as shown in Figure 2.4, are based on ash yield on a dry basis. For sapropelic coals, the upper-grade limit is 50% ash yield on a dry basis, thus excluding oil shales. For humic coals, the upper-grade limit is 80% ash yield on a dry basis. This implies the existence of a subdivision termed carbonaceous rock with ash yield greater than 50% and less than 80% (Flores, 2014).

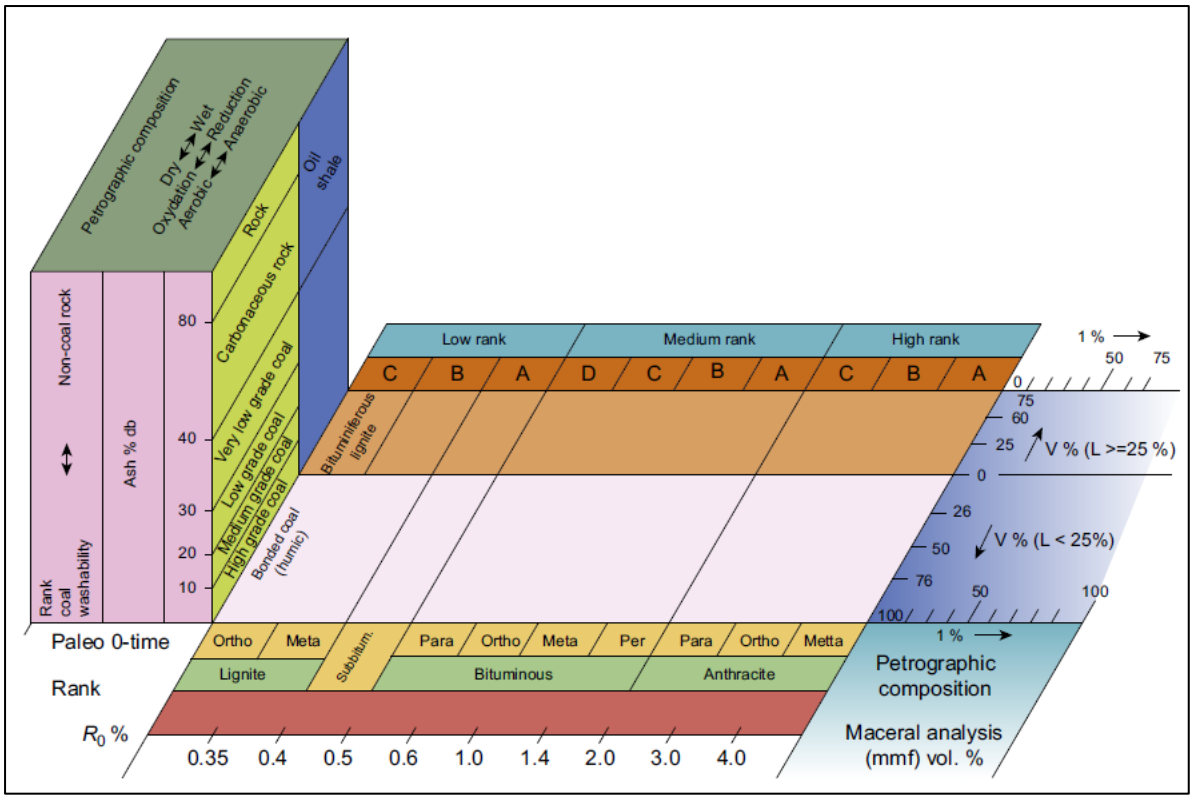

Figure 2.4: General version of the United Nations Economic Commission for Europe in-seam coal rank classification (Flores, 2014).

2.7.3 Domestic Coal Specifications

The domestic market can utilize grades A to D coal. As demonstrated in Table 2.3, the classification of coal grades is based on ash content and calorific value. The grade of coal increases as the ash content decreases and the calorific value increases, as shown below. The calorific value of domestic coal is measured in MJ/kg, while that of coal intended for export is measured in kcal/kg. These products are produced through

an active screening process. Three types of coal products are utilized domestically, based on their size: duff (0 to 6 mm), peas (6 to 25 mm), and small nuts (25 to 40 mm). The cement and lime industry can be supplied with duff, and the metallurgical industry with small nuts. The specification for using domestic products for thermal purposes suggests that A-C grade coal has very little potential for substitution, but D-grade coal could potentially be substituted for Eskom products (Table 2.4). However, using sized products for export substitution results in a loss of value. It is expected, according to the standard, that A and B grade coal can be substituted with export products (Steyn and Minnitt, 2010)

Table 2.3: Steyn and Minnitt (2010) domestic coal specifications

Domestic Coal Specifications					
Parameter	**Units**	**A grade**	**B grade**	**C grade**	**D grade**
Calorific Value	MJ/kg	>27.5	>26.5	>25.5	>24.5
Total Sulphur	Maximum% (AR)	12.0	12.0	8.0	8.0
Ash	Maximum% (AR)	15	16	18	21
Volatile Matter	Maximum% (AR)	24.0	23.0	23.0	23.0
Sulphur	Maximum% (AR)	1.0	1.0	1.0	1.5

Table 2.4: Grade and sizing of material for use by the local industry (Steyn and Minnitt, 2010)

Industry	Coal Grade	Coal Sizing
Gold and uranium mines	A; B	Small nuts
Agriculture	B; C; D	Peas
Brick and tile	C; D	Duff
Mining	A, B	Peas, Small nuts
Cement and lime	A; B; C	Duff
Arcelor mittal steel	A; B	Small nuts
Electricity	B; C; D	Small nuts, peas
Metallurgical	A; B	Small nuts, peas
Chemical industries	A; B	Small nuts
Iron and steel	A; B	Small nuts
Industries	A; B; C; D	Small nuts, peas
Merchants and domestic	A; B; C; D	All

CHAPTER 3 : MATERIALS AND METHODS

This chapter presents the methods and procedures used in the study (Fig. 3.1). The study was divided into preliminary work, fieldwork, data acquisition, laboratory work, data analysis, discussion, conclusions and recommendations.

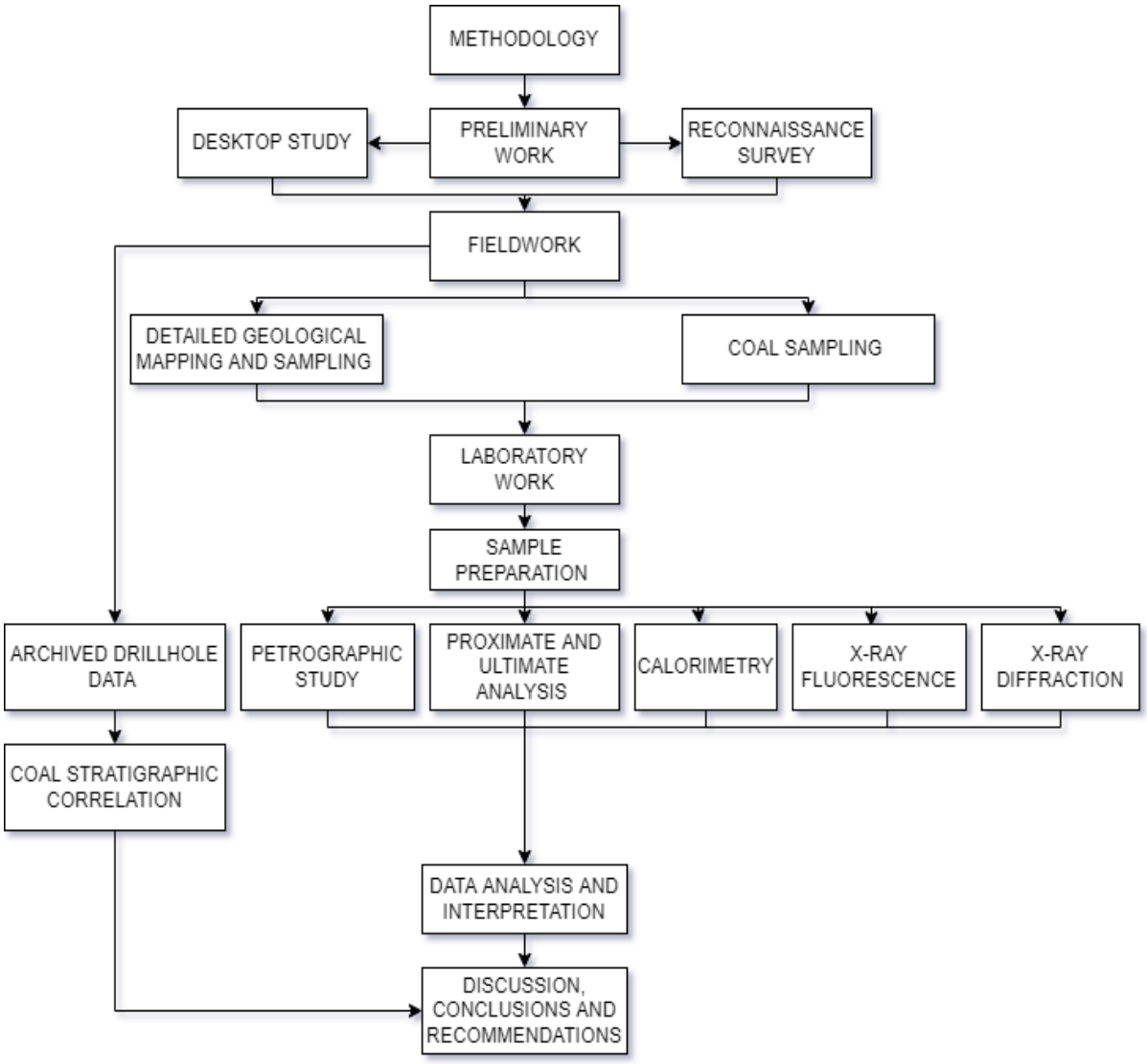

Figure 3.1: Flow chart illustrating methods and procedures applied in the study.

3.1 Preliminary Work

Preliminary work refers to the process of preparing for fieldwork by identifying essential methods and materials for the study. Its objective is to gain knowledge about the study area and identify any potential constraints that may impact the attainment of objectives. This information is used to develop a field plan that outlines the methods,

resources, and personnel required for the fieldwork, as well as its duration and appropriate techniques to be employed.

3.1.1 Desktop Study

A desktop study involves obtaining information about the study area using published and unpublished literature that may be useful in conducting the study. The literature to be used includes but is not restricted to books, journals, reports, photographs, online resources, maps, and unpublished sources. The data and information attained are in line with the planned work. The desktop study also prepares the researcher psychologically and contributes to the selection of the required equipment to undertake the study.

3.1.2 Reconnaissance Survey

A reconnaissance survey was conducted before the actual field work. The objective was for the researcher to familiarise with the study area, identify areas of interest, check accessibility and where needs be, seek permission from the local authorities.

3.2 Fieldwork

3.2.1 Geological Field Mapping and Rock Collection

Geological field mapping was carried out to produce a detailed geological map of the study area on a scale of 1:10 000. The survey area was delineated into an area of 5140 m by 3220 m. The area was divided into 6 profiles, each 857 m wide, oriented perpendicular to the strike direction of lithologies. A topographic base map of 2230 DB HAMAKUYA covering the study area was used for navigation and indicating measured contacts, attitudes, and structures (Fig. 3.2). Field data was collected by mapping rock exposures and structures along traverses in a zig-zag motion across the general strike direction of the area to encounter as many outcrops as possible.

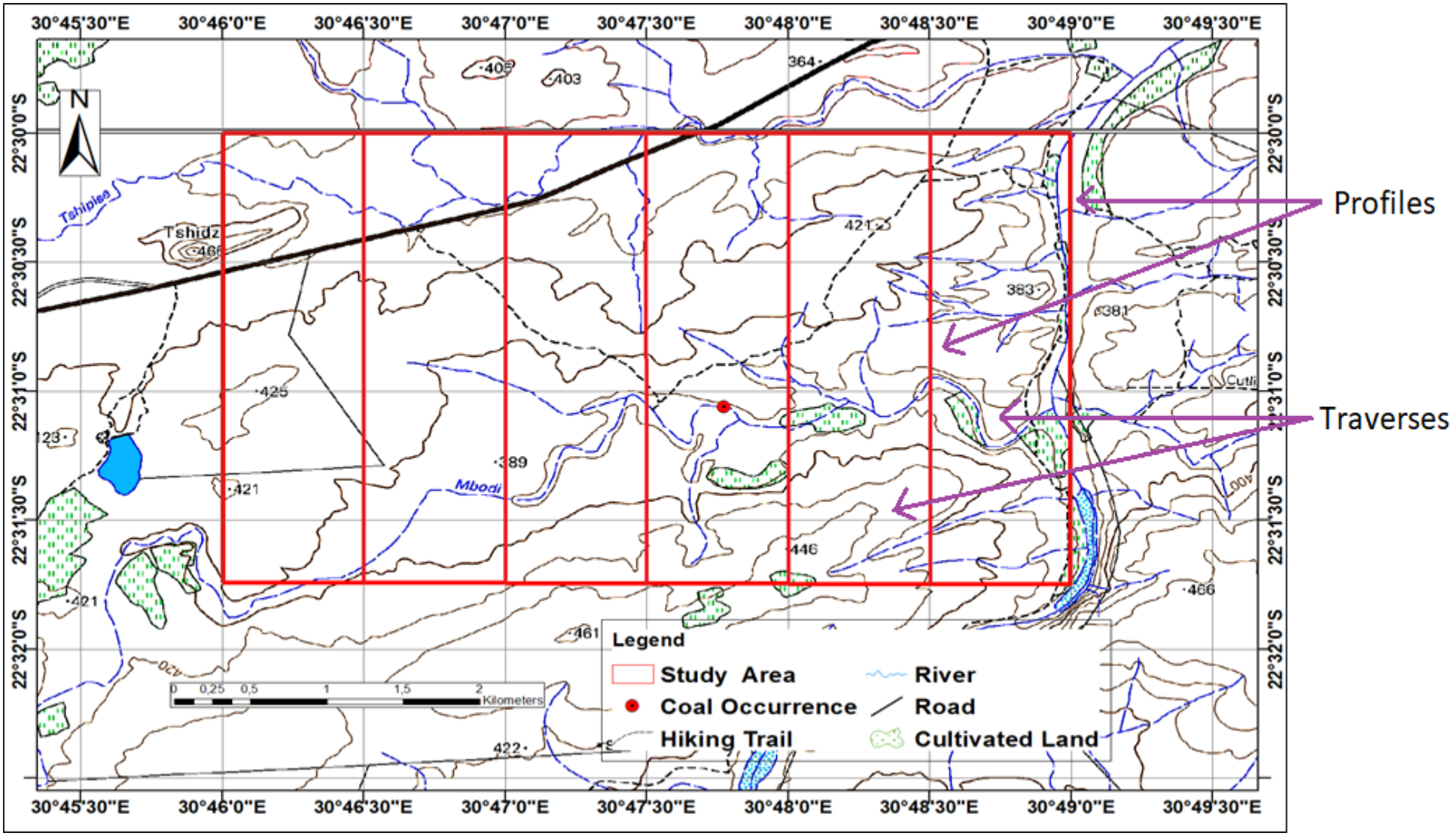

Figure 3.2: Topographical map illustrating traverses adopted for geological field mapping.

A field book was used to record the characteristics of each outcrop and the description of rock types, focusing on colour, grain size and texture, geological contacts, and structures. Global Positioning System (GPS) for navigation and for recording the location of outcrops; Brunton compass for measuring strike, dip angle and dip direction of outcrops; Diluted hydrochloric acid was used to conduct acid tests on rocks with carbonate minerals. A 50 m measuring tape was used to measure the thicknesses of rock beds and igneous intrusions. A magnifying glass and jeweller's loupe hand lens were used to magnify minerals and structures within rock specimen for rock description. A Geological hammer and sledgehammer were used for sampling rock chips. Collected rock specimen were placed in sample bag with a label tag for further laboratory analysis (Fig. 3.3). A total of 34 rock specimen were collected.

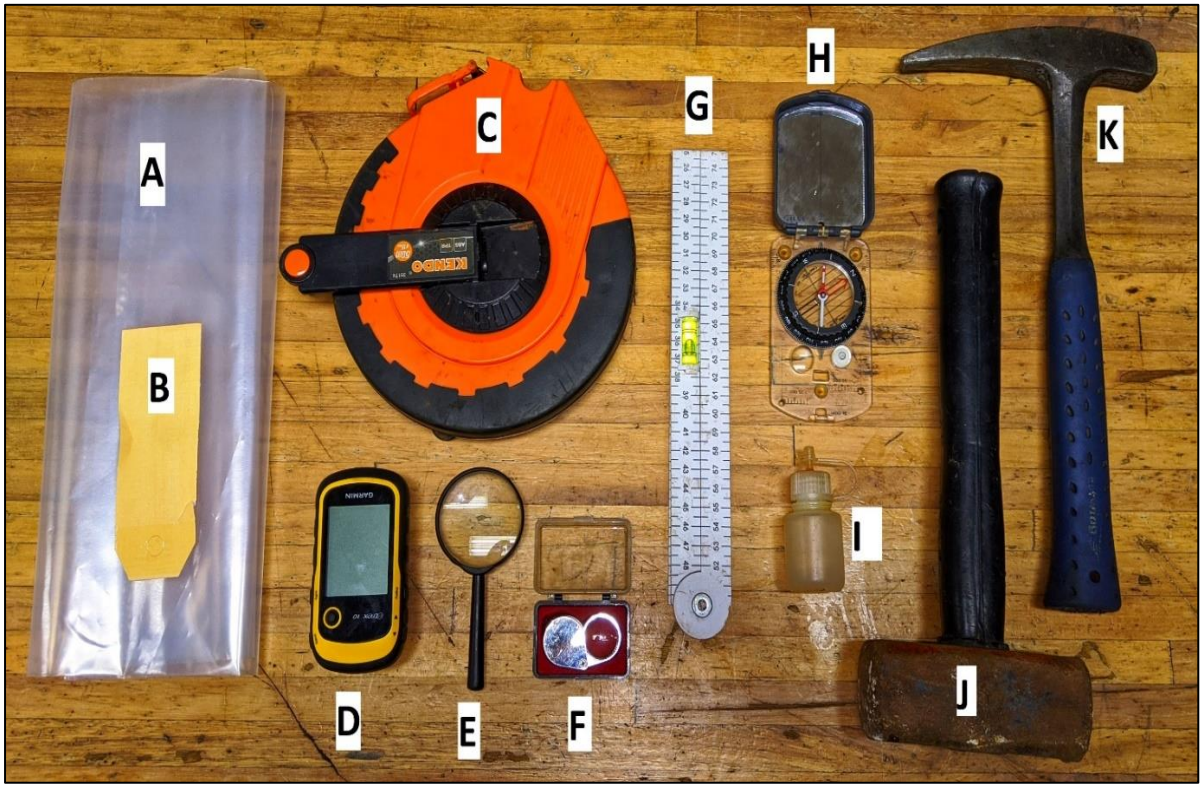

Figure 3:3: Geological field mapping tools: (A) sample bags, (B) Tags, (C) 50 m measuring tape, (D) Garmin eTrex 10 GPS, (E) magnifying glass, (F) jeweller's loupe hand lens, (G) clino ruler, (H) Brunton Compass, (I) Diluted hydrochloric acid, (J) sledgehammer, (K) geological hammer.

3.2.2 Coal Sampling

Coal Sampling was carried out within a coal outcrop exposed along the Mbodi River. The outcropping seam is located roughly at 22°31'0.4" S and 30°48.4" E. Coal was sampled using a Mac Africa MAUGER-02 2 stroke 68 CC petrol-powered mechanical earth auger. The earth auger was attached to a MAUGER-150 drill bit with a shaft diameter and length of 15 cm and 60 cm respectively. Auger drilling was done along the dip direction of the coal seam to avoid cross-contamination with host rock (Fig. 3.4). Coal beds were sampled at an interval of 0-20 cm, 20-40 cm, and 40-60 cm. Each sample was described in detail following: sample ID, drilling interval and coal characteristics. Sampled coal was placed in an airtight sample bag to prevent contamination and oxidation. Drill holes were rehabilitated after sampling. A total of six coal samples, each weighing around 2 kg, were collected.

Figure 3.4: Coal sampling: (A) earth auger, (B) drilling along the dip direction, (C) sample collection, (D), Rehabilitation.

3.3 Secondary Data Acquisition

Secondary borehole data for 10 borehole logs were acquired from the Council for Geoscience interactive web portal (Council for Geoscience, 2021). Borehole data includes drillhole data from the Mushithe area with data from Tshikondeni Coal Mine and Zwigodini areas for comparison purposes. Data from exploration boreholes were gathered over the course of 50 years as various companies conducted extensive exploration activities in the Soutpansberg Coalfield (Malaza, 2014).

3.4 Laboratory Work

3.4.1 Sample Preparation

Thin Section Preparation

Representative rock samples were split into two equal parts and half of the samples were used for the preparation of thin sections and the other half was reserved for X-ray fluorescence spectrometry and X-ray diffraction analysis. Rock specimens were cut using a diamond saw (Fig. 3.5A). Samples were cut into rectangular blocks of about 30 mm by 20 mm. The surfaces of the rectangular blocks were polished with silicon carbide grit mixed with deionised water on a lapping plate to create a smooth surface. Silicon carbide grit sizes mixed with water were used sequentially from coarsest to the finest: #120, #220, #400, #800 and #1000. #800 grit was used to frost 45 mm by 25 mm glass slides on a lapping plate. Samples and glass slides were thoroughly cleaned with deionised water after polishing. Samples were dried in a drying oven for 2 hours at 70°C. Samples were allowed to cool at room temperature for 15 minutes before bonding.

Aka-Resin Epoxy liquid resin was thoroughly mixed with EpoFix hardener using a ratio of 15:2 (15 parts resin and 2 parts hardener). Samples were bonded on frosted glass slides using the epoxy solution. Samples were then carefully placed bonding jig for a period of 24 hours for effective bonding (Fig. 3.5B). Bonded samples were cut to reduce the thickness from about 20 mm to 10 mm using the Streuers Accutum-50 cutting and grinding machine attached to a diamond cutting disc for about 15 minutes per sample. Bonded samples were then ground to a thickness of about 50 µm with Streuers Accutum-50 cutting and grinding machine attached with a grinding disc (Fig.

3.5C). The machine was programmed to grind off 5 µm per run for around 20 minutes. The thickness of the sample was periodically measured with a digital vernier calliper to ensure accurate grinding.

Ground samples were then polished with a Streuers RotoPol-35 polishing machine attached to a 300 mm polishing disc for approximately 2 hours (Fig. 3.5D). The polishing machine was continuously supplied with water and DiaDublo Mono 6 µm diamond suspension solution for lubrication purposes. Samples were periodically measured with a digital vernier calliper to check if the samples have reached the required thickness of around 30 µm. Polished samples were inspected using a Nikon Eclipse E200 petrographic microscope to ensure that the mineral grains are visible, and the polished surface is scratch free.

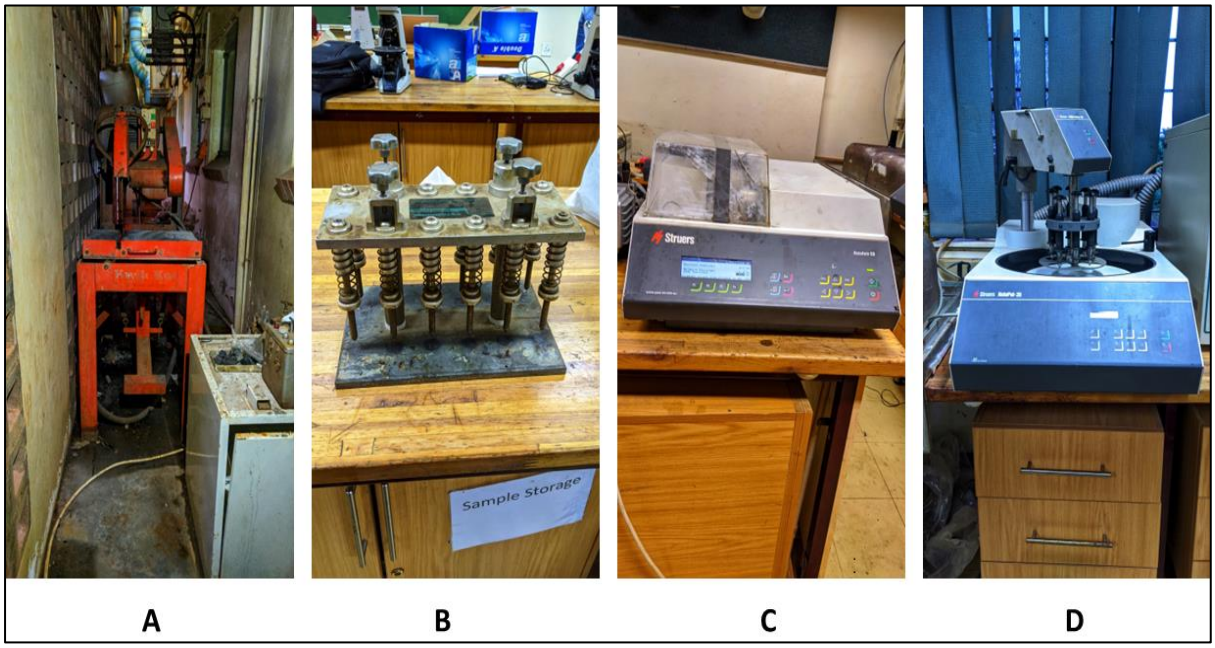

Figure 3.5: Thin section preparation equipment: (A) Diamond cutting saw, (B) Bonding Jig, (C) Cutting and grinding machine, (D) Polishing machine.

Polished Blocks Preparation

Coal petrographic polished blocks were prepared at the University of Johannesburg, Department of Geology following the SABS ISO 7404 part 2 standard. To create these blocks, representative 1 mm coal particle splits were mixed with a blend of Aka-Resin Epoxy liquid resin and EpoFix hardener. The mixture was then left to solidify under a vacuum overnight. A total of 6 coal blocks were prepared.

Sample Preparation for Geochemical Analysis

Coal samples were crushed using a porcelain mortar and pestle to obtain a particle size of about 4 mm. The 4 mm sample was split using a riffle splitter and half of the 4 mm was milled to 212 µm using a Retsch RS 200 milling machine for performing proximate and ultimate analysis, Calorimetry, X-ray fluorescence spectrometry and X-ray diffraction.

A jaw crusher was used to crush rock specimen to a size of less than 10 mm (Fig. 3.6A). To avoid cross-contamination, the jaw crusher was cleaned by crushing pure quartz aggregate and cleaning with a cloth dipped in acetone. After crushing, samples were stored in labelled and sealed Kraft sample bags. The sealed samples were dried for 12 hours at a temperature of 110°C using the Vacutec 970 drying oven (Fig. 3.6B). Samples were allowed to cool for 2 hours at room temperature. Crushed samples were milled with a Retsch RS 200 tungsten carbide milling machine for 8 minutes at 700 revolutions per minute to a particle size of less than 75 µm (Fig. 3.6C). Pure quartz sand was pulverised for 2 minutes at 750 revolutions per minute to clean the surfaces of the tungsten carbide milling pots before milling the samples. A cloth dipped in acetone was also used to clean the surfaces of the milling pots. Pulverised samples were split using a riffle splitter to perform different geochemical analyses on representative samples. Split pulverised samples were stored in sealed Kraft sample bags (Fig. 3.6D).

The process of preparing rock samples for XRF analysis involved placing the crushed samples into pallet cups and incorporating boric acid powder as a binding agent. The mixture consisted of about 15 g of sample powder and 50 g of boric acid, which were then pressed together with a force of approximately 30 tons for 30 seconds using a manual laboratory hydraulic press. After pressing, the pallet cups were cleaned with acetone to prevent any cross-contamination of samples. The resulting pressed pellets were then removed from the pallet cups and placed in labelled containers with their respective sample IDs. In preparation for this study, 14 samples of rock and 6 samples of coal were prepared.

Figure 3.6: Laboratory equipment: (A) Jaw crusher, (B) Drying oven, (C) Milling machine, (D) Riffle splitter.

3.4.2 Petrographic Study

A petrographic study was undertaken using 9 preprepared thin sections and 6 coal samples. Physical characterisation of different rock types was done with an emphasis on mineralogy, texture, colour, structures, and grain size. The optical properties of the minerals as well as micro-structures within the rock samples were studied using the Olympus BX51 petrographic microscope (Fig. 3.7). Both optical and physical properties of rocks were used to identify rock types. A ZEISS AxioCam ICc 1 camera connected to the Axiovision computer software was used to take photomicrographs of thin sections. The photographs and photomicrographs of the samples are fully described in chapter 4.

A Zeiss Axio Imager M2m reflected light petrographic microscope equipped with a Hilgers Fossil system was used to analyse Coal polished blocks (Fig. 3.8). The analysis was carried out under reflected light at a magnification of x500 with oil immersion. The purpose of the analysis was to identify maceral groups and determine

vitrinite reflectance. Additionally, the mineral matter was identified according to the SABS ISO standard 7404-part 4. The full description of the microphotographs is given in chapter 4.

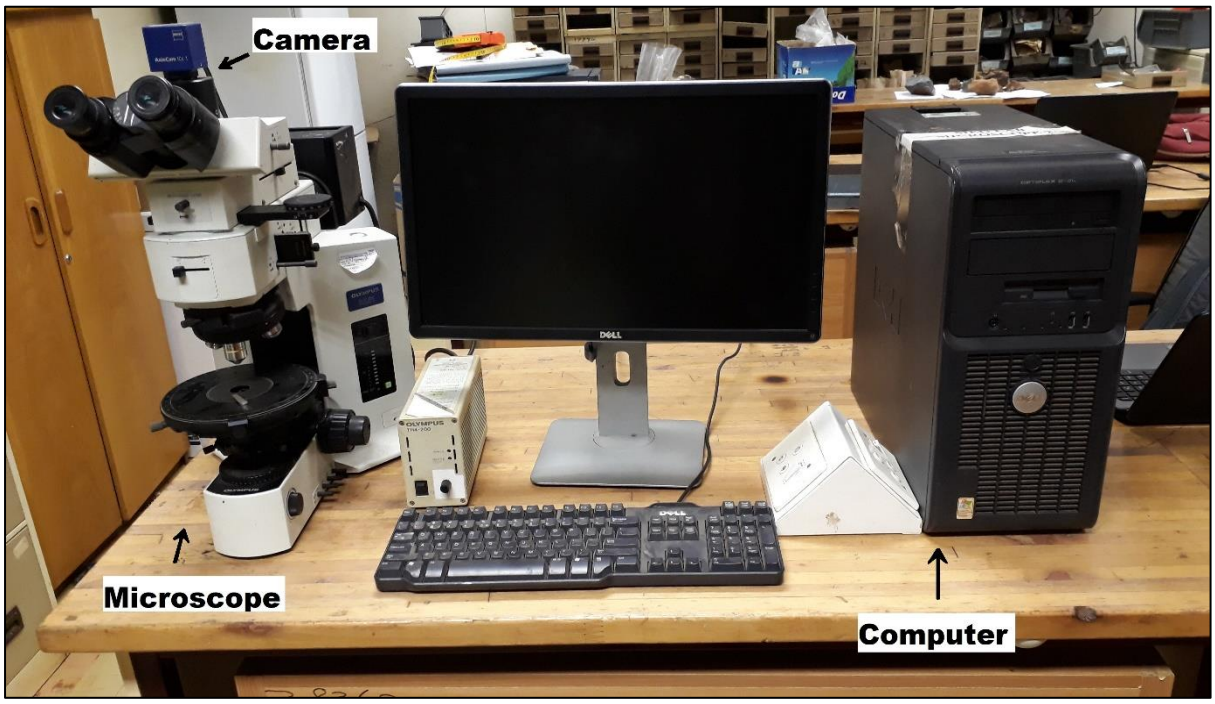

Figure 3.7: Olympus BX51 petrographic microscope fitted with a ZEISS AxioCam ICc 1 camera.

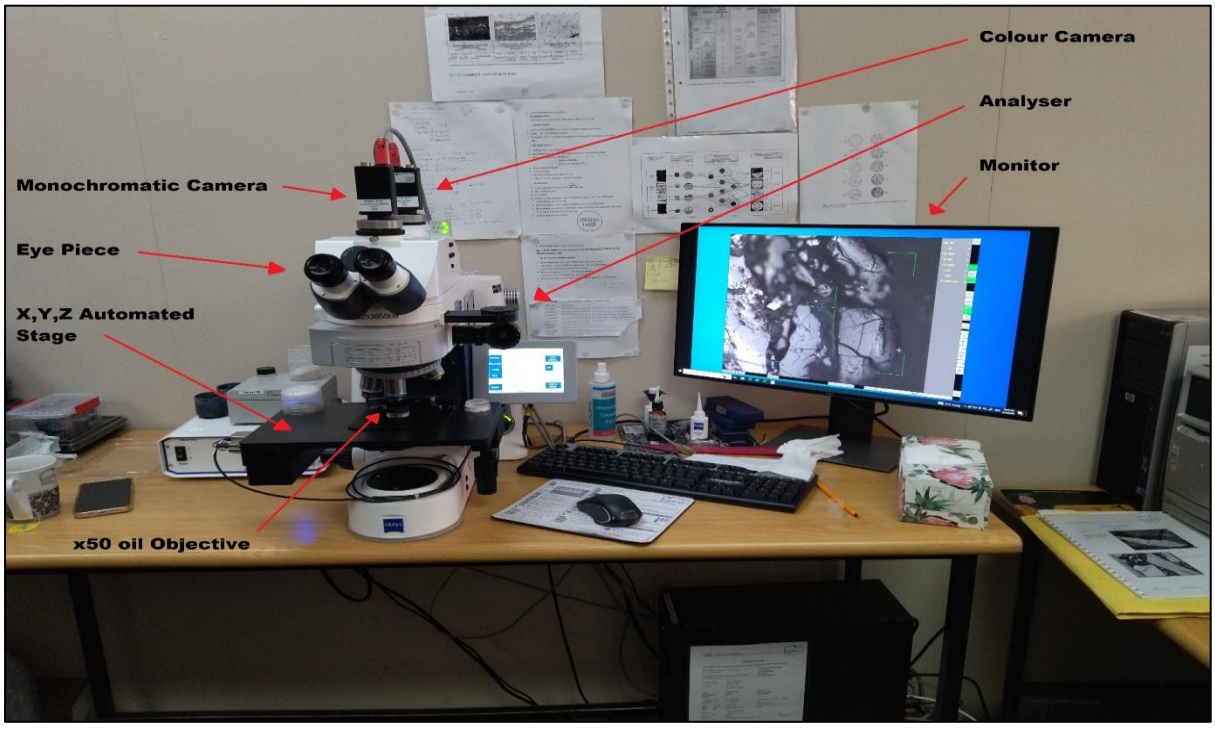

Figure 3.8: Zeiss Axio Imager M2m reflected light petrographic microscope.

3.4.3 Coal Quality Analysis

Proximate analysis, ultimate analysis, and calorimetry were utilised for coal quality analysis. Coal quality analysis was carried out at SGS Middelburg Laboratory, Mpumalanga.

3.4.3.1 Proximate Analysis

According to Thomas (2012), proximate analysis is a comprehensive analysis that determines the amounts of ash, fixed carbon, volatile matter, and moisture in the coal. Proximate analysis has been used widely as the basis for the characterisation of coal in connection with coal utilization (Speight, 2005). Six coal samples were analysed using proximate analysis.

Moisture

Total moisture in coal is the determination of all forms of moisture that resides within the coal matrix, excluding water of crystallization of the mineral matter. Moisture content was measured following the standard procedures of ISO 11722. The first step was to heat the empty vessel at 108 ± 2°C then weighed it after cooling it for 20 minutes in a desiccator. A coal sample was prepared and ground in a vessel so that there was no more than 0.15 g of the material per cm^2 area and weighed again. The vessel was uncovered in the drying oven and heated at a temperature of 108 ± 2°C for approximately one and a half hours. The vessel was cooled in a desiccator for 20 minutes and weighed. The moisture in the sample was expressed as the loss in the mass due to drying as a percentage of the total mass of the sample. The following equation adopted from Speight (2005) was used to determine moisture content in coal:

$$\text{moisture content}\% = \left(\frac{M_i - M_f}{M_i}\right) \times 100 \quad \text{.....(Equation 1)}$$

where: M_i = mass of the sample before heating

M_f = mass of the sample after heating

Ash Yield

The ash yield is the mineral matter that remains after the volatile components of coal have been burned off during combustion (Thomas, 2012). This inorganic residue is obtained by incinerating a coal sample in a ventilated furnace at a temperature of 700±50°C for 4 hours. The burnt coal is then weighed along with the porcelain dish used, and the ash yield is calculated using a formula adapted from Speight (2005). The standard procedures of ISO 1171 were followed to measure the ash yield:

$$\text{ash content } (\%) = \frac{M_i - M_f}{Mi} \times 100 \quad \text{.....(Equation 2)}$$

where: M_i=mass of coal before incineration

M_f = mass of coal after incineration

Volatile Matter

The term "volatile matter" in coal refers to the elements that are released at high temperatures in the absence of air, excluding moisture. These components have a significant impact on coal combustion and primarily consist of flammable gases like hydrogen, methane, carbon monoxide, and tar, as well as non-flammable gases such as carbon dioxide and steam (Speight, 2013). To determine the volatile matter content, the standard ISO 562 method was followed. A pre-weighed platinum crucible with a tight-fitting cover was used to hold one gram of coal, which was then suspended at a specified height in a furnace chamber maintained at 950 ± 20°C. After the rapid release of volatile matter was observed by the disappearance of the luminous flame, the crucible cover was tapped to ensure it remained securely in place, preventing air from entering. The crucible was heated for 7 minutes before being removed from the furnace and allowed to cool. The difference between the percentage loss in weight (excluding moisture) and the percentage of moisture content corresponds to the volatile matter.

Fixed Carbon

The fixed carbon or carbonaceous residue yield of coal is the carbon found in the material which remains after the volatile matter has been liberated (Speight, 2013).

Fixed carbon was calculated following the standard procedures of ISO 17246. Fixed carbon yield is calculated by subtracting the percentage of moisture, ash, and volatile matter from 100%. The following equation adapted from Speight (2005) was used to calculate fixed carbon:

$$\text{Fixed Carbon} = (\text{Moisture} + \text{Volatile matter} + \text{Ash Yield})\% - 100 \ldots\ldots\ldots\ldots \text{(Equation 3)}$$

3.4.3.2 Calorific Value

The calorific value (CV) or heating value of coal is the amount of heat per unit mass of coal when combusted. CV is a direct indicator of coal energy content and is regarded as the most important property for determining the usefulness of coal for combustion purposes (Speight, 2013). Calorific value was measured following the standard procedures of ISO 1928. Calorific value measurement was carried out in pure oxygen at 2500 kPa. This was performed by using a bomb calorimeter connected to Supercal software. The system was used after the stabilisation temperature of about 36.3°C was reached. Before analysis of the actual coal samples, a benzoic standard of calorific value 26.428 MJ/kg was used for verification and calibration. Following this, pulverised coal was weighed to 0.4 g in a crucible, with a cotton thread dipped in the coal and placed in a bomb for analysis. The bomb was filled with oxygen and then placed in a calorimeter where the analysis started automatically after closing the lid. Six coal samples were analysed using calorimetry. To acquire accurate findings, the analysis was repeated, and the averaged data were reported.

3.4.3.3 Ultimate Analysis

The process of ultimate analysis comprises of identifying the proportion of carbon, hydrogen, nitrogen, sulphur, and oxygen, calculated by difference (Speight, 2013). This analysis is combined with calorific value to perform combustion calculations like sulphur emissions, feed rates, and boiler performance. To determine carbon, nitrogen, and hydrogen, a LECO CHN non-dispersive infrared analyser was used, and the ASTM D 5373-08 standard procedures were followed. Six samples of coal underwent ultimate analysis.

Carbon and Hydrogen

The procedure involved taking a measured quantity of coal and placing it in a glazed porcelain crucible. This crucible was then inserted into the combustion tube of the first furnace, where the coal was burned in the presence of oxygen. To achieve combustion, the coal was ground and passed through a sieve with a size of 250 µm, and then exposed to dry oxygen at temperatures ranging from 850°C to 900°C. The resulting combustion products were directed towards copper oxide and lead chromate, which served to absorb different components of the combustion. The copper oxide was responsible for completely combusting the carbon and hydrogen in the coal, while the lead chromate absorbed sulphur oxides. Pre-weighed absorbers in the absorption train were used to absorb water, carbon dioxide, and carbon and hydrogen from the sample, and their increase in weight was used to determine the amounts of these components in the coal (Speight, 2013).

Nitrogen

In order to speed up the digestion process, a mercury salt catalyst was added to a concentrated sulphuric acid solution containing potassium sulphate, and this mixture was used to boil pulverized coal. The nitrogen content of the coal was analysed by digesting a 1 g sample of the coal with selenium oxide, potassium sulphate, and sulphuric acid in a Kjeldahl flask. The analysis was then completed through distillation and titration (Niksa, 2018).

Sulphur

To perform the analysis, a mixture of one gram of coal and three grams of Eschka mixture was prepared. The Eschka mixture consisted of a blend of one part anhydrous sodium carbonate and two parts of light calcined magnesium oxide by weight. The mixture was then placed in a 30 ml porcelain crucible and covered with an additional gram of Eschka mixture. The crucible was heated in a muffle furnace at 800 ± 25°C until the sample was fully oxidised. During the combustion process, any sulphur compounds that were released reacted with the magnesium oxide and sodium carbonate, resulting in the formation of magnesium sulphate and sodium sulphate. The sulphate residue was then extracted, and its weight was determined using the gravimetric method (Speight, 2013).

Oxygen

The percentage of oxygen was calculated through deduction from 100, based on the combined percentages of moisture, ash, carbon, hydrogen, nitrogen, and sulphur. The following equation was employed to achieve this (Speight, 2005):

$$\text{Oxygen} = 100 - (\text{Ash Yield} + \text{Moisture} + \text{Hydrogen} + \text{Carbon} + \text{Nitrogen} + \text{Sulphur}) \quad \text{(Equation 4)}$$

3.4.4 X-Ray Fluorescence Spectrometry

X-ray fluorescence spectrometry is a technique for analysing the chemical composition of various types of substances, including liquids, solids, powders, and filtered materials. The method involves the displacement of electrons from their atomic orbitals, resulting in the emission of energy that is unique to each element. The emitted energy is subsequently detected by the spectrometer and sorted by element. X-ray fluorescence spectrometry is a reliable analytical method for determining the chemical composition of materials (Brouwer, 2010).

XRF analyses were conducted on 6 coal samples and 14 selected representative host rock samples. Coal samples were analysed at the University of Pretoria, Faculty of Natural and Agricultural Sciences and host rock samples were analysed at the University of Venda, Department of Earth Sciences. Coal samples were dried and roasted in alumina refractory crucibles at 100°C & 1000°C respectively, to determine Loss on Ignition (LOI). 1g Sample was mixed with 6 g of Lithiumtetraborate flux and fused at 1030°C to make a stable fused glass bead. The Thermo Fisher ARL Perform'X Sequential XRF instrument with Uniquant software was used for analyses. The software analyses for all elements in the periodic table between Na and U, but only elements found above the detection limits were reported. The values were normalised, to include LOI, to determine crystal water and oxidation state changes. A standard sample material (BHVO-1) was prepared and analysed in the same manner as the samples and is reported as such.

BRUKER AXS S2 RANGER XRF spectrometer linked to a computer was used to analyse pelletised representative host rock samples. To guarantee the accuracy of the analysis, the calibration of the instrument commenced by using a copper disk. Each

sample was run for around 10 minutes and the results were exported via Excel spreadsheet. The results were recorded and are presented in chapter 4.

3.4.5 X-ray Diffraction

X-Ray diffraction (XRD) utilizes x-ray radiation on crystalline organic and inorganic samples. The rays are diffracted in a pattern determined by the position, arrangement, and size of the constituents of the crystal. Scattered photons, which may undergo subsequent interference, lead to a characteristic diffraction pattern, which is specific to the crystalline powder and may serve as its 'fingerprint'. Sensitivity is usually in the microgram to milligram range (Holder & Schaak, 2019).

XRD analyses were conducted at the University of Pretoria, X-ray Diffraction Facility using the PANalytical X'Pert Pro powder diffractometer in θ–θ configuration with an X'Celerator detector and variable divergence- and fixed receiving slits with Fe-filtered Co-Kα radiation (λ=1.789Å). The samples were prepared according to the standardized Panalytical backloading system, which provides a nearly random distribution of the particles. The X'Pert High Score Plus software was used for the identification and interpretation of the diffraction patterns. The mineralogy was determined by selecting the best–fitting pattern from the ICSD database. XRD analyses were conducted on all coal samples and selected representative host rock samples. The results were recorded and presented in chapter 4.

CHAPTER 4 : RESULTS AND DISCUSSION

4.1 Drillhole Data

Secondary exploration data for 10 boreholes provided by Council for Geoscience are presented below. The collar table indicating drilling depth, elevation and borehole locations is presented in Table 4.1. Most boreholes were drilled along Permian and Triassic rocks of the Karoo sequence (Fig. 4.1). Boreholes 1900658, 1901251 and 1900511 were located within Mushithe area. Boreholes 1901191, 1900219, and 1901162 were located in the Zwigodini area, approximately 12 km west of the coal outcrop. Meanwhile, boreholes 1901211, 1900146, 1900085, and 1900364 were situated in the Tshikondeni deposit, approximately 14 km east of the coal outcrop. Borehole sited with Mushithe area were presented in drillhole data description (Section 4.1.1) and boreholes from Tshikondeni and Zwigodini areas were presented in Appendix A1.

Table 4.1: Collar table indicating drilling depth, elevation, and borehole locations

Borehole ID	Depth From (m)	Depth To (m)	Elevation (m)	Latitude	Longitude
1901191	0	456.82	456.4	22°30'54.93"S	30°37'29.16"E
1900219	0	201.07	465.7	22°31'55.47"S	30°37'51.05"E
1901162	475	501.76	443.3	22°30'38.28"S	30°40'29.33"E
1900658	0	404.50	380.2	22°30'1.45"S	30°46'28.06"E
1901251	0	279.91	406.0	22°30'39.4"S	30°48'16.25"E
1900511	0	547.05	3515	22°29'12.72"S	30°49'19.03"E
1901211	0	75.90	346.7	22°30'22.39"S	30°55'44.39"E
1900146	0	197.27	333.3	22°29'43.25"S	30°56'59.03"E
1900085	0	103.76	327.0	22°29'4.91"S	30°57'23.18"E
1900364	0	280.65	333.2	22°30'21.1"S	30°58'09.75"E

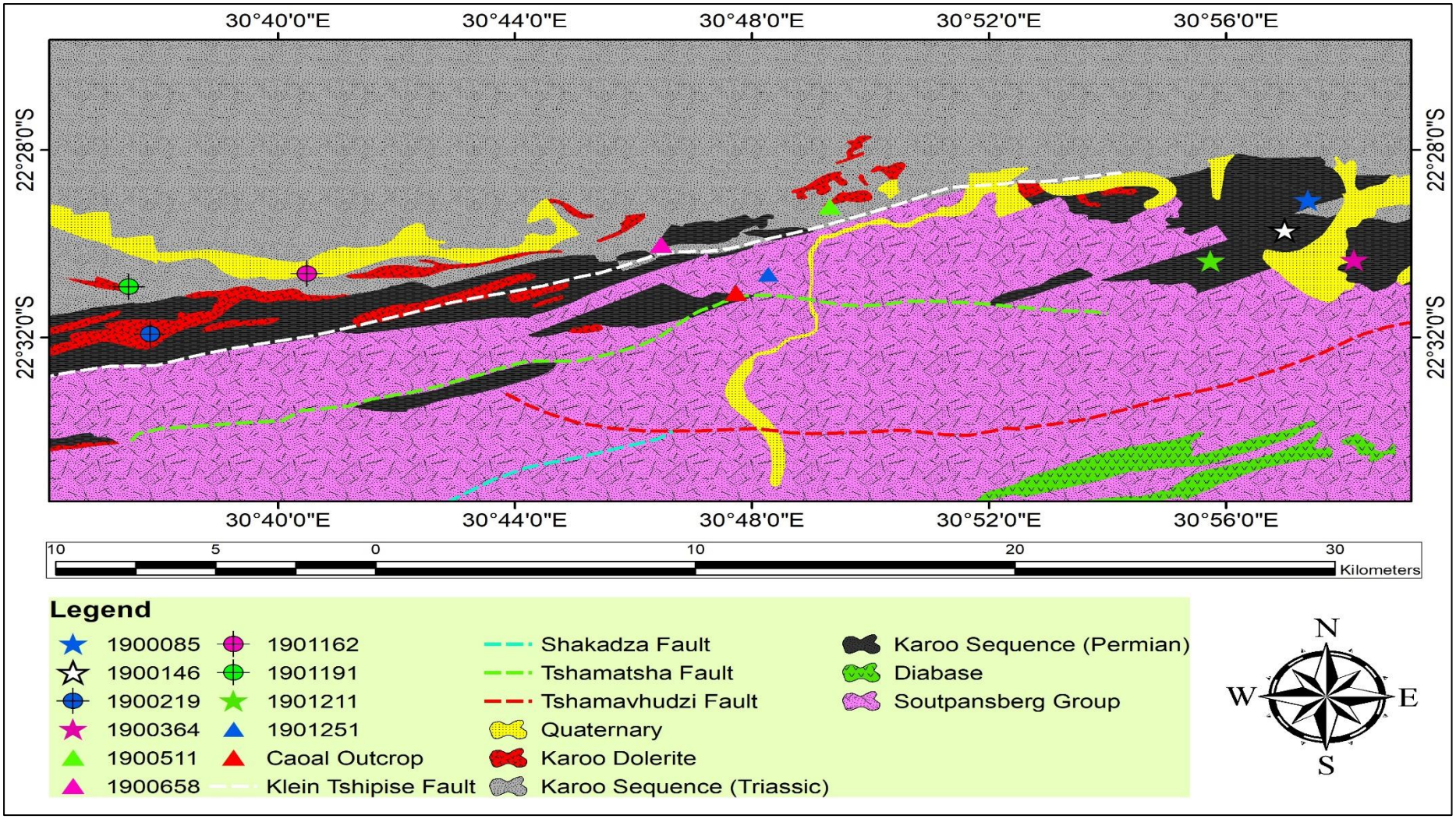

Figure 4.1: Map showing borehole locations overlay on 2230 Musina 1: 250 000 geological map compiled from (Council for Geoscience, 2020) data.

4.1.1 Drillhole Data Description

Borehole 1900658

Borehole 1900658 is located about 3 km northwest of the coal outcrop, within Mushithe Village. The borehole was drilled to a depth of 404.50 m, and it encountered four coal seams (No. 1, 2, 3, and 4) at depths ranging from 265.12 m to 370.99 m (Fig. 4.2). Deep coal seams intercepted at Borehole 1900658 are a result of the overlying Triassic formations overlying the coal-bearing Permian Formations. No. 1 seam (1.06 m thick) along borehole 1900658 was intersected at a depth interval of 265.12 to 266.18 m, hosted by shale on both roof and foot rock, with carbonaceous shale partings. No. 2 Seam (7.32 m) consisted of coal, shaly coal, interbedded with shale, carbonaceous shale, and coaly mudstone. Seam No.3 (4.19 m) consists of coal and shaly coal interbedded with carbonaceous shale and sandstone. Seam No. 4 (0.42 m) was the lowermost seam intersected within borehole 1900658, consisting of coal and coaly shale interbedded with carbonaceous shale.

Outcrop

The exposed coal seam is located along the bank of the Mbodi River, within the Mushithe Village. The coal seam was about 1.13 m and consisted of highly fractured coal hosted and interbedded within carbonaceous shale (Fig. 4.3). Two coal plies were identified. The upper ply was 0.30 m thick, hosted by shale roof rock and carbonaceous shale foot rock. The bottom ply was 0.33 m, hosted by carbonaceous shale on both the roof and foot rock. The exposed coal seam strike 42° northeast, and dips towards the northwest at an angle of 16°. This is consistent with the findings of Brandl (1981), who noted that coal-bearing Karoo Supergroup rocks dip between 3-20° northwards. The outcrop at Mushithe resulted from dip slip displacement along the east-northeast trending Tshamatsha fault resulting from extensive horst and graben systems and faults which have exerted major structural controls on the geology of the area (Mphaphuli, 2017).

Borehole 1901251

Borehole 1901251 was the closest to the coal outcrop and sited about 1 km northwest of the coal outcrop, within Mushithe Village. The borehole intersected seven seams (No. 2, 4, 5, 7, 12, 13, and 14) at depths between 59.14 m to 260.95 m (Fig. 4.4). Seam No. 2 was at the upper section of the coal zones with a thickness of 0.86 m,

while seams No. 4, 5 and 7 was at the middle section with thicknesses of 0.34 m, 0.35 and 2.52 m respectively. Seams No. 12, 13 and 14 was at the lower section with thicknesses of 11.38 m, 11.38 m, and 4.8 m respectively. No. 2 seam was hosted by mudstone on both hanging wall and footwall and consists of mixed and shaly coal interbedded with carbonaceous shale. No. 4 seam consists of mixed coal interbedded with shale and hosted by sandstone on both hanging wall and footwall.

Seam No. 5 consisted of mixed coal interbedded with carbonaceous shale hosted by shale on both the hanging wall and footwall. Seam No. 7 consisted of mixed coal, bright coal interbedded with shale and carbonaceous shale, hosted by coarse sandstone hanging wall and shale footwall. Seam No. 12 consisted of mixed and dull coal, interbedded with shale, medium-grained sandstone, and carbonaceous shale, hosted by carbonaceous shale on both the hanging wall and footwall. Seam No. 13 consists of dull, shaly, and mixed coal interbedded with shale, carbonaceous shale, and fine sandstone with carbonaceous shale hanging wall and shale footwall. No. 14 seam consists of dull, mixed, and bright coals, hosted by shale as hanging wall and footwall.

Borehole 1900511

Borehole 1900511 was sited about 4.3 km northeast of the coal outcrop, within Mushithe Village. The borehole comprises seven coal seams, namely, No. 1, 2, 3, 4, 5, 6, and 7, intercepted at depth distances between 508.5 m and 533.08 m (Fig. 4.5). Deep coal seams intersected within Borehole 1900511 can be attributed to the overlying Triassic Formations overlying coal-bearing Permian Formations. No. 1 seam (2.82 m thick) is the uppermost seam, consisting of coal and shaly coal interbedded with carbonaceous shale. The seam was hosted by coaly mudstone (hanging wall) and carbonaceous shale (footwall). Seam No. 2 (5.51 m thick) was the thickest seam intercepted within borehole 1900511, the seam consisted of coal interbedded with carbonaceous shale and shale and hosted by carbonaceous shale on both hanging wall and footwall.

Seam No. 3 (2.06 m thick) consisted of coal interbedded with carbonaceous shale and shale and hosted by carbonaceous shale on both the hanging wall and footwall. Seam No. 4 was approximately 3.8 m thick, the seam consisted of coal interbedded with shale and carbonaceous shale, hosted by shale (hanging wall) and sandstone

(footwall). Seam No. 5 (4.97 m thick) consisted of coal hosted by carbonaceous shale (footwall) and medium-grained sandstone (hanging wall), interbedded with carbonaceous shale, coaly mudstone and mudstone. Seam No. 6 was 1.61 m thick, consisting of coal interbedded with carbonaceous shale and coaly mudstone, hosted by carbonaceous shale on both hanging wall and footwall. Seam No. 7 (0.89 m thick) was the lowermost seam of the borehole, the seam was hosted by carbonaceous (hanging wall) shale and shale (foot rock).

Borehole 1901191

Borehole 1901191 was sited approximately 18 km northwest of the coal outcrop, within Zwigodini Village. Borehole 1901191 was drilled to a depth of 456.82 m and logging was done from 33.65 m due to surface weathering. No coal seams were intersected. Coal seams were not intercepted at Borehole 1901191 as it was drilled within the northern margin of the Triassic Solitude Formation which only have occasional bands of bright coal in some areas (Malaza, 2014).

Borehole 1900219

Borehole 1900219 was sited about 17 km west of the coal outcrop, within Zwigodini Village. The borehole intersected two coal seams (Seam No.1 and No. 2) at depth distances between 56.78 m and 171.5 m. Seam No. 1 was approximately 0.8 m, hosted by carbonaceous shale (footwall) and shale (hanging wall), interbedded with carbonaceous shale and coaly mudstone. Several dolerite intrusive bodies were observed above and below No.1 seam. Seam No. 2 (8.15 m) consisted of coal interbedded with carbonaceous shale, coaly mudstone and mudstone, with a footwall and hanging wall of shale.

Borehole 1901162

Borehole 1901162 was located about 12 km northwest of the coal outcrop within Sagole Village. The borehole was logged from 475.25 m to 501.76 m. One seam (No. 8) was intersected between 492.62 m to 499.53 m. The sandstone-hosted seam consisted of shaly, mixed, and bright coal interbedded with carbonaceous shale, shale, and sandstone.

Borehole 1901211

Borehole 1901211 was sited about 14 km east of the outcrop, within the Tshikondeni deposit. The borehole intersected one seam (Seam No. 13) at a depth between 74.55 m and 66.61 m. Coal was hosted by a 66.61 m thick coaly mudstone (hanging wall) and siltstone (footwall). Seam No. 13 was about 7.94 m thick, interbedded with coaly mudstone and shale. Seam No. 13 was dominated by dull coal with occasional bright coal occupying the lower section of the seam.

Borehole 1900146

Borehole 1900146 was sited about 16 km east of the outcrop, within the Tshikondeni deposit. The borehole was drilled to a depth of 197.27 m and logging was done from 65.64 m. Four seams (No. 6,7,8 and 9) were intercepted at depth distances between 119.31 m and 196.39. Seams No. 6,7 and 8 have were having thickness of 2.41 m, 3.83 m, and 1.19 m respectively, consisting of coal interbedded with shale. Seam No. 9 (18.23 m) was at the lower section of the borehole and consisted of coal hosted within shale-coal-sandstone facies.

Borehole 1900085

Borehole 1900085 was sited about 17 km northeast of the outcrop, within the Tshikondeni deposit. The Borehole was drilled to a depth of 103.76 m and logging was done from 18.2 m due to surface weathering. Two seams (No. 6 and 7) were intersected at depth distances between 85.76 m (top) and 90.48 m (bottom). Seams No. 6 (2.11 m) and No. 7 (2.61 m) consisted of thermally metamorphosed coal hosted within shale and burnt shale. Dolerite encountered at a depth between 96.88 to 100.39 m was likely the source of heat responsible for the overlying burnt coal.

Borehole 1900364

Borehole 1900364 was sited about 18 km east of the outcrop, within the Tshikondeni deposit. The borehole was drilled to a depth of 280.65 m and logging was done from 18.54 m due to surface weathering. Twelve seams (No. 3, 4, 5, 6, 7, 8, 9, 10, 12, 13, 14 and 15) were encountered at depth between 26.22 m and 271.23 m. Seam No. 3, 6, 7, 12, 13, 14 and 15 attained thicknesses of 6.69 m, 1.83 m, 3.5 m, 6.54 m, 6.32 m, 11.13 m, and 16.62 m respectively, consisting of coal and shaly coal, hosted within shale and interbedded with shale, carbonaceous shale, coaly mudstone and

sandstone. Seam No. 4, 5, 8, 9 and 10 attained thicknesses of 5.7 m, 24.53 m, 1.58 m, 10.99 m, and 5.47 m respectively, consisting of coal hosted by shale (roof rock) and sandstone (foot rock), and interbedded with shale carbonaceous shale, and sandstone.

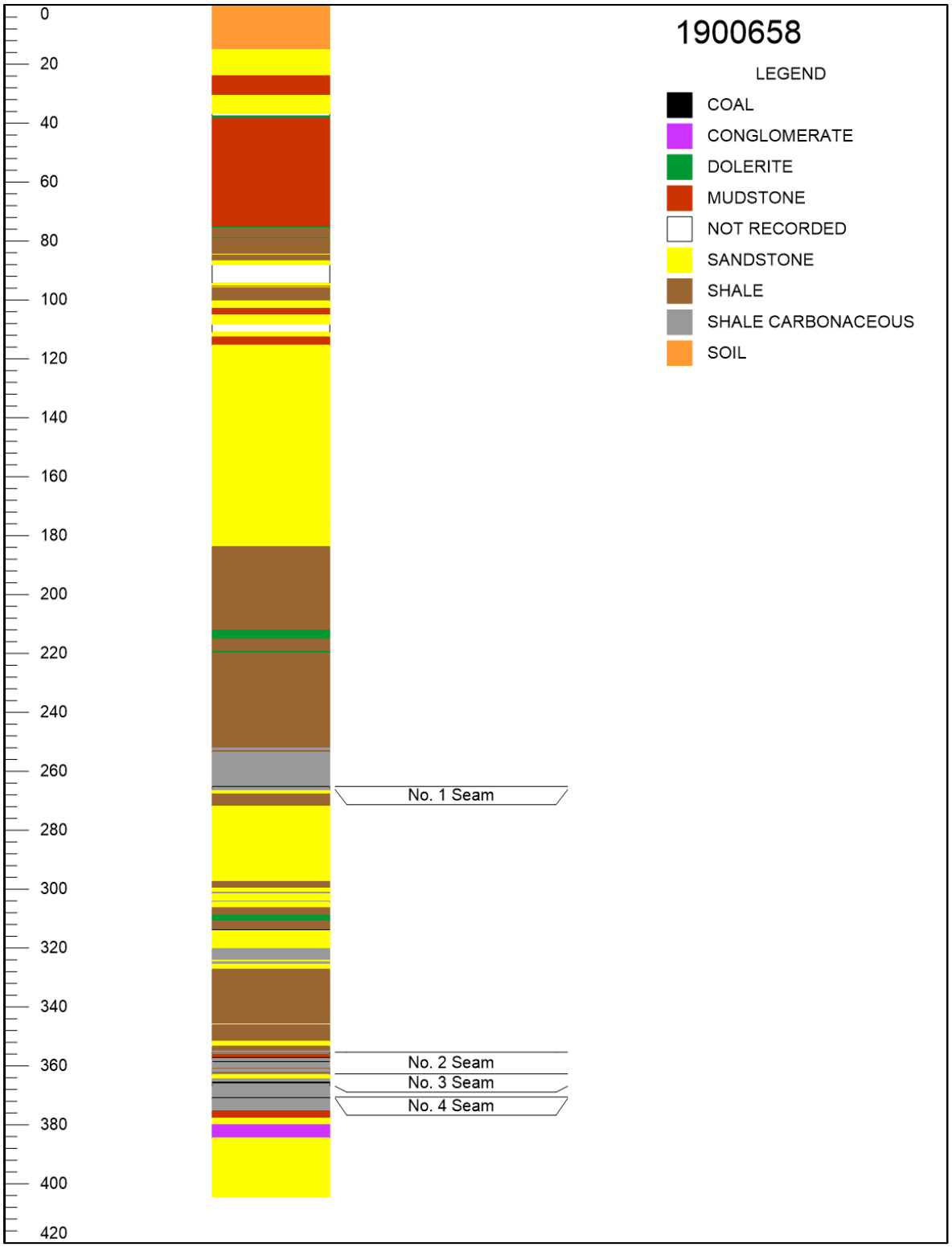

Figure 4.2: Borehole 1900658 log showing lithological variations.

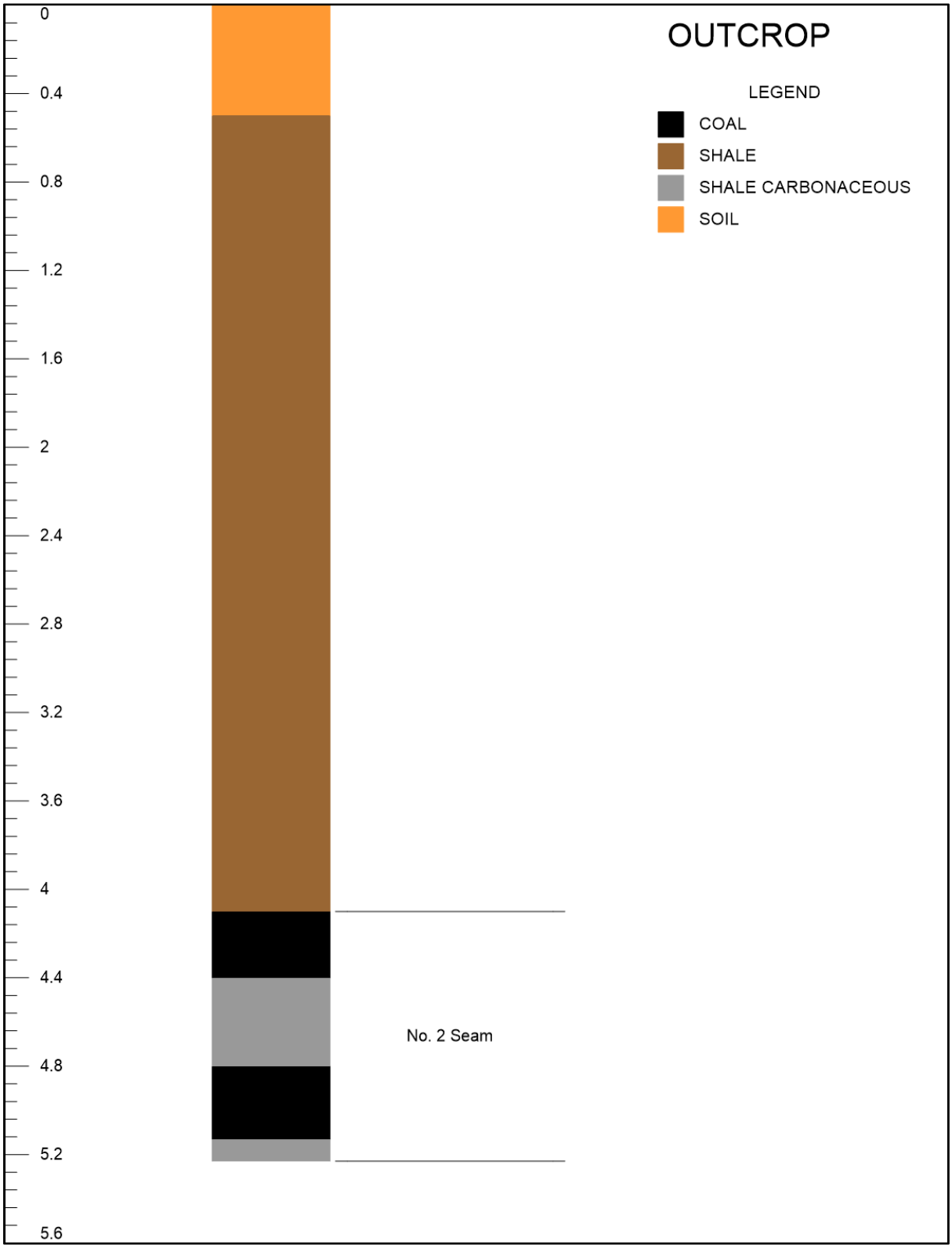

Figure 4.3: Coal outcrop borehole log showing lithological variations.

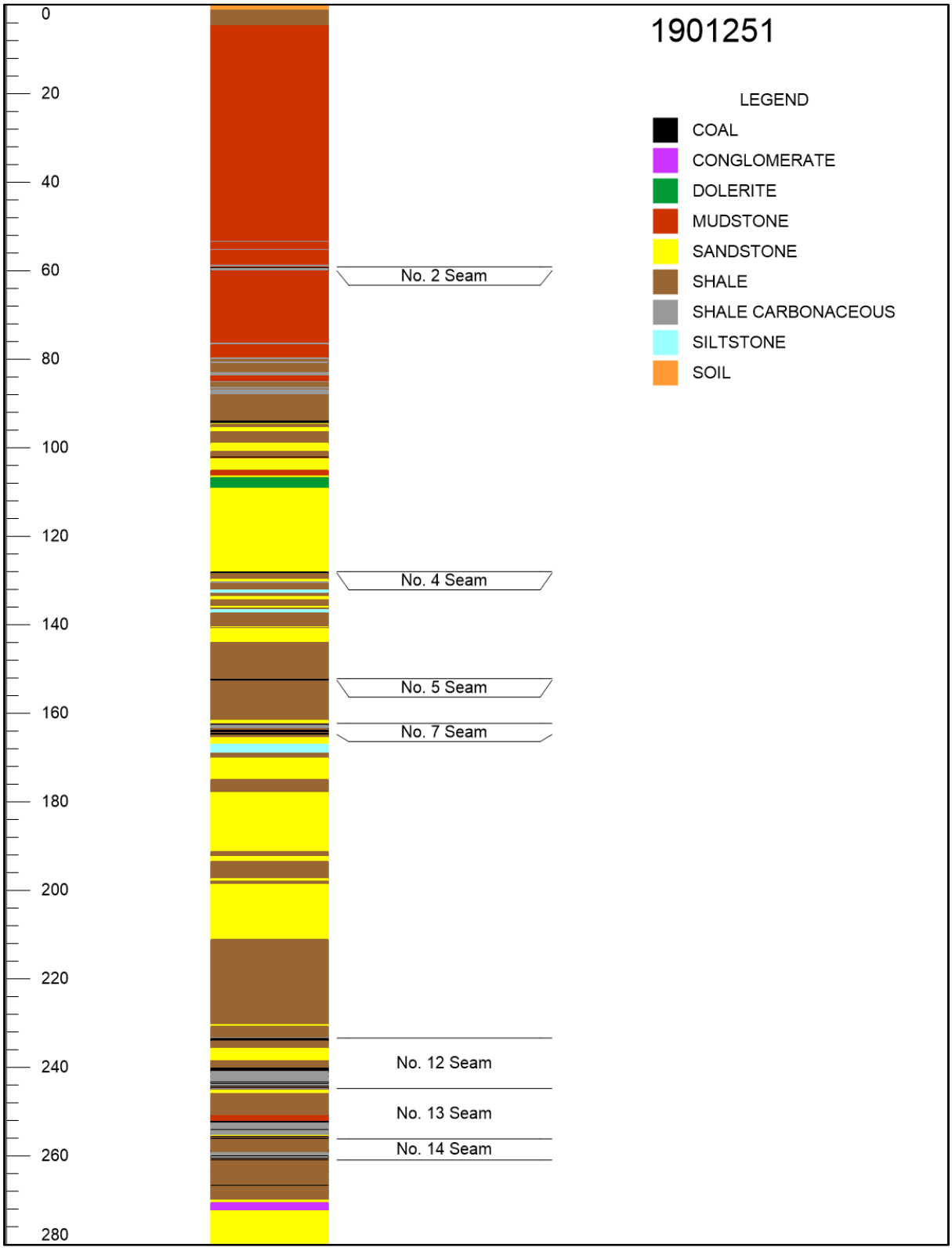

Figure 4.4: Borehole 1901251 log showing lithological variations.

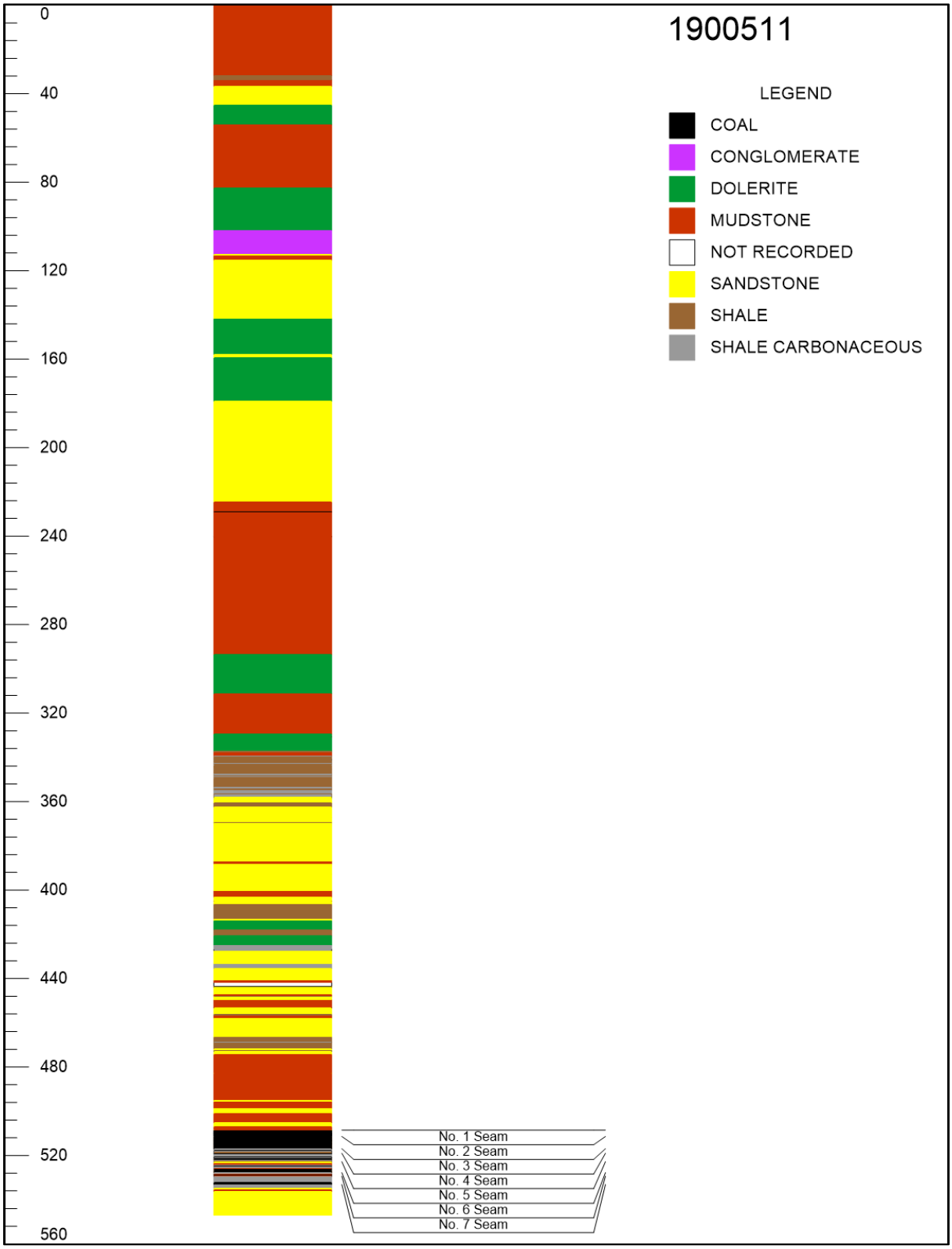

Figure 4.5: Borehole 1900511 log showing lithological variations.

4.1.2 Coal Seam Correlation

The data from the boreholes 1900219, 1901251, and 1900364 was used to create a west-east borehole correlation profile along the strike (Fig. 4.6). Additionally, data from the boreholes 1900511, 1901251, and the coal outcrop was used to create a north-south profile (Fig. 4.7).

Coal measures within the Mushithe area consist of four to seven coal seams, with thicknesses ranging from 0.35 m to 11.38 m and notable lateral and horizontal variations. Coal seams intersected within the Tshikondeni area ranged between one and twelve while Coal seams intersected ranged between one and two. The nature of the coal in the area changes from a multi-seam coal-mudstone association in the east, which includes twelve seams in the Tshikondeni area, to seven seams in the central Mushithe area and two seams in the west (Zwigodini area). Coal seams in the Mushithe area become deeper towards the north, reaching depths of 511.39 m to 533.08 m.

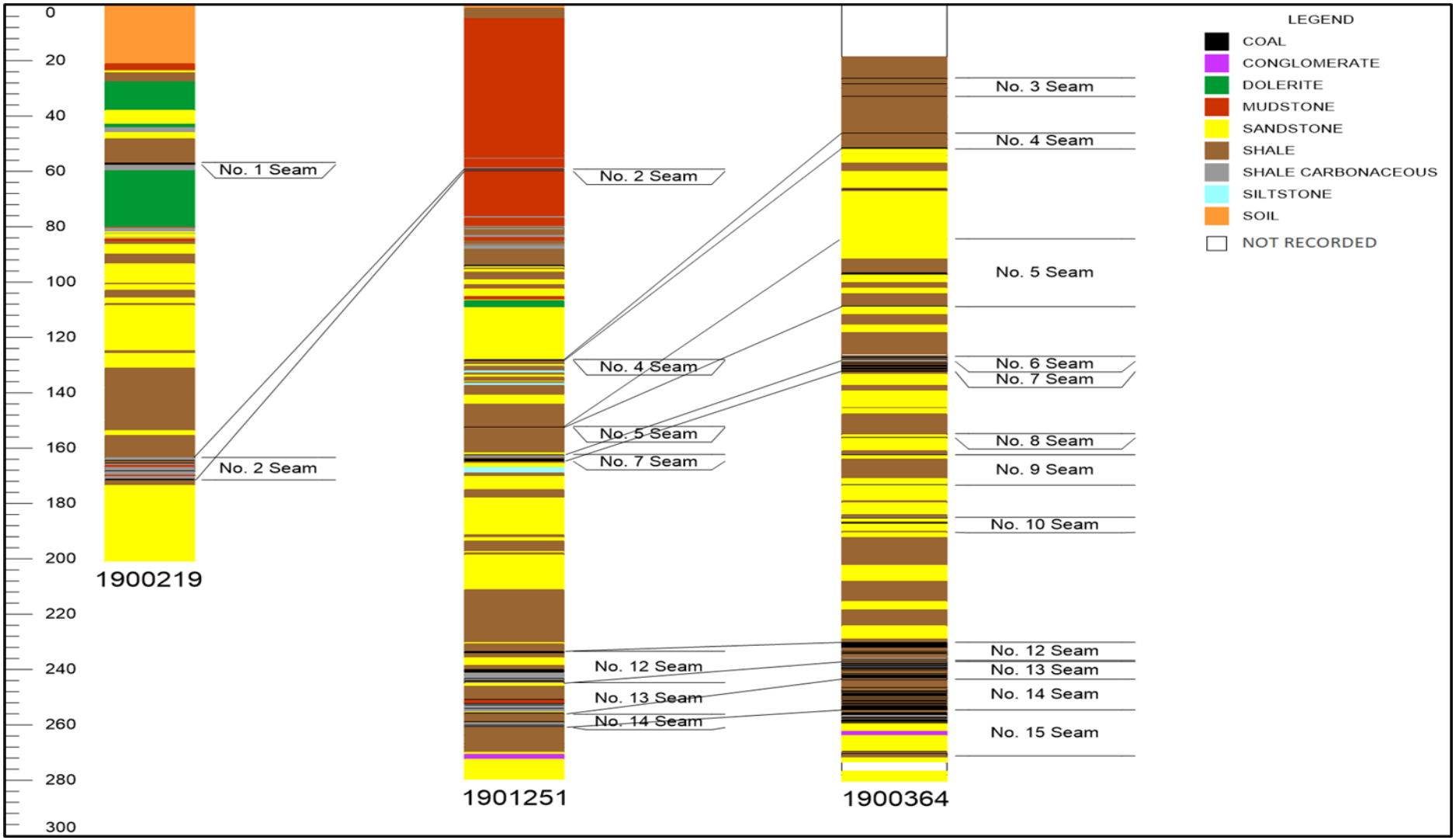

Figure 4.6: West-east profile along boreholes 1900219, 1901251 and 1900364.

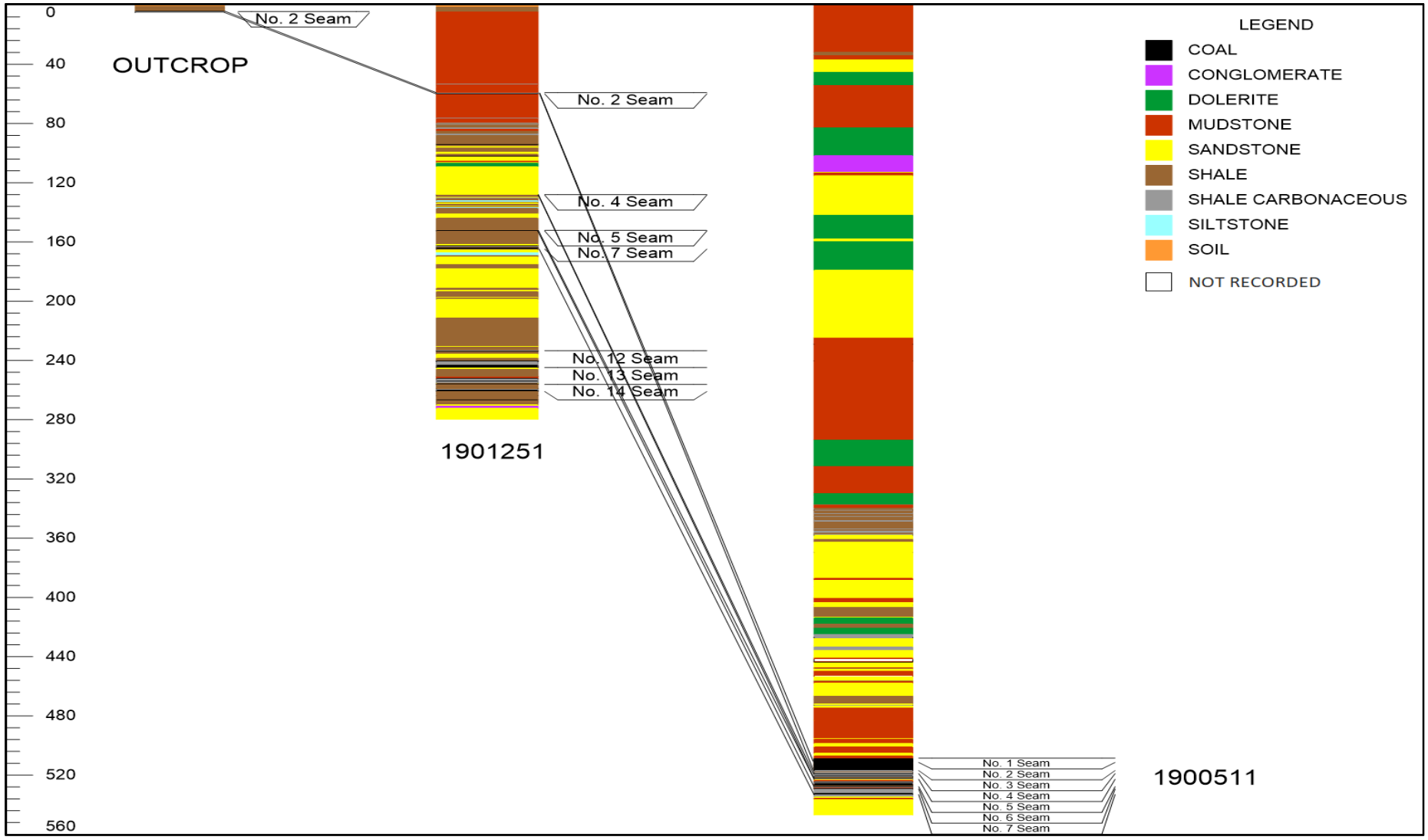

Figure 4.7: North-south profile along boreholes 1900511, 1901251 and the coal outcrop.

4.2 Geological Map

The following rocks were encountered at Mushithe area: Pink quartzite, red quartzite, mudstone, basalt, sandstone, quartz vein, carbonaceous shale, coal and calcrete (Fig. 4.8). Quartzites and sandstones were the most widely distributed lithological units. General strike direction rock units were north-east direction with an average dip of angle of 23°. Mudstone was limited to the north-eastern portion of the study area. Mudstone was in sharp contact with red quartzite. Quartzites were found adjacent to sandstone and basalt, and this is indicative of contact metamorphism of sandstone by Basalt to form quartzite. All quartzite outcrops were striking in the northeast direction. Quartzite often formed hilltops within the study area due to its extreme resistance to chemical weathering.

Basalt was limited to the eastern portion of the study area. Basalt was in sharp contact with quartzite. A sharp contact between basalt and quartzites is indicative of contact metamorphism of sandstone. Sandstone was found in sharp contact with shale and in gradual contact with red and pink quartzite. Quartz vein was found north of the study area intruding red quartzite and in the eastern portion intruding red quartzite and basalt. Occurrence of quartz veins within basalt indicates that the vein is younger than the basalt. Carbonaceous shale and shale found along Mbodi River were identified as host rocks for coal at Mushithe area. Coal occurrence at Mbodi River was interbedded with carbonaceous shale and shale. Shale and carbonaceous shale were highly fractured.

Calcrete was limited to south-west of the study area. The outcrop was highly weathered, and in gradual contact with quartzite. The cross-section (Fig. 4.8) of the Mushithe coal occurrence was done from point A to point B from the geological map, this was done to allow representation of all lithologies with depth. Lithological units were plotted on the cross section using their dip angles and dip directions as well their altitudes. The coal-bearing rocks located along the Mbodi River were isolated from the main coal-bearing rocks situated to the north of the study area. Hancox and Götz (2014) indicated that coal deposits within a particular basin may be located in distinct areas that are commonly referred to as valleys. This observation is consistent with the current findings. The outcropping resource block like Mushithe coal occurrence situated south of the edge of the Pafuri sub-basin can be suitable to surface mining by small, medium, and micro enterprises as noted by Jeffrey (2005).

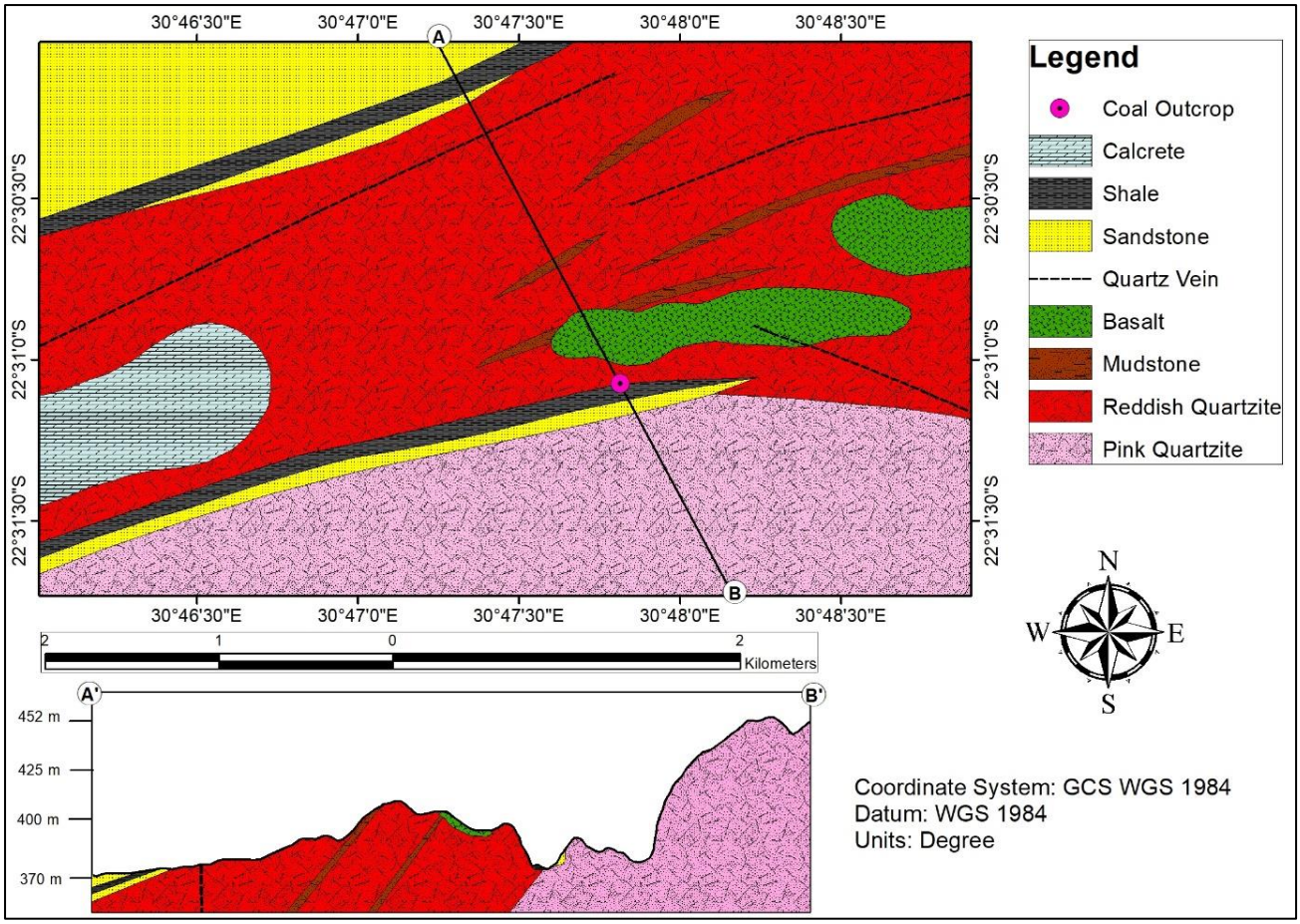

Figure 4.8: 1:10 000 Geological map and cross section of Mushithe area.

4.2.1 Rock Description

Rocks were described both macroscopically and microscopically. Macroscopic analysis was done using a magnifying glass. Consideration was given to colour, mineralogy, texture, grain size and structures. Microscopic analysis was done using Olympus BX51 petrographic microscope to identify optical properties in the rocks. A detailed description of the rocks that were identified in the study area is presented below.

Pink Quartzite

Pink quartzite was generally found south of Mbodi River. The specimen was light pink in colour (Fig. 4.9). The specimen showed interlocking crystalline structure dominated by quartz. In thin section (Fig. 4.10), pink quartzite was dominated by interlocked quartz grains. In plane-polarised light (PPL), quartz grains were colourless with low relief, no cleavage and low birefringence. In cross-polarised light (XPL), quartz showed first order white-grey interference colours and undulatory extinction.

Figure 4.9: A photograph of pink quartzite outcrop and hand specimen.

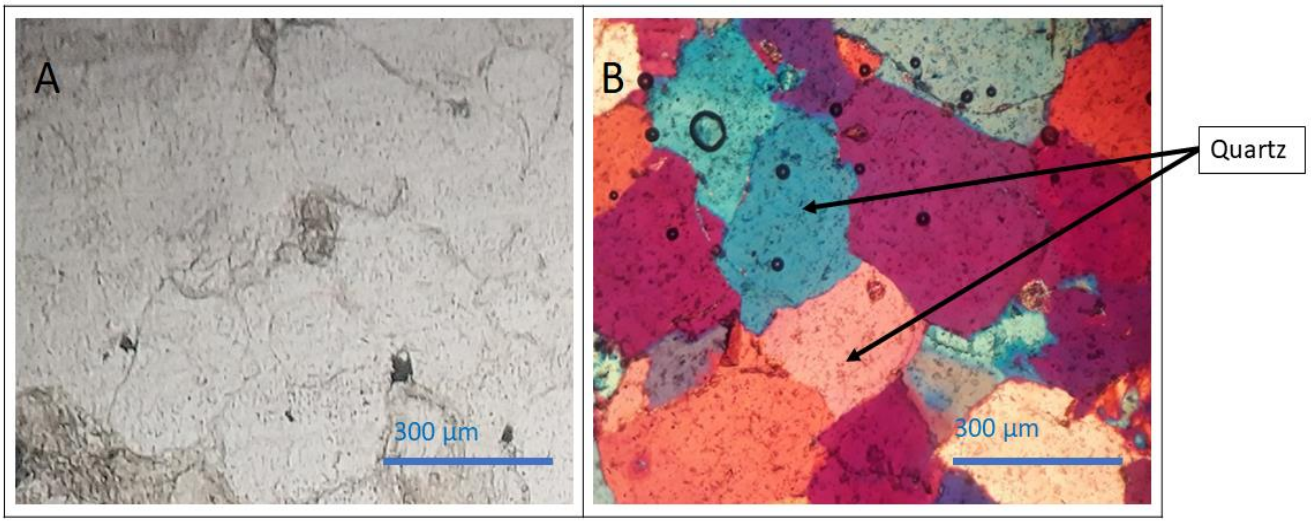

Figure 4.10: Photomicrograph of pink quartzite captured using both plane polarised light (A) and cross-polarised light (B).

Red Quartzite

Red quartzite was generally found north of the Mbodi River (Fig. 4.11). The hand specimen was reddish in colour. The specimen showed interlocking crystalline structure. When viewed with a magnifying glass, the specimen was dominated by quartz. The reddish colour of the sample indicates the clasts of the protolith were cemented by iron oxide. In thin section (Fig. 4.12), the sample was dominated by interlocked quartz with minor plagioclase. Quartz and plagioclase showed low relief in plane-polarised light. Quartz showed low birefringence and first order white-gray

interference colours, and undulatory extinction cross-polarised light. Twinning can be observed on plagioclase.

Figure 4.11: A photograph of red quartzite outcrop and Hand specimen.

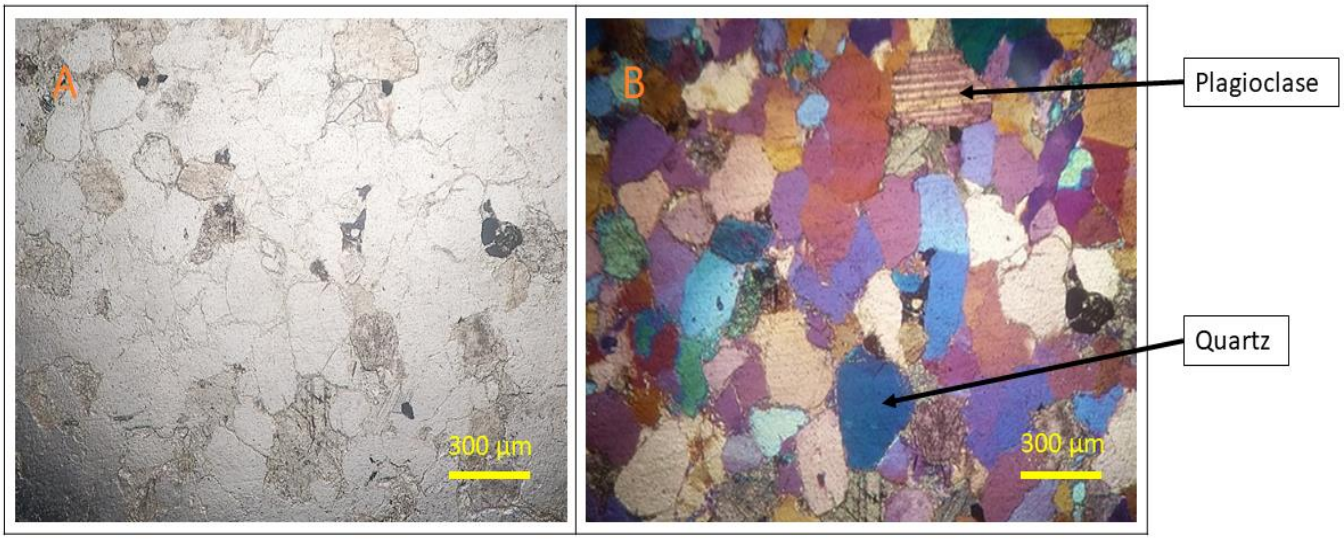

Figure 4.12: Photomicrograph of red quartzite captured using both plane polarised light (A) and cross-polarised light (B).

Mudstone

Mudstone was generally found along the north-eastern porting of the study area, and it was interbedded with red quartzite (Fig. 4.13). The specimen was reddish brown, and it consists of a mixture of clay and silt-sized particles. The red colour can be attributed to the presence of an iron oxide cementing agent. In thin section (Fig. 4.14), the sample was dominated by quartz, clay minerals and iron oxide. Clay minerals exhibited a very fine texture. In plane-polarised light (PPL), quartz grains were

colourless, low relief, no cleavage and low birefringence. In cross-polarised light (XPL), quartz showed first order white-grey interference colours and undulatory extinction. Since iron oxide do not transmit light in thin section, it appeared black in both PPL and XPL.

Figure 4.13: A photograph of Mudstone outcrop and hand specimen.

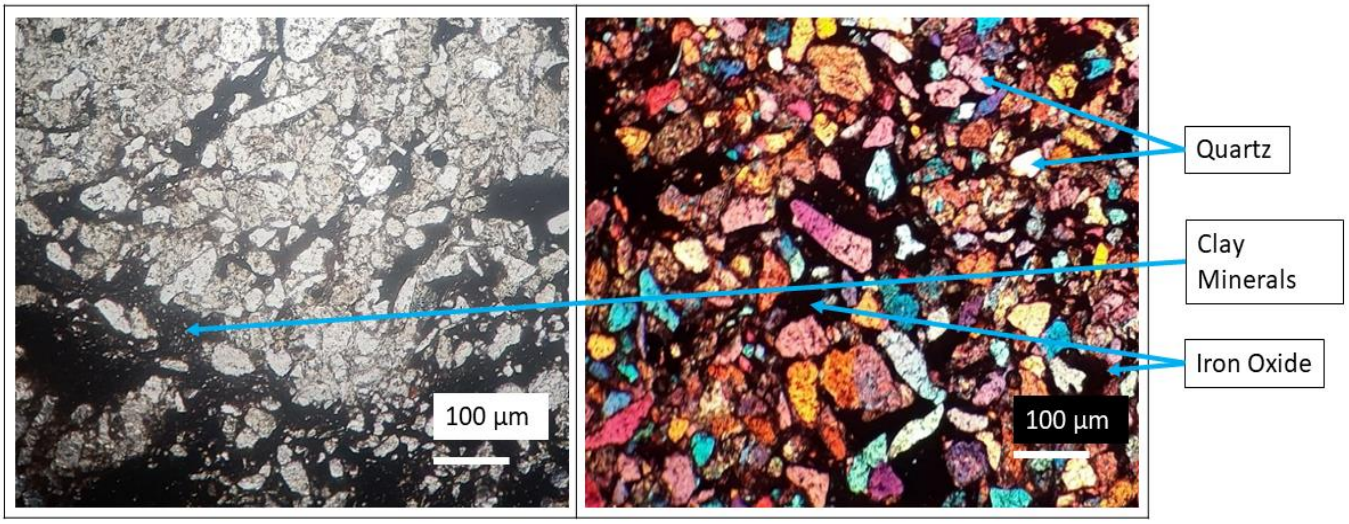

Figure 4.14: Photomicrograph of mudstone captured using both plane polarised light (A) and cross-polarised light (B).

Basalt

Basalt outcrops in the area were mostly intruding red quartzites. Outcrops of basalt were generally found along the eastern part of the study area (Fig. 4.15). The hand specimen was dark grey and consists mainly of mafic minerals. Individual minerals

could not be distinguished with the naked eye (aphanitic texture). The texture results from rapid cooling in a volcanic environment.

In thin section (Fig. 4.16) Under plane polarised light (PPL), plagioclase and quartz were colourless, clinopyroxene was pale green, brownish to colourless. Clinopyroxene had high relief, while plagioclase and quartz had a low relief. A typical near 90° pyroxene cleavage can be identified. Under the cross polarised light (XPL), middle second-order interference colours can be observed in clinopyroxene, which ranges from yellowish, brown, pale green to bluish. Quartz showed low birefringence and first order white-grey interference colours. Twinning can be observed in plagioclase.

Figure 4.15: A photograph of basalt outcrop and hand specimen.

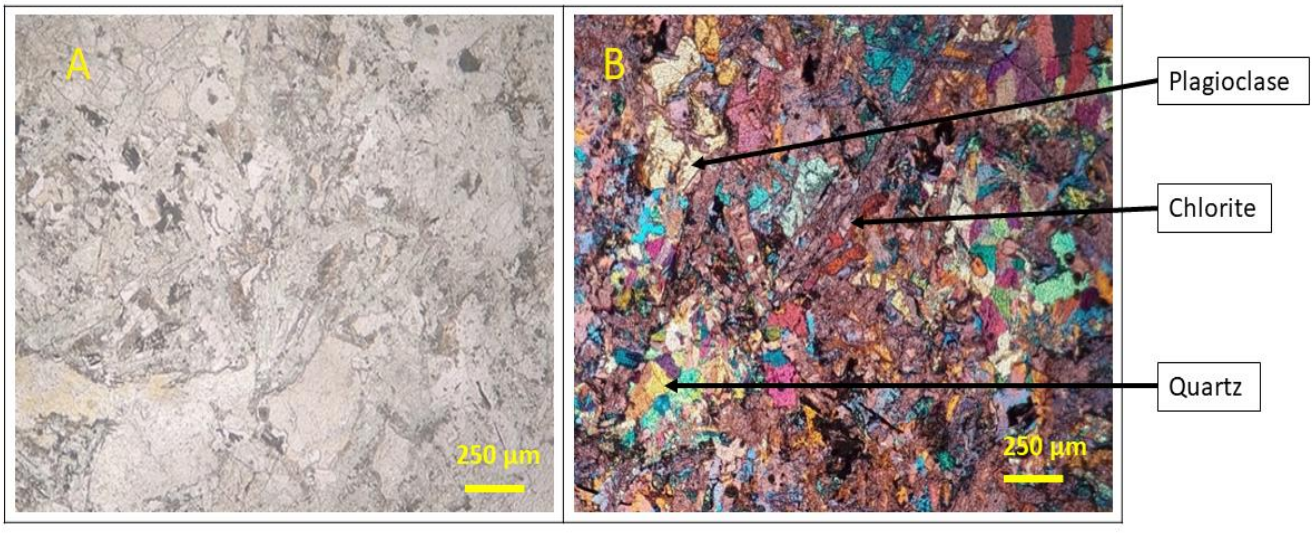

Figure 4.16: Photomicrograph of basalt captured using both plane polarised light (A) and cross-polarised light (B).

Quartz Vein

Quartz vein was intruding quartzite and basalt (Fig. 4.17). The thickness of the vein was around 20 m. The specimen was whitish, and this can be attributed to the presence of milky quartz. In thin section (Fig. 4.18), quartz vein was dominated by quartz. Quartz was colourless with low relief and no cleavage in plane-polarised light (PPL). Quartz showed low birefringence, first order white-grey interference colours, and undulatory extinction under cross-polarised light (XPL).

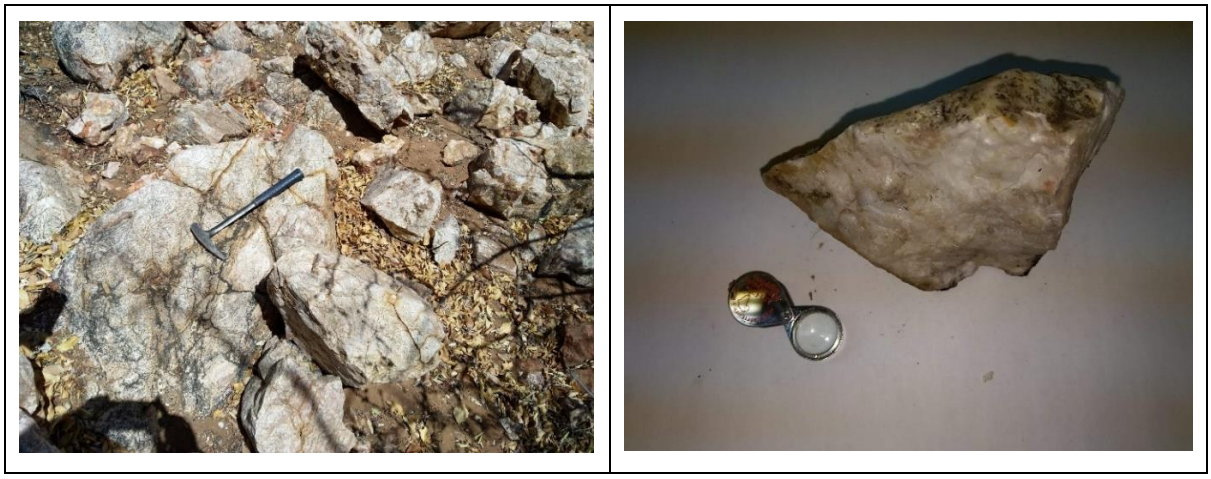

Figure 4.17: A photograph of quartz vein outcrop and hand specimen.

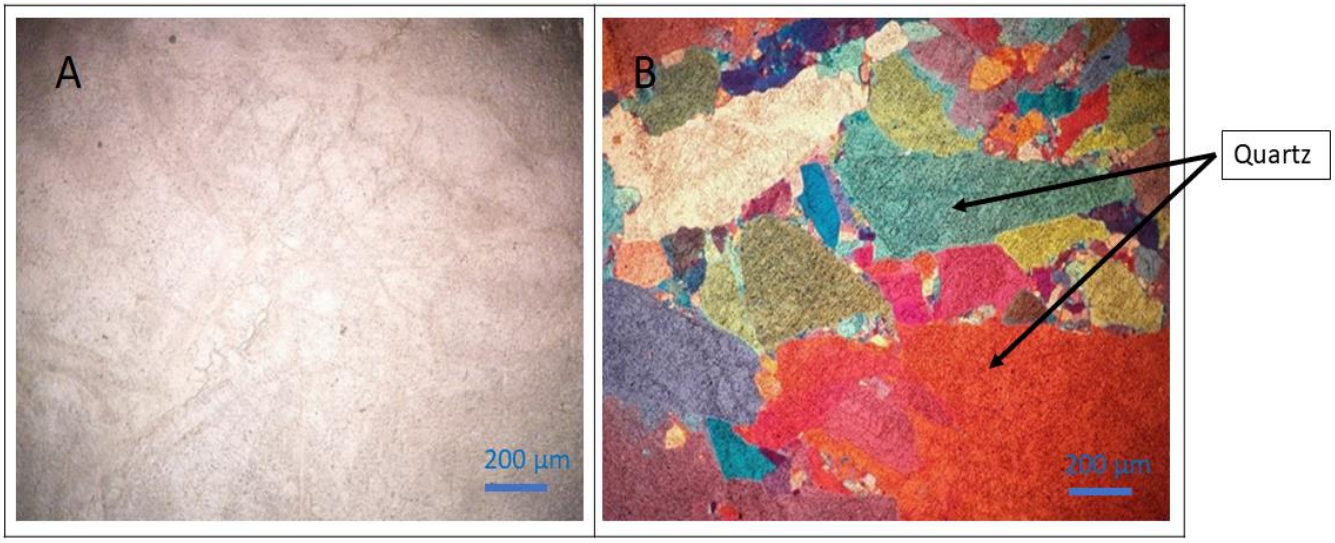

Figure 4.18: Photomicrograph of quartz vein captured using both plane polarised light (A) and cross-polarised light (B).

Sandstone

Sandstone was generally found along the north-western part of the study area and along Mbodi River (Fig. 4.19). The hand specimen was whitish and composed of sand-sized quartz grains. In thin section (Fig. 4.20), sandstone was dominated by quartz grains which were colourless with low relief and no cleavage in plane-polarised light (PPL), and low birefringence, first order white-grey interference colours, and undulatory extinction under cross-polarised light (XPL).

Figure 4.19: A photograph of sandstone outcrop and hand specimen.

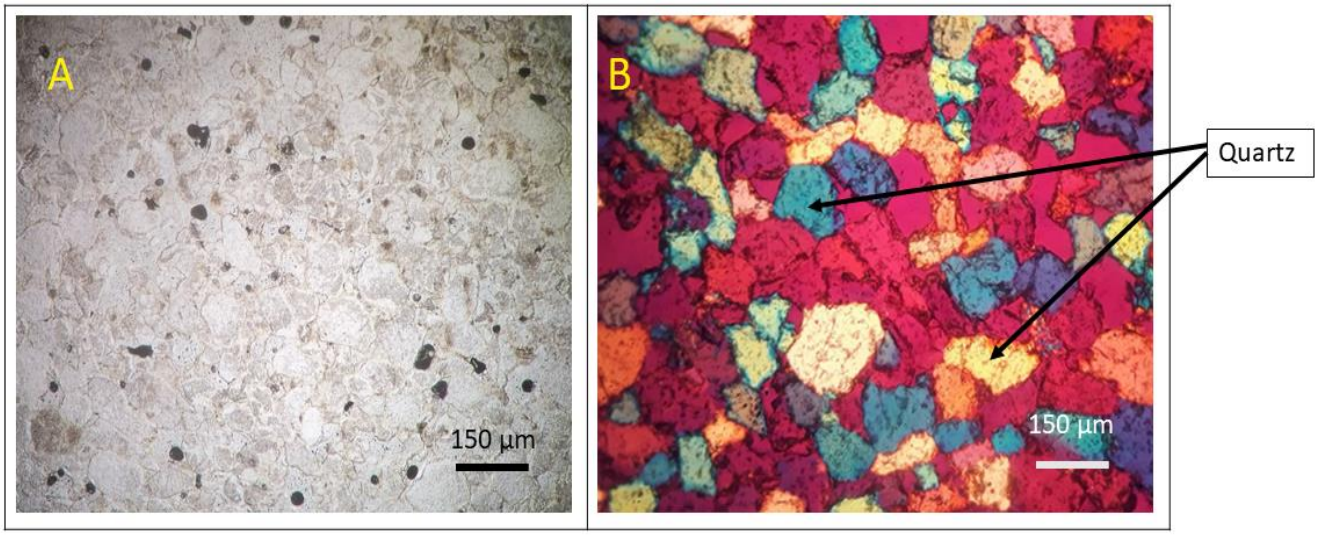

Figure 4.20: Photomicrographs of sandstone captured using both plane polarised light (A) and cross-polarised light (B).

Shale

Shale was found along Mbodi and Tshipise Rivers (Fig.4.21). The hand specimen was grey and composed mainly of clay-sized grains. The hand specimen was exhibiting the tendency to split into thin layers that are parallel to the bedding-plane surface (fissile). Shale was interbedded with carbonaceous shale and coal. In thin section (Fig. 4.22), quartz showed low relief in XPL, low birefringence and first-order white-gray interference colours, and undulatory extinction in PPL. Clay minerals exhibited a very fine texture.

Figure 4.21: A photograph of shale outcrop and hand specimen.

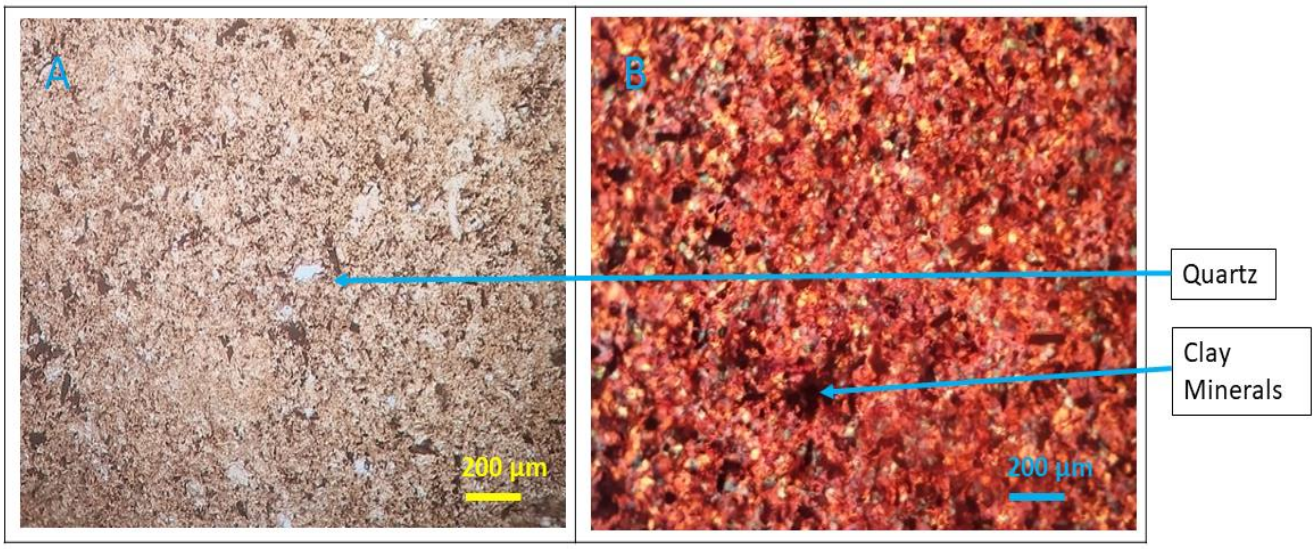

Figure 4.22: Photomicrograph of shale captured using both plane polarised light (A) and cross-polarised light (B).

Carbonaceous Shale

Carbonaceous shale was exposed along the bank of the Mbodi River and interbedded with shale and coal (Fig. 4.23). The sample was dark grey and composed of clay-sized grains. The sample was exhibiting the tendency to split into thin layers that are parallel to the bedding-plane surface (fissile). The dark grey colour of the rock indicates organic-rich composition. In thin section (Fig. 4.24), carbonaceous shale was dominated by clay minerals and minor quartz. Clay minerals exhibited a very fine texture. Quartz showed low relief in PPL, low birefringence and first-order white-grey interference colours, and undulatory extinction in XPL.

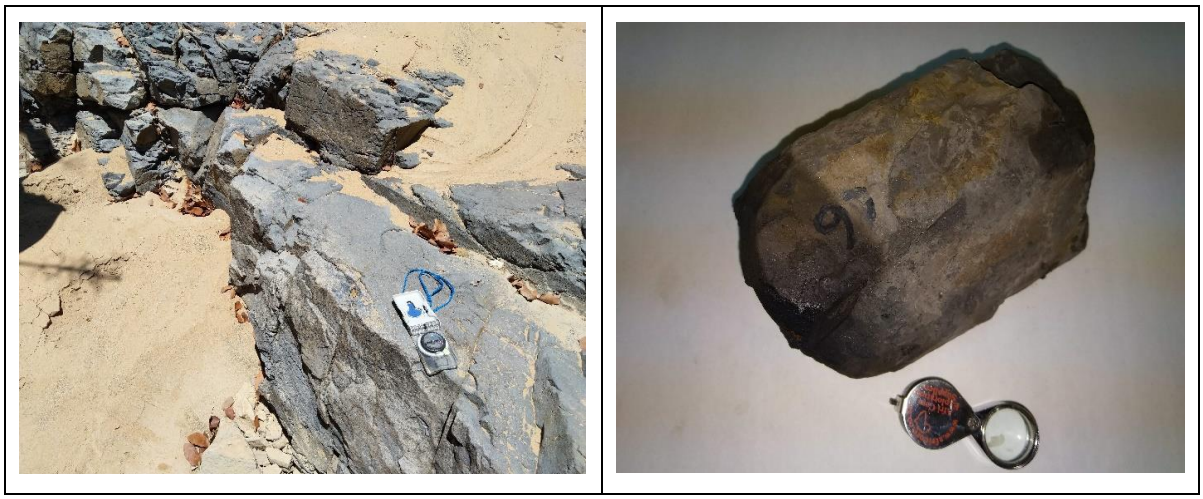

Figure 4.23: A photograph of carbonaceous shale outcrop and hand specimen.

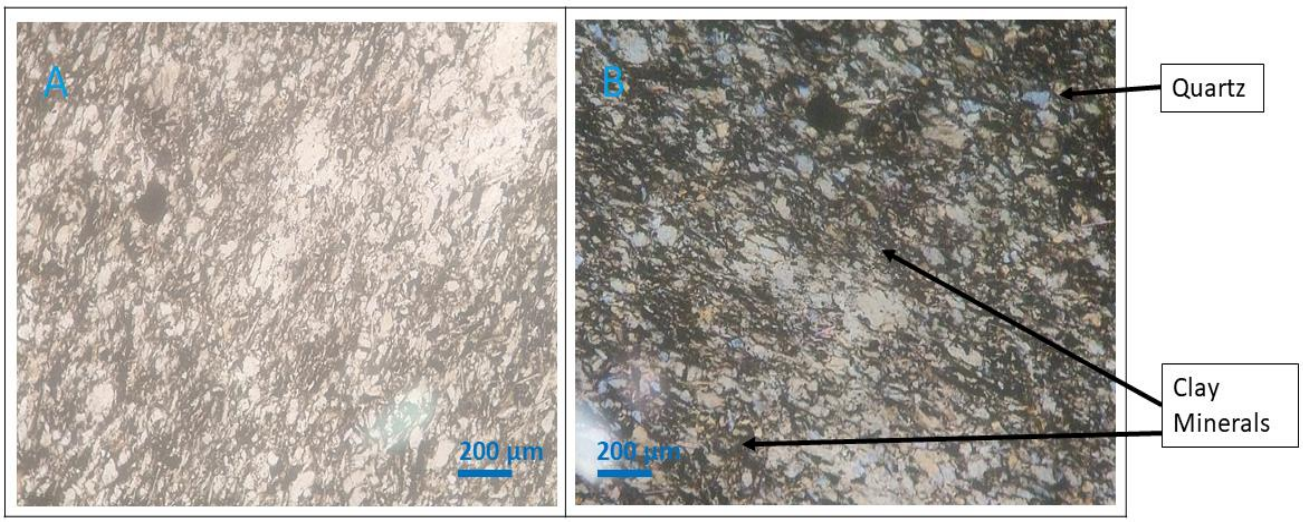

Figure 4.24: Photomicrograph of carbonaceous shale captured using both plane polarised light (A) and cross-polarised light (B).

Calcrete

Calcrete was dominant along the western part of the Mushithe area (Fig. 4.25). The hand specimen was white, and it was dominated by fine-grained cementing material cementing minor visible sand-sized mineral clasts. The hand specimen reacted with diluted hydrochloric acid indicating the presence of carbonate minerals. In the thin section (Fig. 4.26), calcrete was dominated by calcite groundmass. Some calcite grains showed lamellar twins. Calcite exhibited cleavage, extremely high birefringence in XPL and change of relief with the stage being turned in PPL. Quartz grains were colourless, low relief, had no cleavage and had low birefringence in PPL. In XPL, quartz showed first-order white-grey interference colours and undulatory extinction.

Figure 4.25: A photograph of calcrete outcrop and hand specimen.

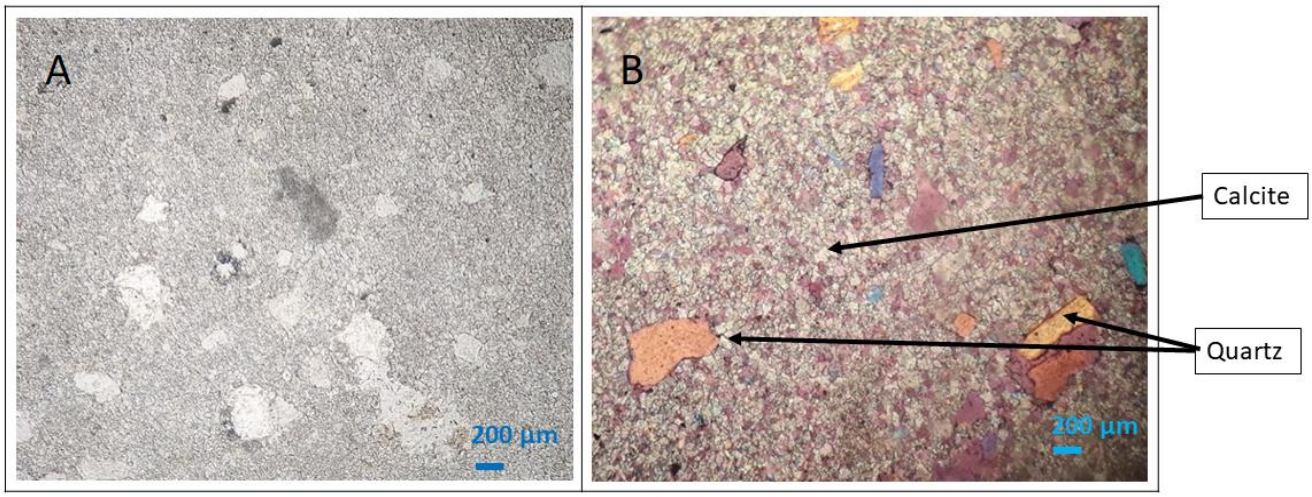

Figure 4.26: Photomicrograph of calcrete captured using both plane polarised light (A) and cross-polarised light (B).

4.2.3 Mineralogical Analysis

A total of 14 host rock samples underwent mineralogical analysis using X-Ray Diffractometry. The results are presented in Table 4.2 and the data was used to plot the mineralogical distribution histogram (Fig. 4.27).

Quartz was the most dominant mineral in quartz vein, sandstone, and quartzite, as demonstrated in Figure 4.27. The weight percentages of quartz in these samples ranged from 97% to 100%, with an average of 99.95% in quartz vein, 98.80% in sandstone, and 98.53% in quartzite. Calcrete samples were dominated by dolomite (24.50 – 91.88 wt %, average 58.19 wt %) and calcite (65.0 wt %) followed by Quartz (10.10 – 8.12 wt %). Shale samples were dominated by kaolinite (61.40 – 63.58 wt %; average 62.49 wt %) followed by amorphous materials noted in Shale 2 sample indicating the presence of organic matter in shale. Basalt samples were dominated by plagioclase (32.40 – 36.62 wt %; average 35.51 wt %), chlorite (23.30 – 28.64 wt %; average 25.97 wt %) and quartz (12.70 – 16.44 wt %; average 14.57 wt %). Mudstone samples were dominated by quartz (42.20 – 2.78 wt %; average 37.49 wt %), plagioclase (21.90 – 19.17 wt %; average 20.54 wt %) and muscovite (22.70 – 25.47 wt %; average 24.09 wt %). The reddish colour in Mudstone samples can be attributed to the presence of hematite (3.6 – 6.76 wt %; average 5.18 wt %).

Table 4.2: Results showing the distribution of minerals in rocks samples.

	Amorphous	Anatase	Augite	Calcite	Chlorite	Dolomite	Epidote	Hematite	Kaolinite	Magnetite	Microcline	Muscovite	Orthoclase	Plagioclase	Quartz	Sepiolite
Mudstone 1	0	0	0	1.30	8,30	0	0	3.60	0	0	0	22.70	0	21,90	42.20	0
Mudstone 2	0	6.34	0	0	9,48	0	0	6.76	0	0	0	25.47	0	19,17	32.78	
Basalt 1	0	0	12.20	0	23,3	0	16.40	0	0	0	0	0.90	0	32,40	14.80	0
Basalt 2	0	0	2.78	9.56	28,64	0	0	0	0	2.53	3,43	0	0	36,62	16.44	0
Quartz Vein 1	0	0	0	0	0	0.10	0	0	0	0	0	0	0		99.90	0
Quartz Vein 2	0	0	0	0	0	0	0	0	0	0	0	0	0	00	100.0	0
Shale	0	0.70	0	0	0	0	0	0	61.4	0	0	8.10	0	0	29.90	0
Carbonaceous Shale	33.0	0	0	0	0	0	0	0	63.58	0	0	0	0	0	3.42	0
Sandstone 1	0	0	0	0	0	0.10	0	0	0.50	0	0	0	0.60	0	98.80	0
Sandstone 2	0	0	0	0	0	0	0	0	1.21	0	0	0	0	0	98.79	0
Calcrete 1	0	0	0	65.0	0	24.50	0	0	0	0	0	0	0	0	10.10	0.40
Calcrete 2	0	0	0	0	0	91.88	0	0	0	0	0	0	0	0	8.12	0
Red Quartzite	0	0	0	0	0	0	0	0	0	0.36	0	2.29	0	0	97.35	0
Pink Quartzite	0	0	0	0	**0**	0	0	0.10	0.20	0	0	0	0	0	99.70	0

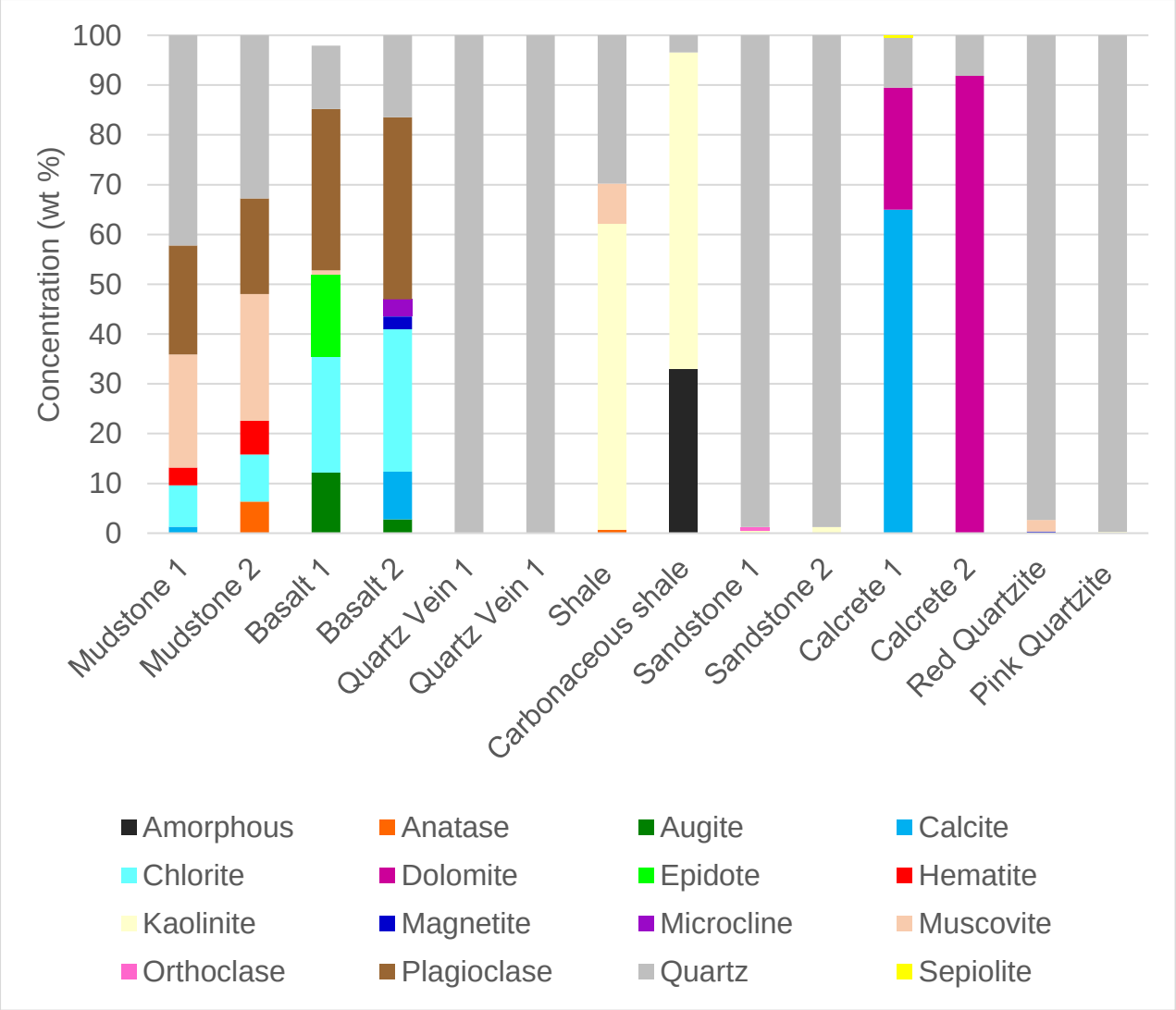

Figure 4.27: graph showing the composition of minerals in rock samples.

4.2.4 Rock Geochemistry

X-ray fluorescence spectrometry was used to analyse the geochemistry of 14 rock samples, examining both major oxides and trace elements. The results are presented in Appendix B. The results from the study were normalised against the upper crustal composition values from Taylor and McLennan (1985) using the following formula:

$$Enrichment = \frac{Value\ from\ the\ Study}{Value\ from\ UCC} \quad \text{.....(Equation 5)}$$

Where: a value greater than 1 indicates enrichment and a value less than 1 indicates depletion.

Major Oxides

Figure 4.28 depicts the concentration levels and distribution of major oxides in rock samples, as determined through X-ray fluorescence spectrometry analysis.

According to the findings, SiO_2 is the most prominent oxide, comprising 68.31 wt % on average and ranging from 16.46 wt % to 99.05 wt % in concentration. Quartz vein samples demonstrated the highest levels of SiO_2, reaching 99.02% and 99.05%, whereas calcrete samples had the lowest levels, reaching only 16.46% and 17.85%. CaO was the second dominant oxide with an average concentration of 10.01 wt %. The highest concentrations of CaO were found in calcrete samples (46.30 wt % and 64.91 wt %). The third most dominant oxide was Al_2O_3 with an average concentration of 8.54 wt %. The highest concentrations of Al_2O_3 were found in shale followed by mudstone and basalts. No concentration of Al_2O_3 was recorded in Quartz vein and calcrete samples. Fe_2O_3 had an average concentration of 4.90 wt % ranging from 0.42 wt % to 15.24 wt %.

Basalt samples showed the highest concentration of Fe_2O_3 followed by shale and mudstone samples. MgO recorded an average concentration of 3,3 wt %. Calcrete and mudstone samples recorded the highest concentration of MgO while no MgO was recorded in quartz vein samples. Other major oxides include Na_2O, K_2O, TiO_2, P_2O_5, and MnO. The average concentration of Na_2O was 2.46 wt %. The highest concentration of Na_2O was noted in Calcrete samples (12.61 wt % and 12.50 wt %). Na_2O was not recorded in quartz vein and sandstone samples. The concentration of K_2O varied from 0.04 wt % to 5.25 wt % with an average of 1.30 wt %. The highest concentration of K_2O was noted in mudstone and shale samples. The average concentrations of TiO_2 and P_2O_5 were 0.58 wt % and 0.20 wt % respectively. MnO was the least dominant oxide with an average of 0.09 wt %.

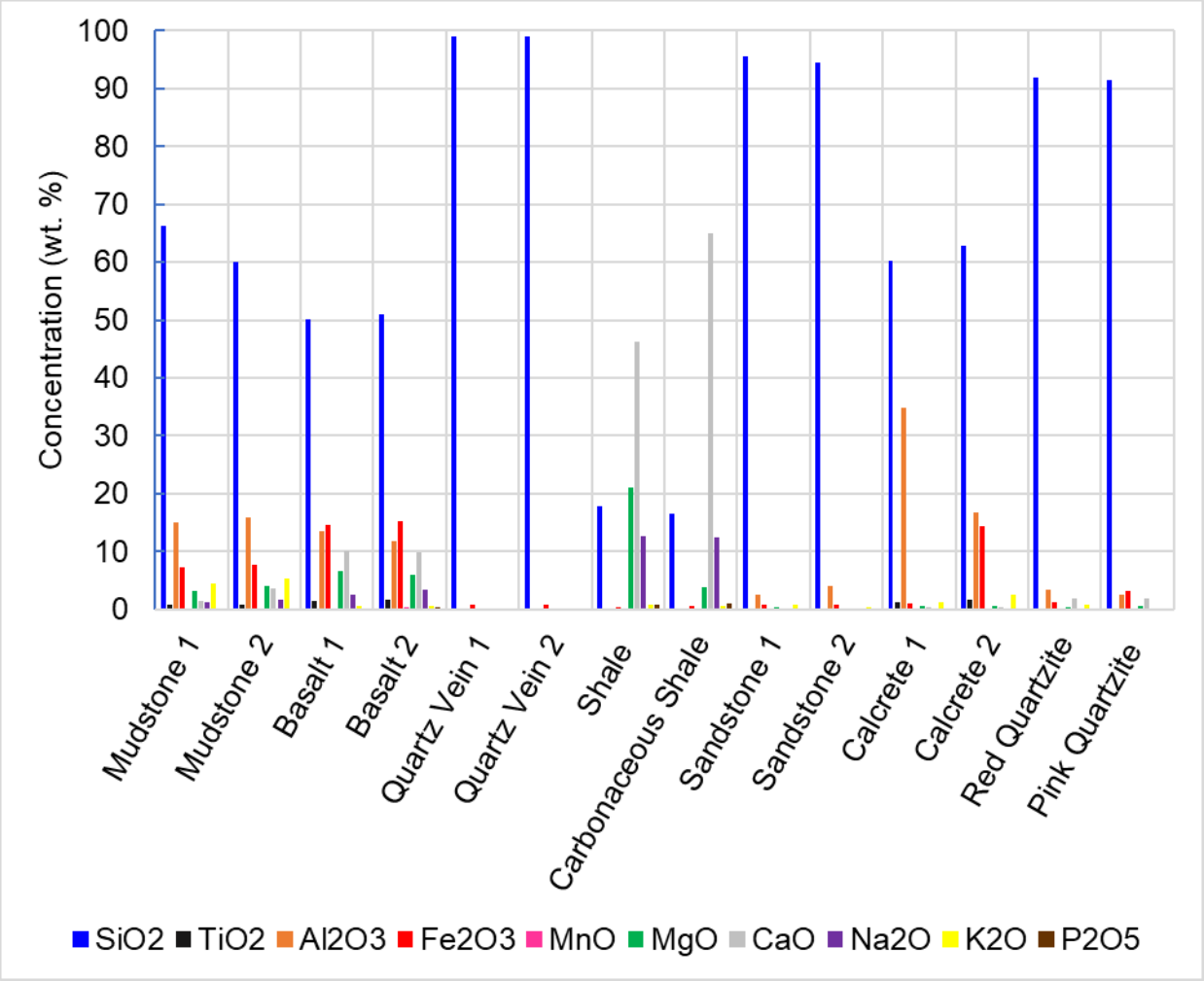

Figure 4.28: Major oxides associated with host rocks.

Within the selected representative samples, quartz vein, sandstone, and quartzite samples were enriched in SiO_2 (Fig. 4.29). The enrichment of SiO_2 in these rocks indicates the dominance of quartz and silicate minerals. Shale, Basalt samples were enriched in TiO_2. Shale samples were enriched in Al_2O_3. The enrichment of aluminium oxide in shale indicates the prominence of clay minerals. Mudstone and basalt were enriched in Fe_2O_3. The enrichment of Fe_2O_3 can be attributed to the reddish colour of the mudstone samples indicating the presence of a hematite cementing agent. MnO was enriched in mudstone, basalt, and quartzite samples. Calcrete and basalt samples were enriched in CaO and MgO indicating the dominance of calcite and dolomite minerals in calcrete and ferromagnesian minerals in basalts. Calcrete samples were enriched in Na_2O.

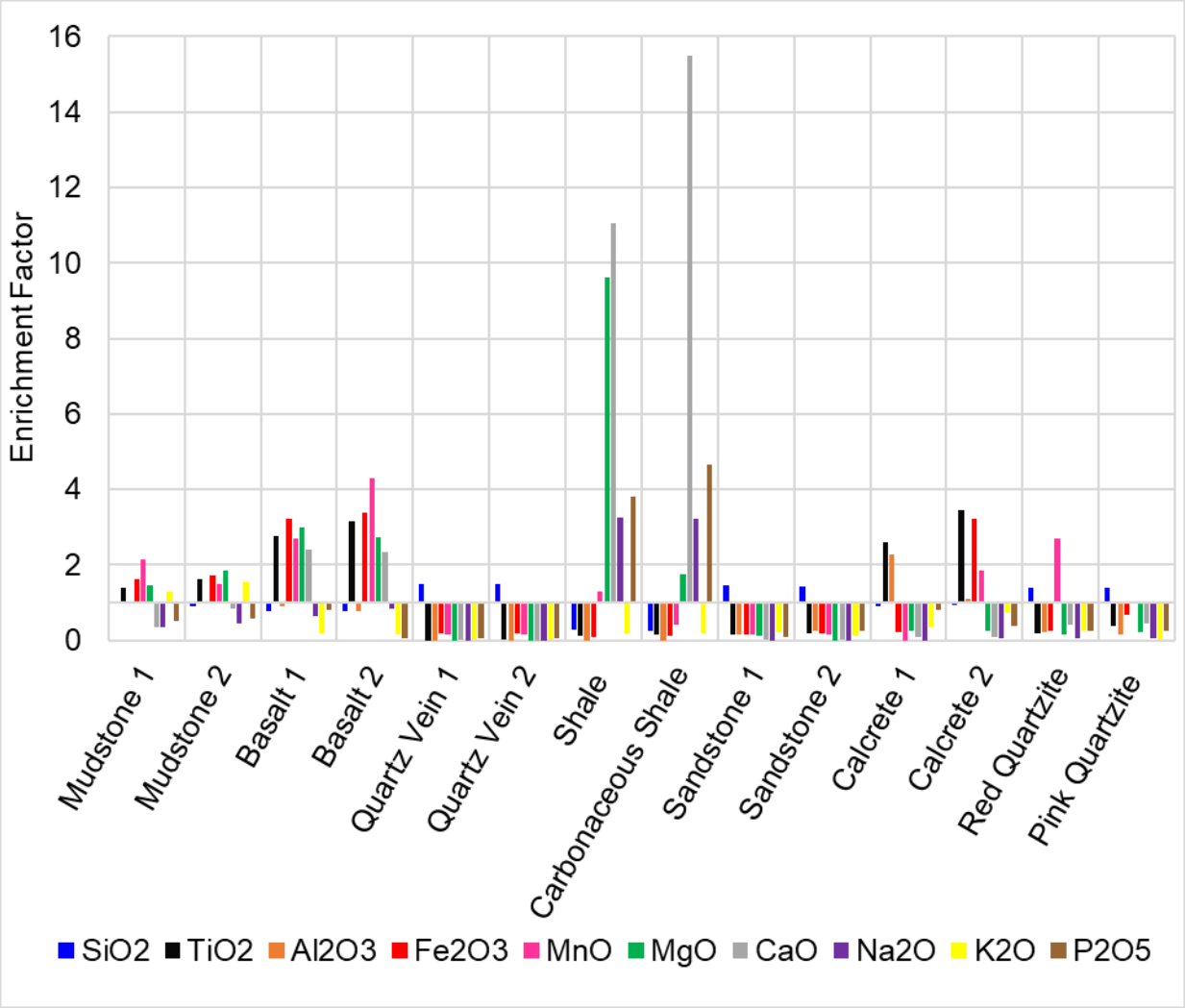

Figure 4.29: Enrichment of major oxides normalised against the upper crustal composition.

Trace Elements

The proportions of trace elements associated with host rocks, derived from X-ray fluorescence spectrometry, are presented in Appendix B. Trace elements were grouped into Large Ion Lithophile Elements, High Field Strength Elements, and Transition Elements. The results from the study were normalised against the upper crustal composition values from Taylor and McLennan (1985).

Large Ion Lithophile Elements

This group includes elements such as Rb, Ba, Sr, Th and U (Fig 4.30 and Fig 4.31). Ba was the generally most abundant element within all rock types with concentrations ranging from 60.00 ppm to 1338.40 ppm with an average concentration of 486.56 ppm.

Barium was enriched in mudstone, basalt, and shale samples. Sr was the second most abundant Large Ion Lithophile Element. The concentration of strontium ranges from 4.40 ppm to 507.00 ppm with an average concentration of 155.04 ppm.

The concentration of Rb ranges from 1.60 ppm to 126.60 ppm with an average concentration of 38.01 ppm. The concentration of Rubidium was depleted in all rocks except in mudstone. Th had an average concentration of 15.16 ppm ranging from 1.1 ppm to 70.3 ppm. Basalt and shale samples were enriched in thorium. Compared to other Large Ion Lithophile Elements, the concentration of U was generally low within all rock types. Compared with the uranium UCC concentration of 2.8 ppm, the average concentration of uranium was 1.51 ppm. All rocks except shale were depleted in uranium.

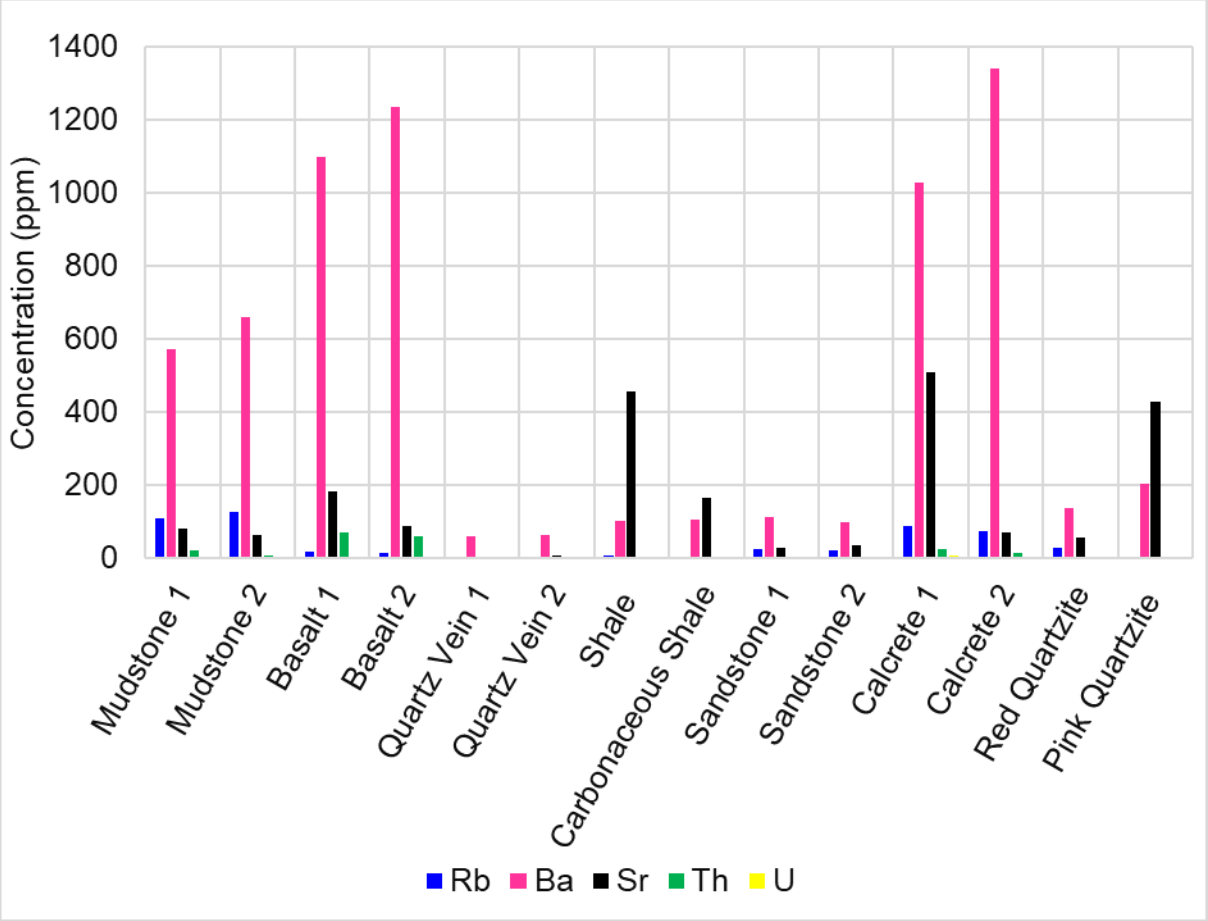

Figure 4.30: Concentration of Large Ion Lithophile elements associated with host rock samples.

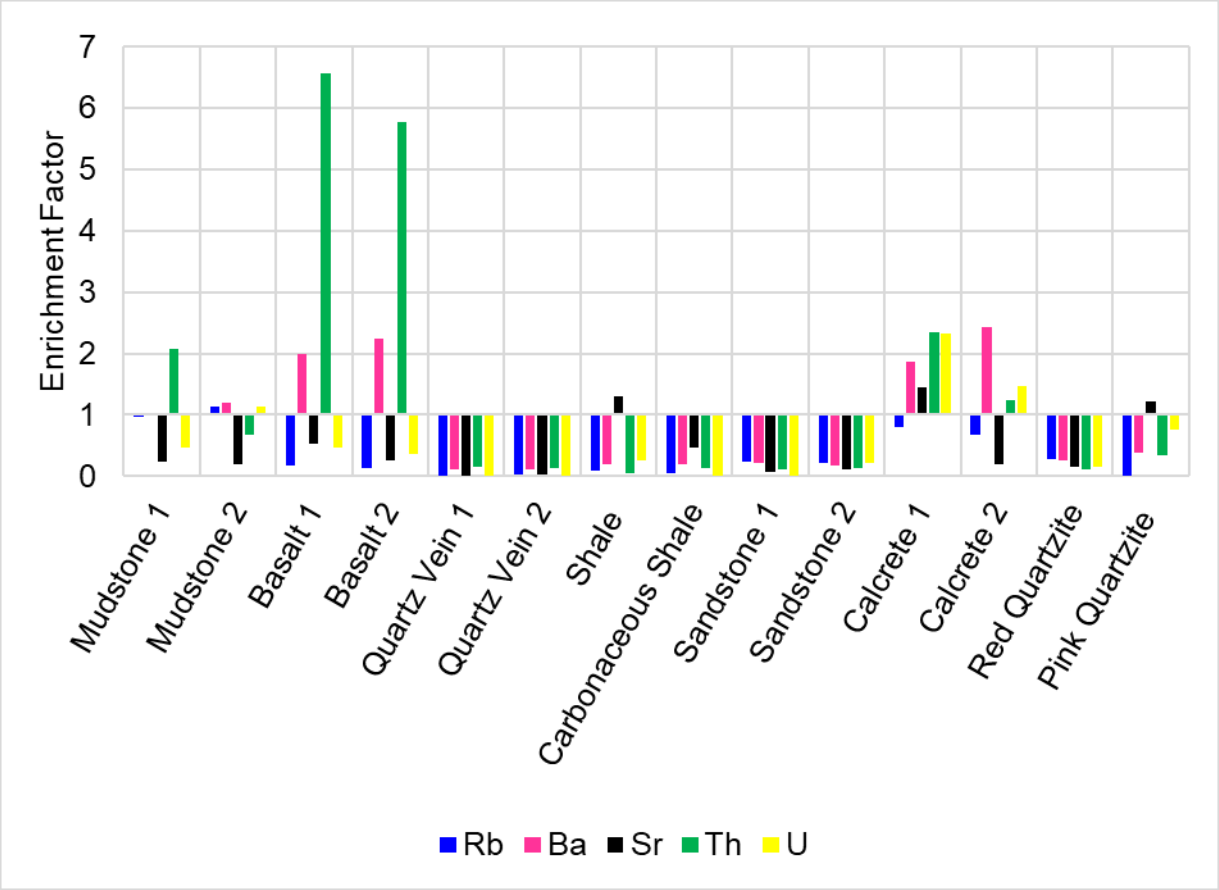

Figure 4.31: Enrichment of Large Ion Lithophile elements normalised against the upper crustal composition.

High Field Strength Elements

This group includes elements such as Y, Zr, Nb and Hf (Fig 4.32 and Fig 4.33). Rock samples showed variation in High Field Strength elements concentrations, and the general trends of average high field strength elements concentrations were Zr > Y > Hf > Nb. The concentration of Zr ranges from 0.5 ppm to 558 ppm with the lowest concentration noted in quartz veins and the highest noted in shale and mudstone samples. The average concentration of Zr was 153.53 ppm compared to 190 ppm from UCC. All rocks were depleted in zirconium except in shale samples. Y concentration ranges from 0.6 ppm to 55.50 ppm with an average of 17.91 ppm compared to 22 ppm from UCC. The highest concentration of yttrium was noted in shale and mudstone samples while the lowest was noted in quartz vein samples. Yttrium was only enriched in shale and mudstone. The average concentration Hf is 10.23 ppm compared to 5.8 ppm from UCC. Hf was only enriched in shale samples. The average concentration of

Nb was ppm 6.31 ppm compared to 12 ppm from UCC. Nb was enriched in mudstone, basalt, and quartz vein.

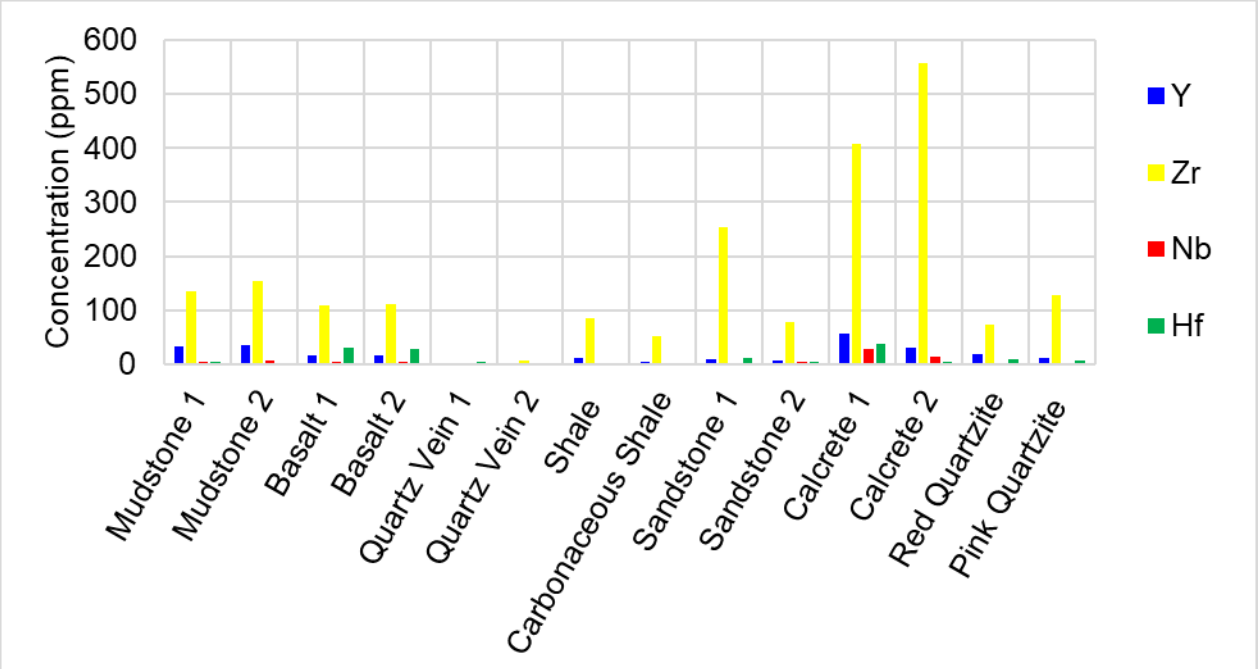

Figure 4.32: Concentration of High Field Strength elements associated with host rock samples.

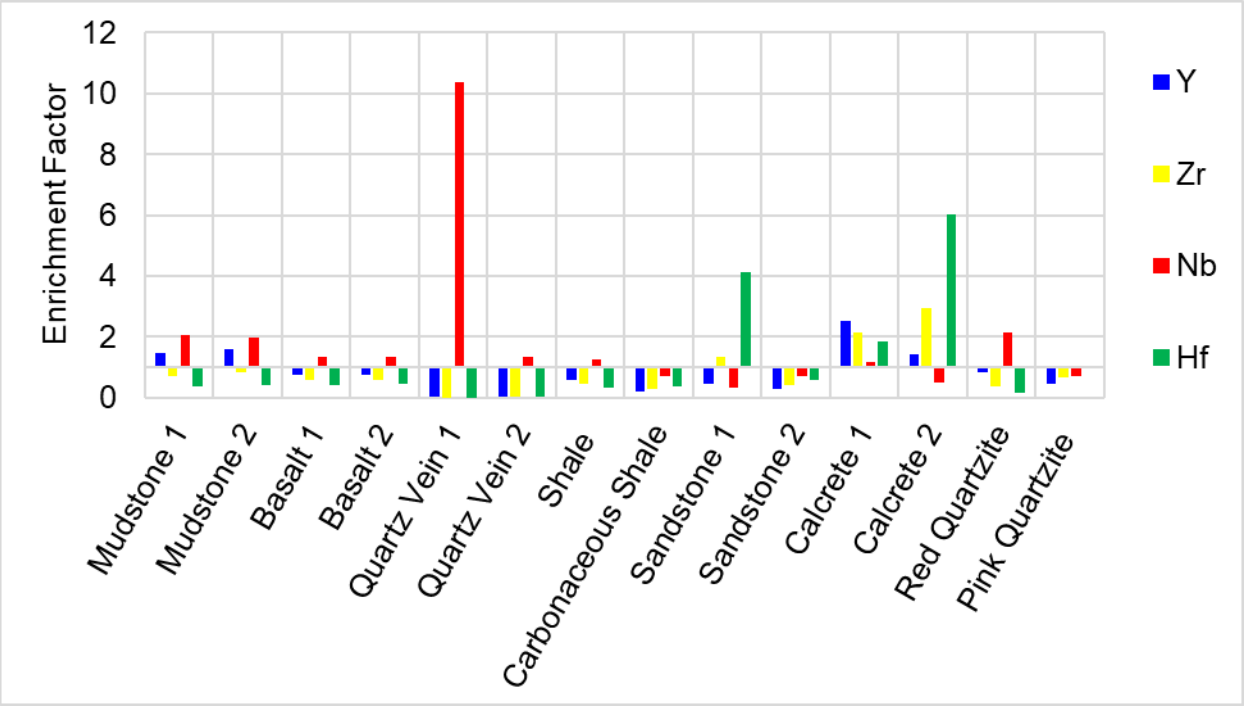

Figure 4.33: Enrichment of High Field Strength elements normalised against the upper crustal composition.

Transition Trace Elements

This group includes elements such as V, Co, Cu, Ni and Sc (Fig 4.34 and Fig 4.35). V was the most dominant with N being the second most dominant. Co and Sc were the least dominant. V had an average concentration of 134.52 ppm. V was enriched in basalt, Shale, and Mudstone. Ni had an average concentration of 134.52 ppm compared to 44 ppm from UCC. Ni was enriched in mudstone and basalt.

The concentration of copper ranged from 0 ppm to 274.4 ppm with an average concentration of 64.47 ppm compared to 25 ppm. The highest concentration of copper was noted in basalt and shale samples. Cu was enriched in basalt, shale, and quartzite samples. Co was the 3rd most dominant Transition Trace element with an average concentration of 12.15 ppm and a range of 1.0 – 37.40 ppm. Compared to the cobalt UCC concentration of 17.0 ppm, all rocks are depleted in Co except basalt and mudstone. The concentration of Sc was generally low in all rock types. The average concentration of Scandium was 0.91 ppm compared to 13.6 ppm from UCC. Sc was enriched in quartzite, quartz vein and sandstone samples.

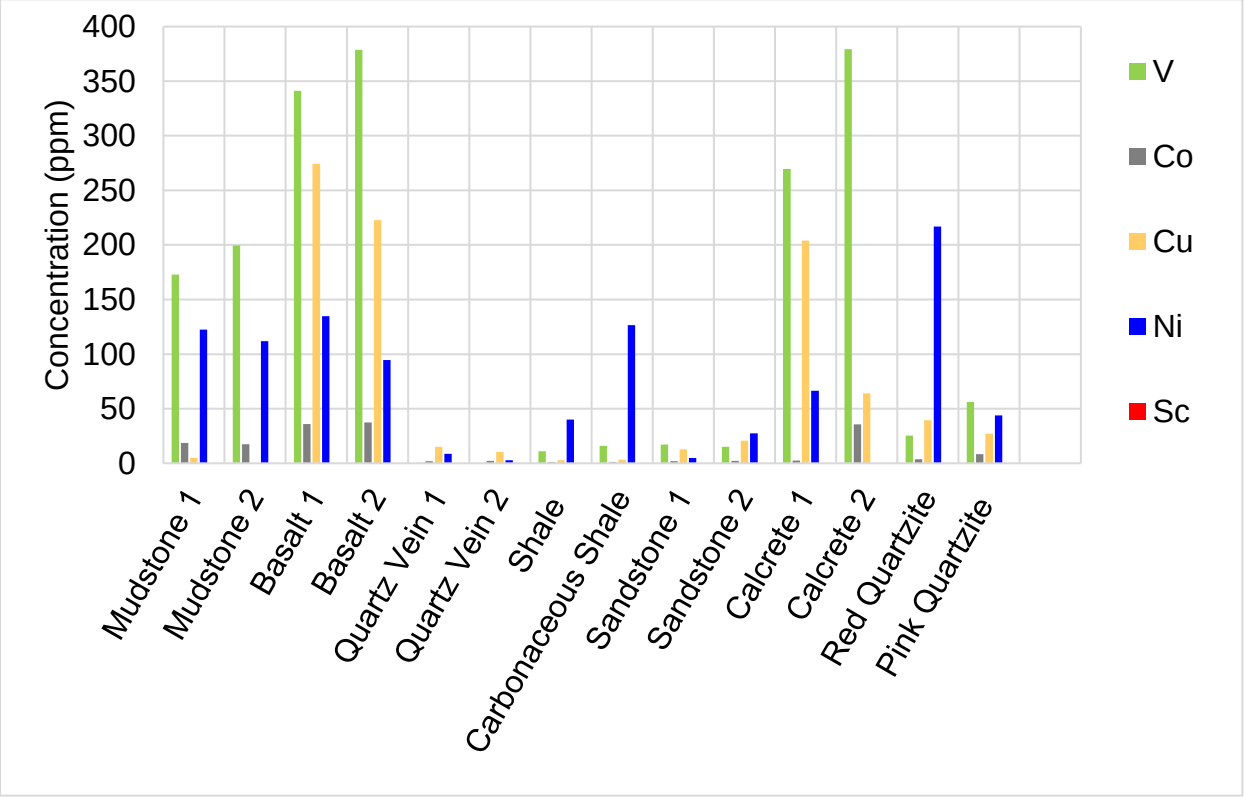

Figure 4.34: Bar graph showing concentration of Transition trace elements associated with host rock samples.

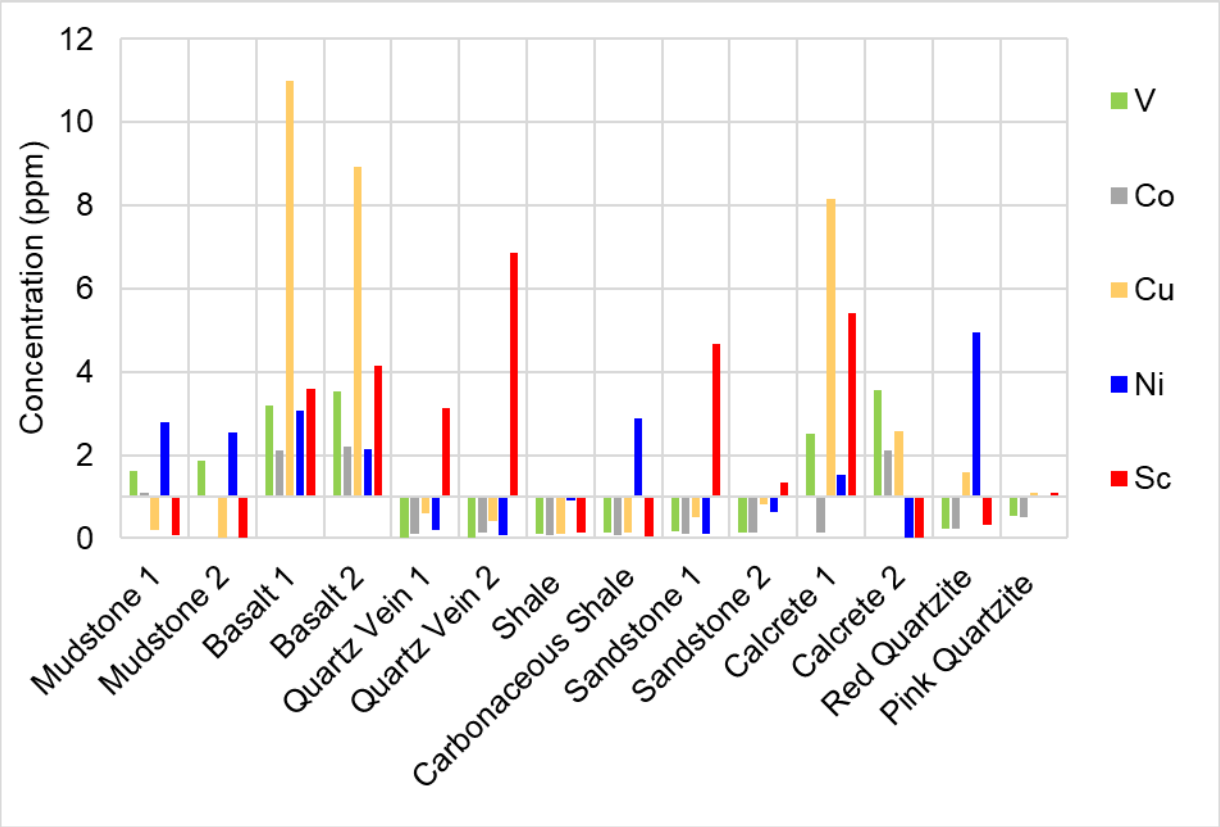

Figure 4.35: Enrichment of Transition trace elements normalised against the upper crustal composition.

4.3 Coal Quality

The data presented in this section included proximate analysis, calorific value, ultimate analysis, and coal geochemistry.

4.3.1 Proximate Analysis

The percentage of moisture, ash, volatile matter and fixed carbon are presented in Table 4.3 and the results were graphically presented in Figure 4.36. Moisture was expressed on an air-dry basis (ad), ash yield, volatile matter, and fixed carbon on a dry basis (db).

The moisture content of the analysed coal samples ranged between 6.07 wt % and 10.94 wt % with an average of 8.73 wt %. The average moisture content of Ply A (10.03 wt %) was higher than Ply B (7.43 wt %). A trend was noted between sampling depth and moisture content, where moisture content decreases with sampling depth (Fig. 4.37). Ash yield ranged between 16.7 wt %.and 41.9 wt % with an average of 25.2 wt %. The average ash yield of Ply A (30 wt %) was higher than Ply B (20.4 wt

%). Based on ash yield, exposed coal at Mushithe can be classified as low-grade according to UNECE (1998).

Volatile matter ranged between 29.7 wt % and 35.8 wt % with an average of 32.33 wt %. The average volatile matter of Ply A (33.13 wt %) was higher than Ply B (31.53 wt %). High volatile matter can be related to the (anticipated) high vitrinite macerals in petrography (Section 4.4). The volatile content of coal at Mushithe is higher than coal in the Tshikondeni area which is about 25 wt % (Hancox and Götz, 2014). The fixed carbon varied between 25.25 wt % and 50.49 wt % with an average of 42.48 wt %. The average fixed carbon of Ply B (48.06 wt %) was higher than Ply A (36.90 wt %).

Table 4.3: Proximate analysis of the exposed coal seam at the Mushithe area.

Ply	ID	Moisture (ad)	Ash (db)	Volatile Matter (db)	Fixed Carbon (db)
	A1	10.94	21.30	35.80	42.89
	A2	10.79	26.80	34.70	38.56
	A3	8.37	41.90	28.90	29.25
A	Average	10.03	30.00	33.13	36.90
	B1	8.29	16.70	32.70	50.49
	B2	7.94	19.20	32.20	48.66
	B3	6.07	25.30	29.70	45.03
B	Average	7.43	20.40	31.53	48.06
Average		8.73	25.20	32.33	42.48

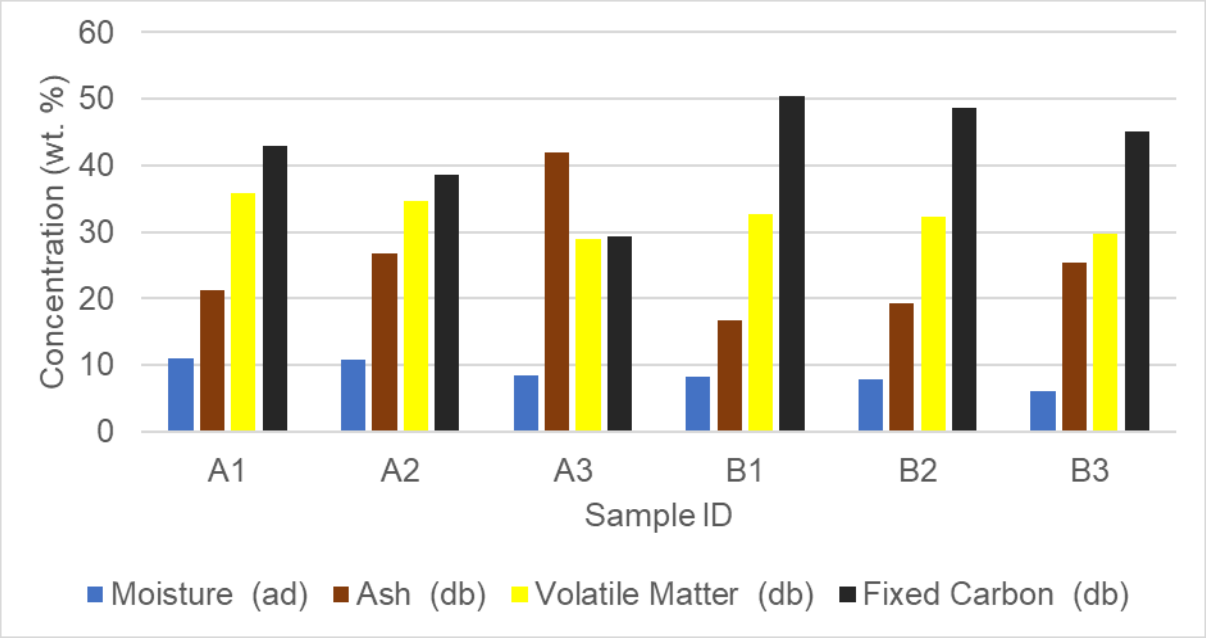

Figure 4.36: Graph showing proximate analysis results of the exposed coal seam at the Mushithe area.

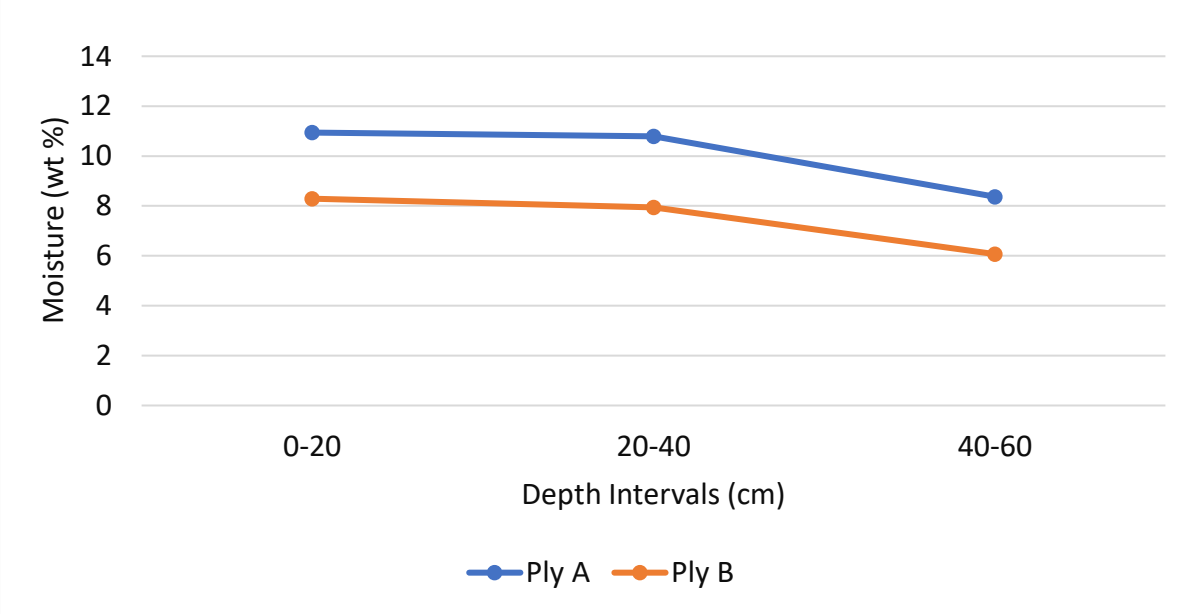

Figure 4.37: Relationship between sampling depth and inherent moisture.

4.3.2 Calorific Value

Table 4.4 displays the results for the calorific value, while Figure 4.36 illustrates the results graphically. Calorific values of coal within the Mushithe coal occurrence range from 12.97 MJ/kg to 23.35 MJ/kg with an average of 19.52 MJ/kg. The average calorific value for Ply A (16.55 MJ/kg) was lower compared to Ply B (22.49 16.55 MJ/kg), this can be attributed

to higher moisture, ash yield and lower fixed carbon within Ply A. Mushithe coals have relatively higher average calorific value compared to coal from Vele (17.53 MJ/kg), Makhado (18,17 MJ/kg) and relatively lower compared to Tshikondeni colliery (28.24 MJ/kg) (Mphaphuli, 2017). According to Steyn and Minnitt (2010), the coal found in Mushithe is categorised as lower than grade D. According to ASTM 388, Coal at Mushithe can be ranked as Sub-Bituminous C coal.

It was observed that there is a correlation between ash yield and the calorific value of coal, where the ash yield increases as the calorific value decreases (Fig. 4.39). Additionally, a connection was found between the amount of fixed carbon present and the calorific value, where the energy value increases as the amount of fixed carbon increases (Fig. 4.40).

Table 4.4: Heat energy of the studied samples

Ply	**Sample ID**	**Calorific Value** (MJ/kg)
A	**A1**	19.40
	A2	17.27
	A3	12.97
	Average	16.55
B	**B1**	23.35
	B2	22.62
	B3	21.49
	Average	22.49
Average		19.52

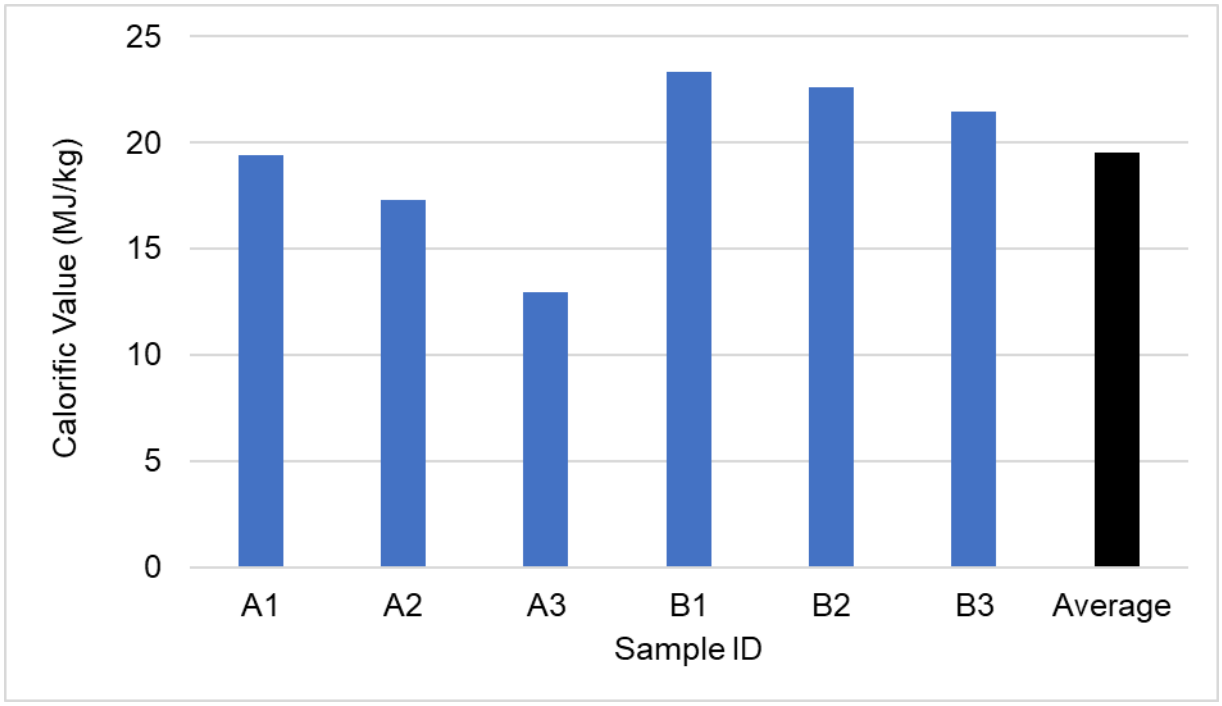

Figure 4.38: Graphical representation of calorific value results of the exposed coal seam at the Mushithe area.

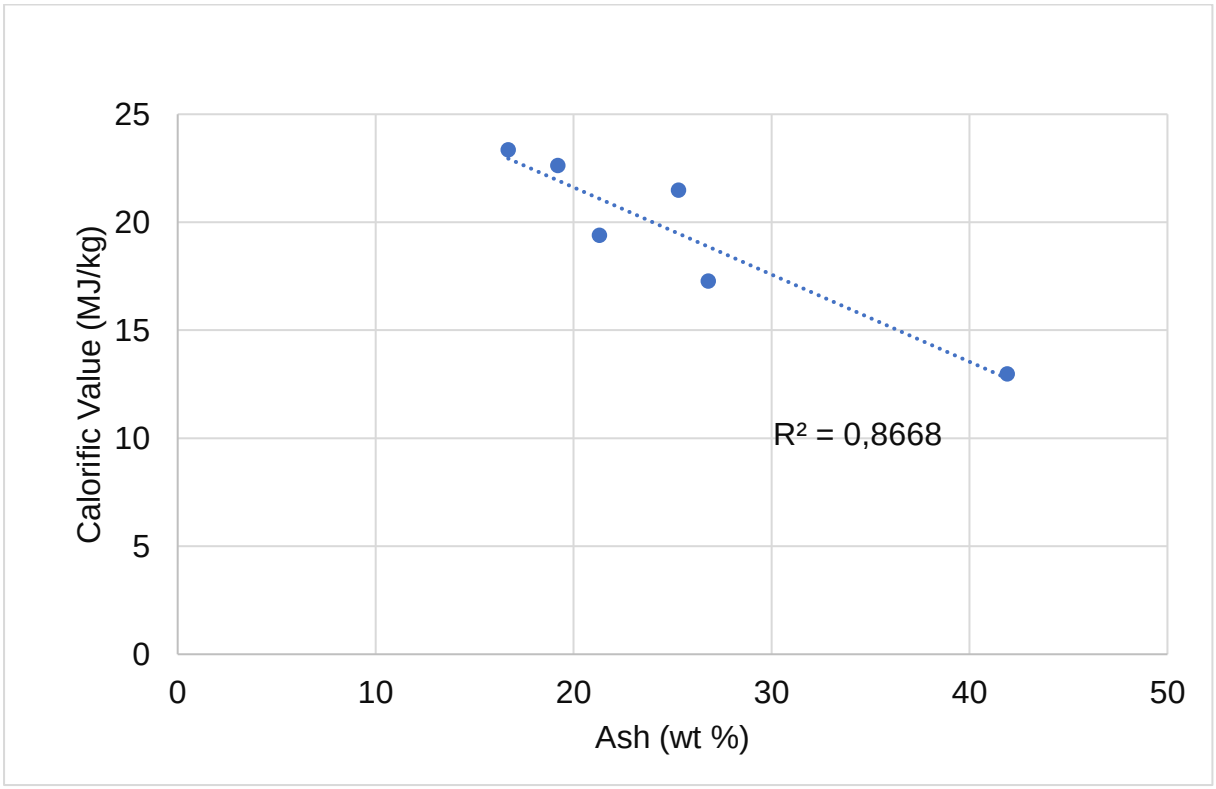

Figure 4.39: Relationship between ash yield and calorific value.

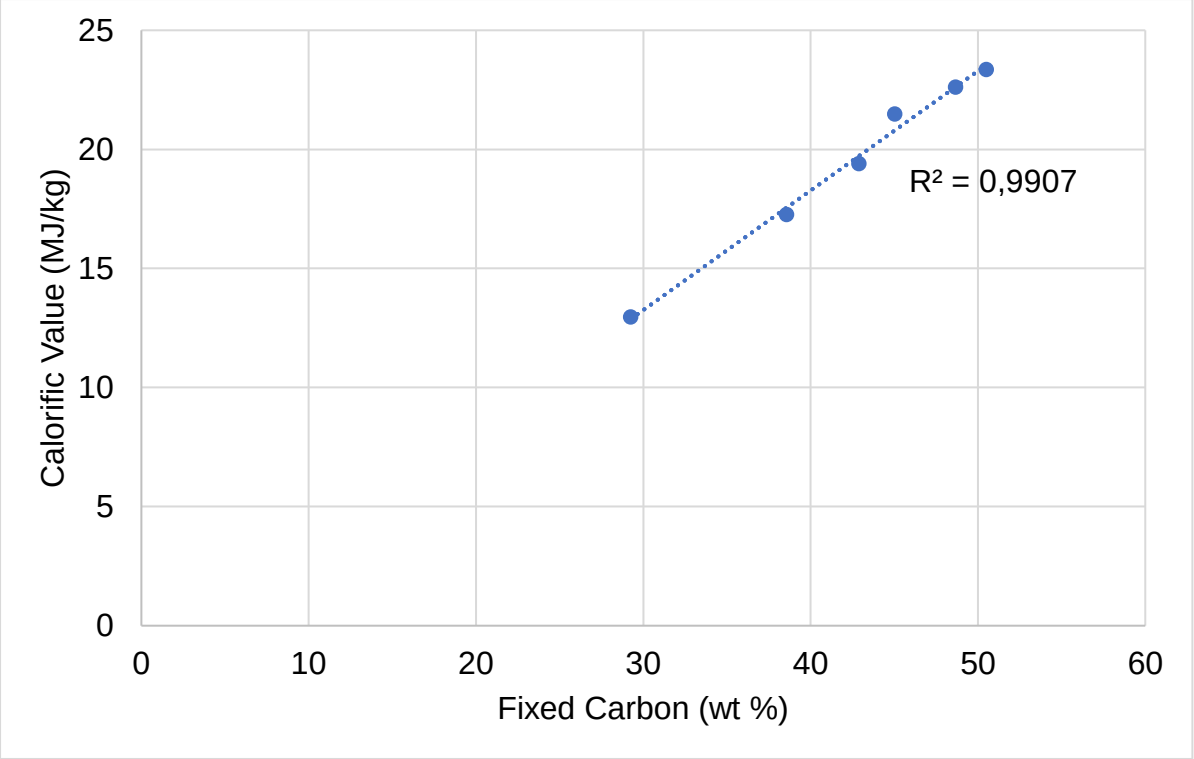

Figure 4.40: Relationship between fixed carbon and calorific value.

4.3.3 Ultimate Analysis

The ultimate analysis results for the exposed coal seam at the Mushithe area are presented in Table 4.5 and graphically presented in Figure 4.41.

The carbon content in the collected coal samples from the study area varies from 25.26 wt % to 50.73 wt % with an average of 41.37 wt %. High concentrations of carbon are normally characteristic of vitrinite macerals. The oxygen content in the samples varies from 20.83 wt % to 24.64 wt % with an average of 23.08 wt %. The high concentration of oxygen is in accordance with higher moisture content. The hydrogen content was found to range between 2.22 wt % and 2.55 wt % with an average of 2.38 wt %. A low concentration of hydrogen can be related to the (anticipated) low liptinite macerals in petrography (Section 4.4). The coal's sulphur content ranges from 0.23 wt % to 0.38 wt %, with an average of 0.30 wt %. Based on Chou (2012) classification, this indicates that the coal is of the low sulphur type, which typically contains sulphur levels of ≤1 wt %. Medium sulphur coal contains sulphur levels of ≥1 wt % to ≤3 wt %, while high sulphur coal contains sulphur levels of ≥3 wt %. It is worth noting that most of the sulphur present in low-sulphur coal is derived from the sulphur content of the original plant material that was incorporated during peat accumulation.

Table 4.5: Ultimate analysis results (wt %) for the exposed coal seam at the Mushithe area

Ply	ID	C	H	N	S	O
A	A1	41.72	2.22	1,27	0,34	24,6
	A2	36,96	2,27	1,16	0,28	24,64
	A3	25,26	2,28	0,85	0,23	24,61
	Average	34,65	2,26	1,09	0,28	24,61
B	B1	50,73	2,55	1,26	0,3	21,47
	B2	48,02	2,47	1,32	0,3	22,35
	B3	45,52	2,48	1,02	0,38	20,83
	Average	48,09	2,5	1,2	0,33	21,55
Average		41,37	2,38	1,15	0,3	23,08

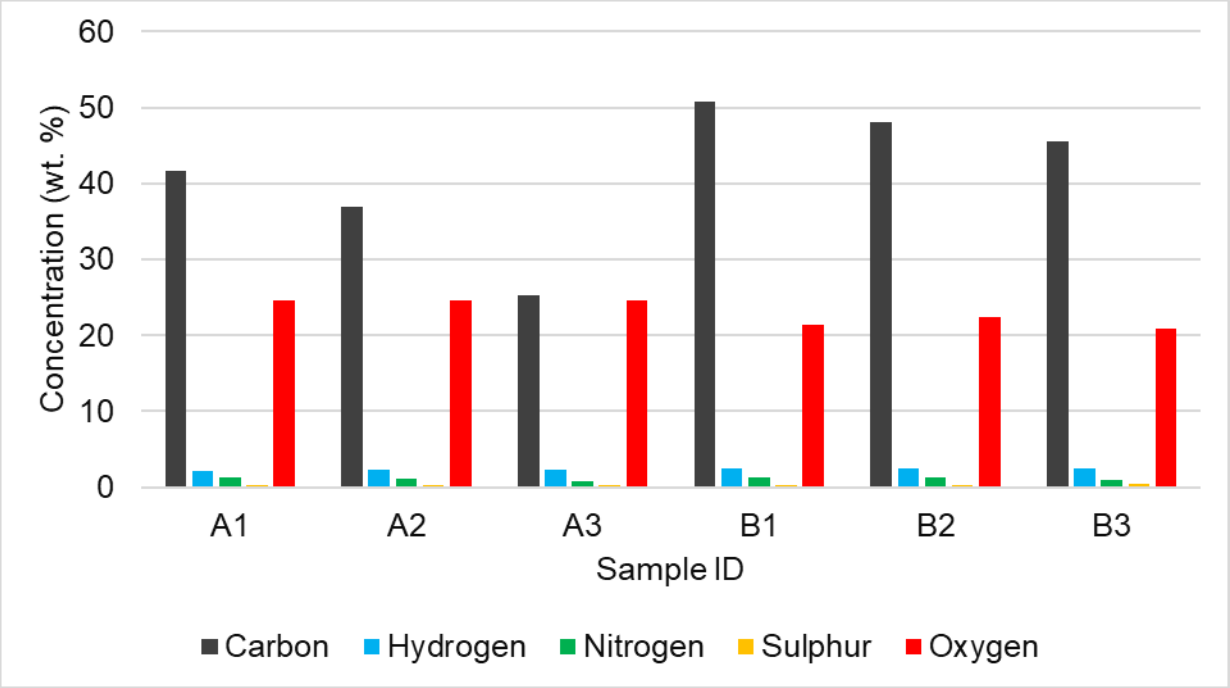

Figure 4.41: Graphical representation of ultimate analysis results of the exposed coal seam at the Mushithe area.

4.4 Coal Petrography

The data presented in this section include maceral composition and reflectance analysis.

4.4.1 Maceral Composition

The results are presented in Table 4.6 and the data was illustrated on Figure 4.42. The coal petrographic characterisation revealed that Mushithe coal samples are generally rich in vitrinite followed by inertinite. Liptinite was not detected. Vitrinite values varied from 36.50 to 90.60 vol. %, while the inertinite values ranged from 9.4 to 63.5 vol. %, on a mineral matter-free basis (mmf). Inertinite macerals such as fusinite, secretinite and fusinite were noted (Fig. 4.43). Fusinite showed characteristic Bogen structures. Secretinite particles were oval shaped with cracks and darker rims around the edges.

Large inert semifusinite particles with cracks were noted. Vitrinite macerals such as collotelinite and collodetrinite were dominant (Fig. 4.44). As result of exposure to the atmosphere, various coal weathering features such as cracks, fissures and oxidation rims were noted. Some large cracks were occupied by trapped minerals which are indicative of water movement (Fig. 4.45).

The coal found in Mushithe has a higher vitrinite content, which aligns with Kruszewska (2003). Kruszewska observed that coals from the Soutpansberg Coalfield tend to be rich in vitrinite, while those from Mpumalanga Coalfields are rich in inertinite. Additionally, the lack of liptinite content in the Mushithe coal supports Speight (2013) who indicated that liptinite content in most global coals is typically less than 7%.

Table 4.6: Maceral composition of the exposed coal seam at Mushithe area

ID	MACERAL (vol%)	MACERAL GROUP		
		VITRINITE	LIPTINITE	INERTINITE
A1	inc. mm	81.40	0	8.50
	mmf	90.60	0	9.40
A2	inc. mm	74.20	0	10.30
	mmf	87.80	0	12.20
A3	inc. mm	50.30	0	13.90
	mmf	78.40	0	21.60
B1	inc. mm	45.0	0	38.60
	mmf	54.0	0	46.0
B2	inc. mm	44.60	0	49.70
	mmf	47.30	0	52.70
B3	inc. mm	32.90	0	57.30
	mmf	36.50	0	63.50

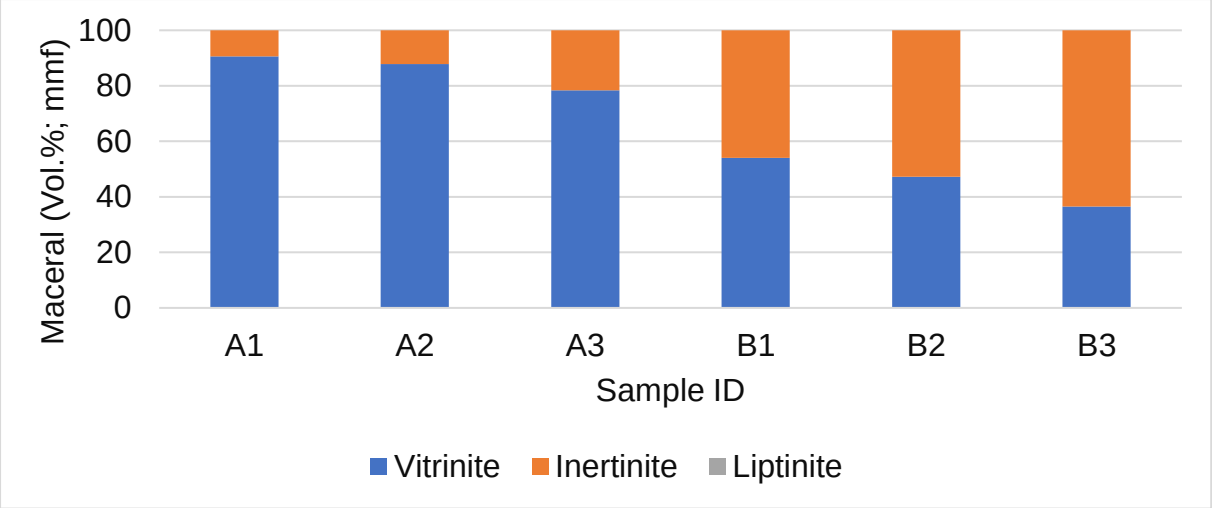

Figure 4.42: Graphical representation of maceral composition of the exposed coal seam at Mushithe area.

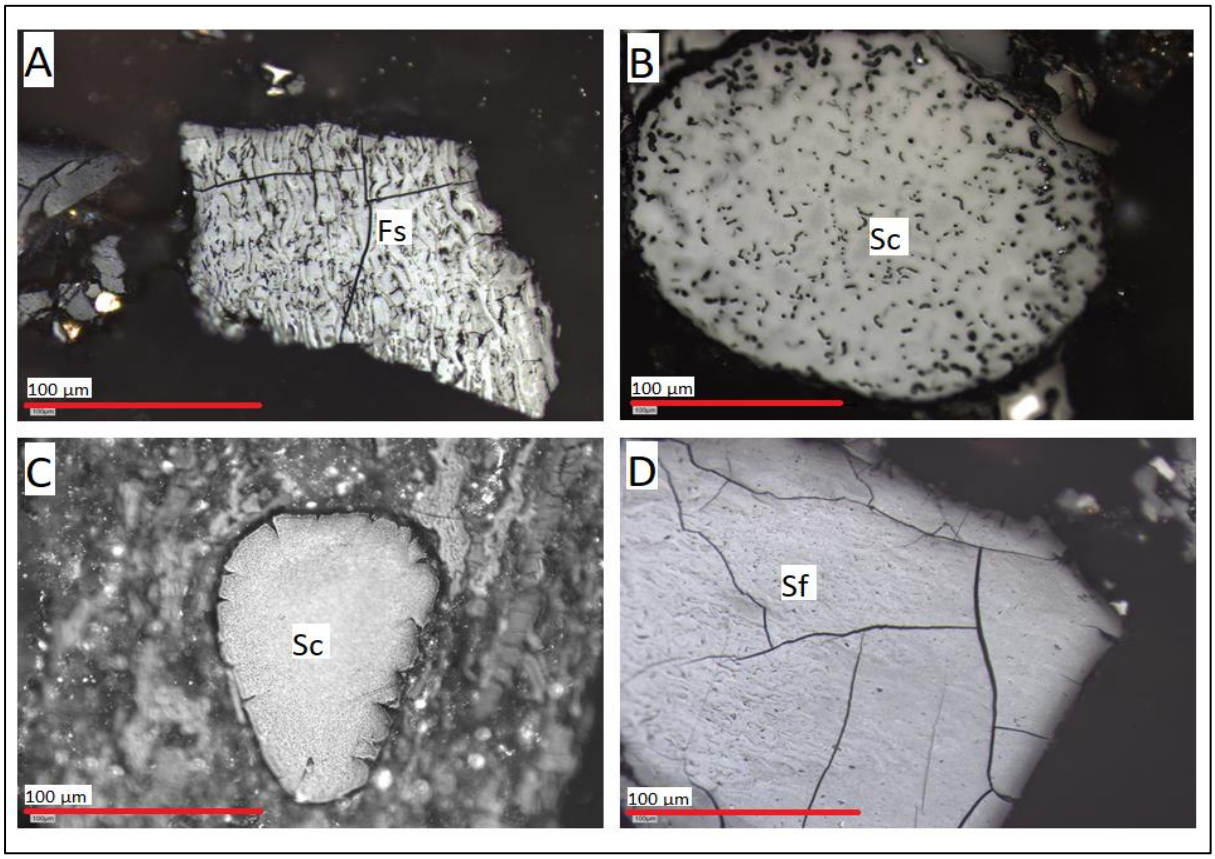

Figure 4.43: Photomicrographs of inertinite macerals. A) Aggregated particle of fusinite showing characteristic Bogen structures (B2); B) Oval-shaped secretinite particle with some vesicles infilled with mineral matter (A2); C) Oval-shaped secretinite with oxidation cracks and darker rims around the edges (B1); D) Large inert semifusinite particle with cracks (B3).

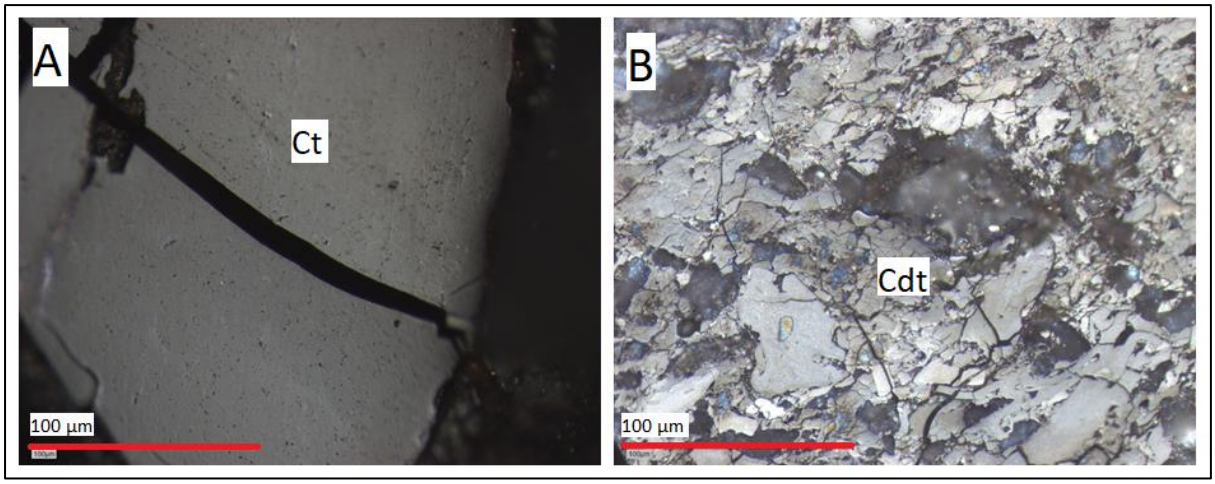

Figure 4.44: Photomicrographs of vitrinite macerals. A) Collotelinite with a large crack; B) Collodetrinite embedded with quartz and clay minerals.

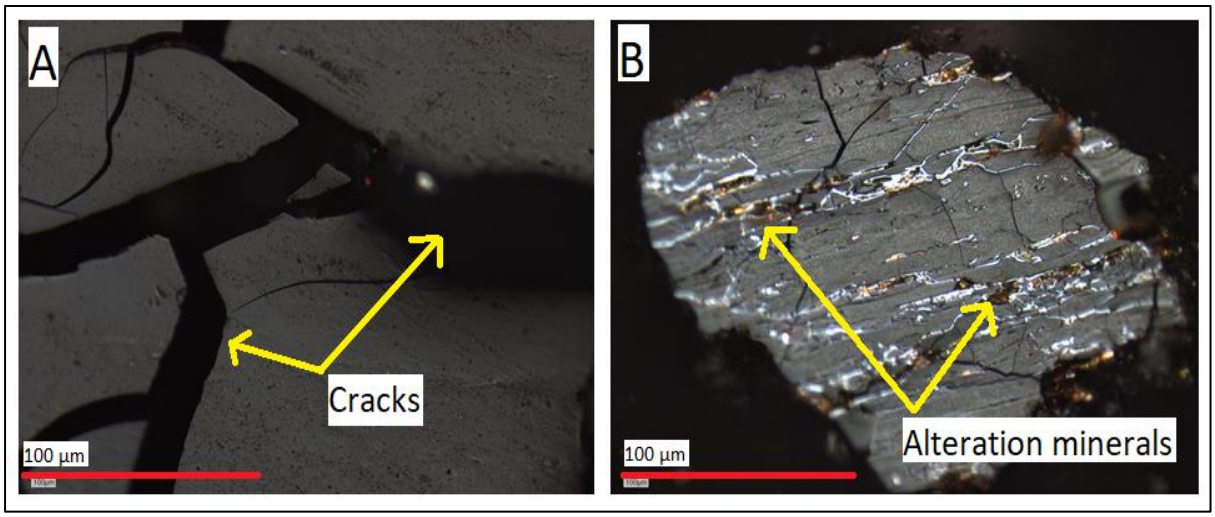

Figure 4.45: Photomicrographs of weathering features. A) Cracks in a vitrinite particle with some minerals trapped in a larger crack, indicative of fluid movement (A1); B) Alteration minerals occurring as epigenetic minerals in a vitrinite particle (A2).

4.2.2 Vitrinite Reflectance Analysis

The results for mean random vitrinite reflectance are shown in Table 4.7 and histograms were constructed for each sample. Figure 4.46 is included as an example of a reflectance histogram, with all the other histograms included in Appendix D. Mushithe coal have a mean random vitrinite reflectance between 0.80 – 0.82%, with an average of 0.81%. Vitrinite reflectance of the exposed coal at Mushithe fall in the Medium Rank C category (UNECE, 1998). Coal rank classification by vitrinite reflectance following UNECE (1998) where similar to rank classification following the standard classification of coals by rank (ASTM D388). The mean vitrinite reflectance

of coal at Mushithe is lower compared to 1.23% in the Tshikondeni area (Mphaphuli, 2017), this is consistent with Sparrow (2012), who noted that coal rank within the Soutpansberg Coalfield increases towards the east. The rank of Mushithe coal is consistent with the findings of Wagner *et al*., (2018) who indicated that most Southern African coals fall into the Medium Rank C Bituminous coal category. The standard deviation for all samples except for sample B2 is below 0.1. The standard deviation ranged between 0.034 and 0.102, indicating narrow reflectance readings. Histograms for all samples indicated a unimodal distribution.

Table 4.7 Vitrinite reflectance readings for the exposed coal seam at the Mushithe area

	A1	**A2**	**A3**	**B1**	**B2**	**B3**
Vitrinite Reflectance	0.80	0.80	0.82	0.82	0.82	0.82
Standard Deviation	0.071	0.065	0.066	0.034	0.102	0.096
points	99	102	100	100	100	90
Rank	C	C	C	C	C	C

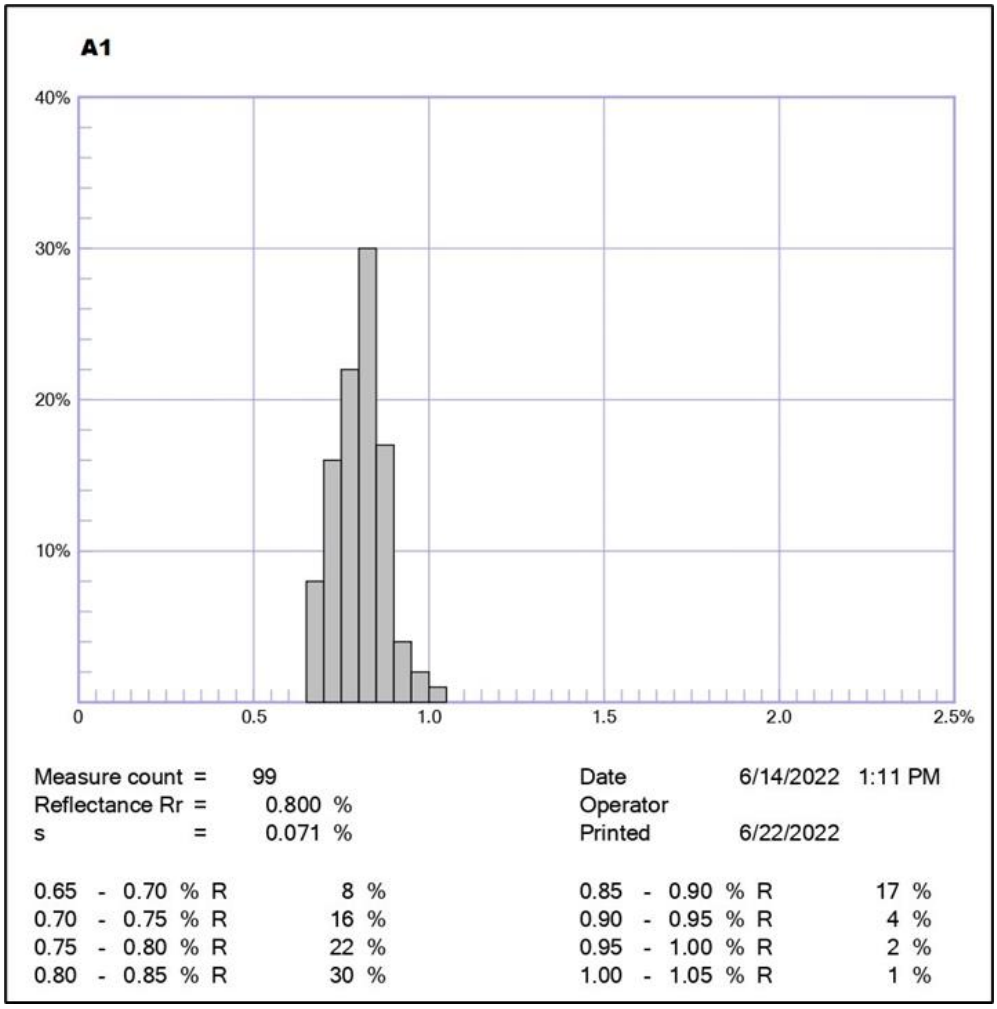

Figure 4.46: Reflectance histogram for sample A1.

4.4.3 Mineralogy of Coal

A total of six coal samples collected from the coal outcrop underwent mineralogical analysis using microscopic study and XRD.

Microscopy

Petrographically observable minerals are presented in Table 4.8 and the data was used to plot the mineralogical distribution histogram (Figure 4.47). Clay, quartz, pyrite, and carbonate minerals were identified petrographically. Quartz was the most dominant mineral with an average of 10.3 vol % followed by clay (3.95 vol %) and carbonate minerals (0.08 vol %). Clay minerals occurred in a form of syngenetic clays infilling macerals and kaolinite worms. Carbonate minerals occurred in a form of siderite nodule imbedded in distorted inertinite bands. Distorted inertinite bands were as result of carbonate mineral growth, indicative of syngenetic formation. Quartz was

intensively embedded with inertinite fragments (Fig. 4.48). The reported low pyrite values align with the ultimate analysis findings that classified the coal as low-sulphur coal according to Chou (2012) classification. Total observable mineral matter content and ash yield were plotted (Fig. 4.49) and a strong positive linear relationship between ash yield and observable mineral matter content. This can be attributed to ash yield from a coal being largely composed of the mineral matter (Thomas, 2012).

Table 4.8: Petrographically observable mineral matter of exposed coal seam at Mushithe area.

Mineral Matter (Vol %)	**A1**	**A2**	**A3**	**B1**	**B2**	**B3**
Clay	6.50	4.70	6.10	5.20	0.70	0.50
Quartz	3.10	9.10	29.70	6.80	5.0	8.10
Pyrite	0	0	0	0.20	0	0
Carbonates	0	0.50	0	0	0	0
Other minerals	0.50	1.20	0	4.20	0	1.20

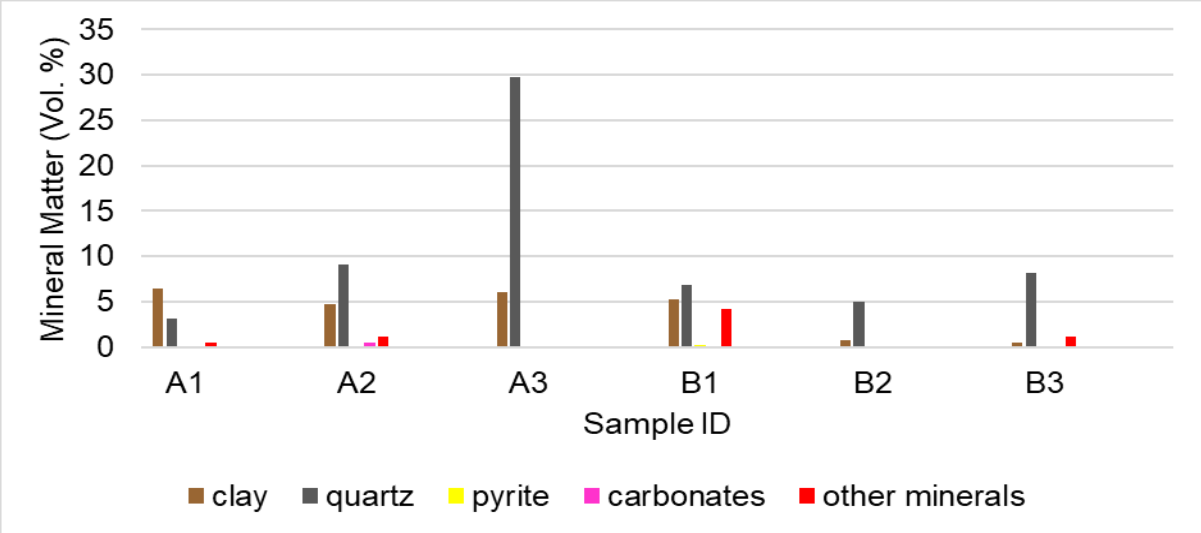

Figure 4.47: Mineralogical distribution of petrographically observable mineral matter content in coal samples.

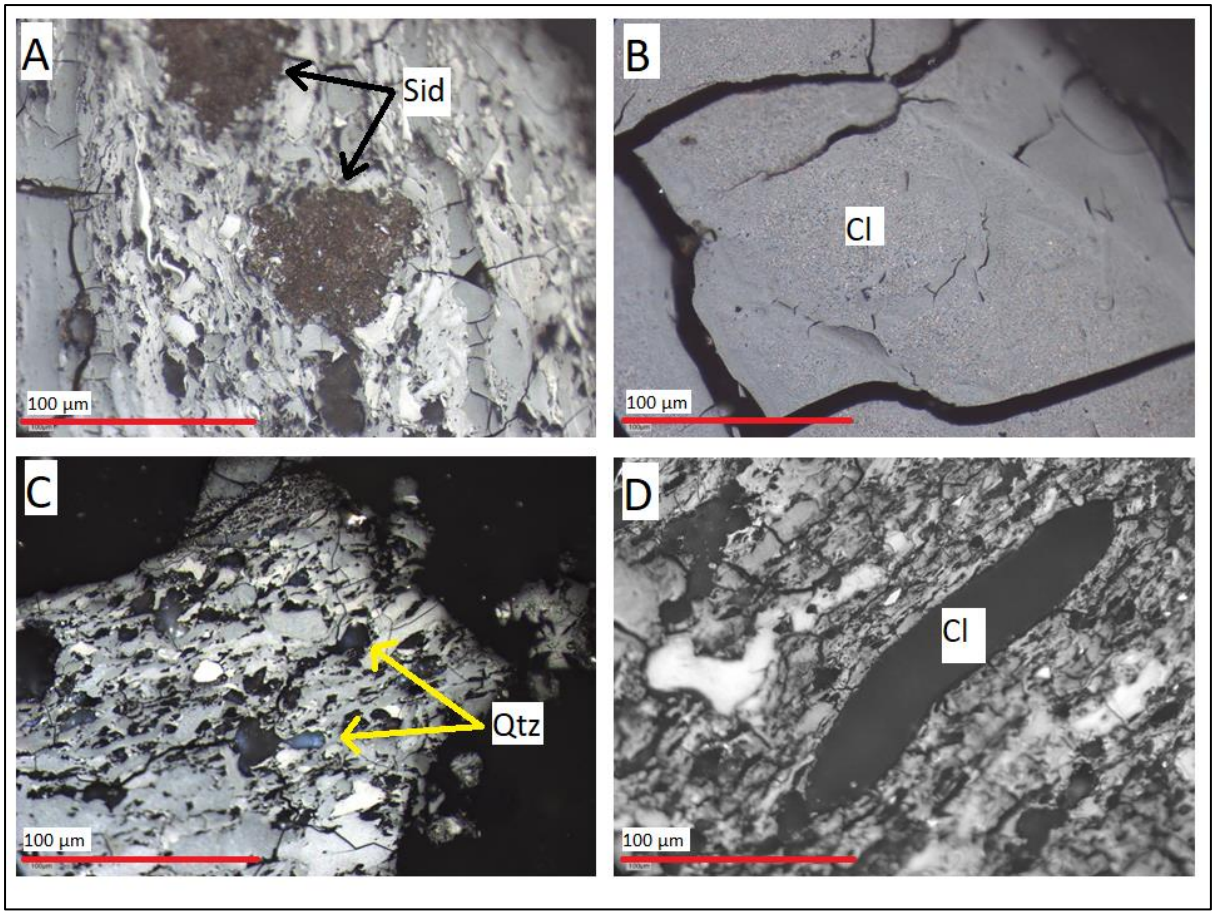

Figure 4.48: Photomicrographs of various minerals. A) Large radial siderite nodule imbedded in an inertinite particle (A2); B) Vitrinite maceral infilled with syngenetic clays (A3); C) Fragmented inertinite particle intensively embedded with quartz grains (B3); D) Kaolinite worm infilled with clay minerals inertinite macerals (A1).

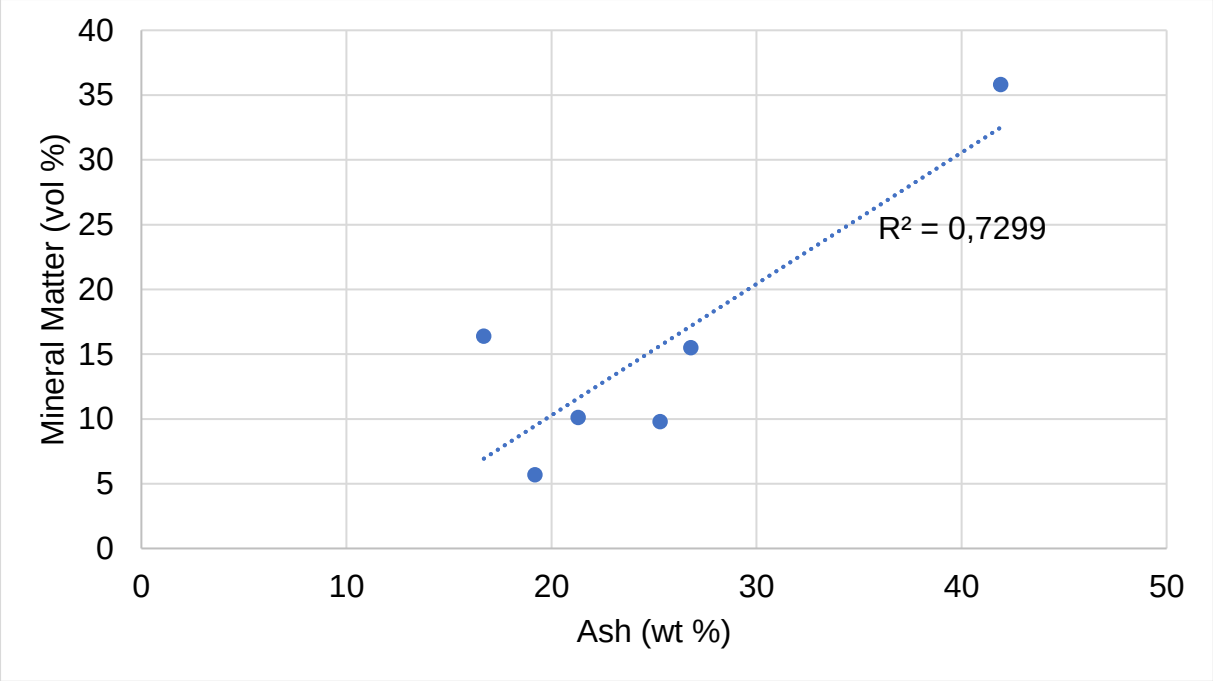

Figure 4.49: Relationship between ash (wt %) and observable mineral matter content (vol %).

X-Ray Diffraction

X-Ray Diffraction results are presented in Table 4.9 and the data was used to plot the mineralogical distribution histogram (Figure 4.50).

Mushithe coal is dominated by amorphous material (61.57 – 75.59 wt %) followed by kaolinite (20.0 – 33.86 wt %) and quartz (4.38 – 7.82 wt %). The dominance of kaolinite and quartz identified by X-Ray Diffraction is consistent with microscopy results where coal was dominated by quartz and clay minerals. High values of kaolinite minerals identified by X-Ray Diffraction as opposed to lower values of clay minerals identified petrographically can be attributed to limitations due to the resolution of the petrographic microscope where minerals particles below 5µm are not identifiable (Mphaphuli, 2017).

Table 4.9: XRD determined minerals from the exposed coal seam at the Mushithe area

ID	Kaolinite	Quartz	Amorphous
A1	24.7	7.82	67.48
A2	26.53	4.38	69.09
A3	33.86	4.57	61.57
B1	31.58	4.52	63.9
B2	20.0	4.79	75.21
B3	21.09	6.32	72.59

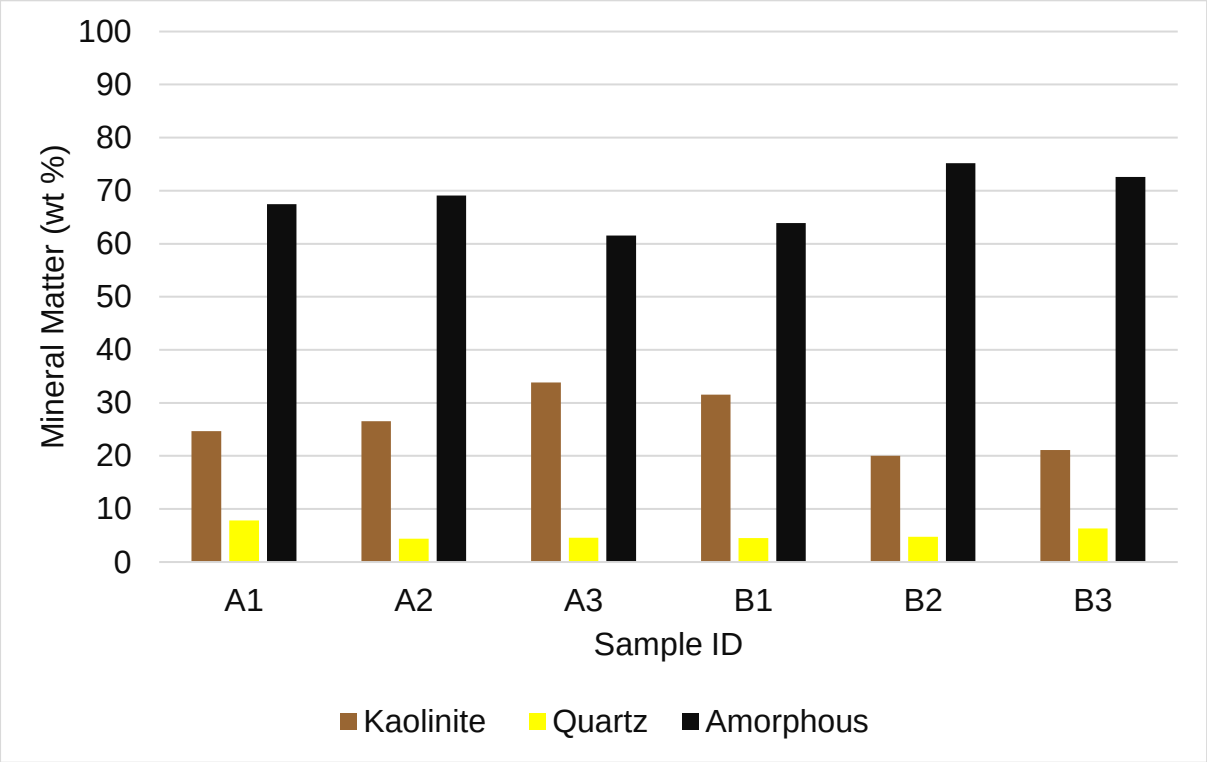

Figure 4.50: Graph showing the distribution of minerals in coal.

4.5 Geochemistry of Coal

Major Oxides

The major element compositions of the ash samples are presented in Table 4.10 and the data was used to plot the geochemical distribution histogram (Fig. 4.51). Ash composition mainly consist of SiO_2 (9.76 – 20.04 wt %; average 13.72 wt %); Al_2O_3 (7.17 – 15.83 wt %; average 10.36 wt %); MgO (0.26 – 2.8 wt %; average 1.19 wt %); and with minor amounts of Fe_2O_3 (0.72 – 1.32 wt %; average 0.93 wt %); Na_2O (0.33 – 1.43 wt %; average 077 wt %); CaO (0.18 – 1.37% wt %; average 0.60 wt %); TiO_2 (0.25 – 0.48 wt %; average 0.36 wt %); K_2O (0.08 – 0.18 wt %; 0.12%); ZrO_2 (0.08 – 0.16 wt % average 0.11 wt %); P_2O_5 (0.07 – 0.13% wt %: average 0.10 wt %). Loss of Ignition was significantly high ranging from 57.27 to 80.03 wt %. The relatively high proportions of SiO_2, Al_2O_3, and MgO coincide with the mineral composition of coal. The SiO_2/Al_2O_3 ratio range from 1.27 to 1.44, with an average of 1.34 which is higher than the theoretical ratio for kaolinite (1.18), suggesting quartz or amorphous silica occurs in the mineral matter portion of the coal.

The TiO_2/Al_2O_3 ratio range from 0.03 to 0.05 with an average of 0.04, indicating intermediate origin, where a silicic, intermediate, and mafic property of deposits are indicated by TiO_2/Al_2O_3 ratios of <0.02, 0.08 – 0.02 and >0.08 respectively. The base acid ratio index was used to predict the potential for ash slagging. Correlation between the high-temperature melting acid group (SiO_2 + Al_2O_3 + TiO_2) (*A*) and the low-temperature melting basic group (Fe_2O_3 + CaO + MgO + K_2O+ Na_2O) (*B*) was expressed by the base to the acid ratio (*B/A*). The *B/A* values for the samples vary from 0.04 to 1.14 with an average of 0.08 suggesting the samples have low slagging potential, where low, medium, and high slagging potential are indicated by B/A values of <0.4, 0.4 – 0.7, and >0.7, respectively (Singer, 1991).

Table 4.10: XRF Analysis of coal ash in the Mushithe area

	A1	A2	A3	B1	B2	B3
SiO_2	10,61	11,27	20,04	18,19	9,76	12,45
Al_2O_3	7,56	8,79	15,83	14,13	7,17	8,66
MgO	0,65	2,80	2,16	0,61	0,63	0,26
Na_2O	0,52	1,43	1,26	0,52	0,54	0,33
P_2O_5	0,12	0,07	0,07	0,11	0,12	0,13
Fe_2O_3	0,79	1,27	1,32	0,71	0,78	0,72
K_2O	0,08	0,14	0,18	0,14	0,07	0,08
CaO	0,40	1,37	0,94	0,32	0,39	0,18
TiO_2	0,30	0,25	0,48	0,44	0,27	0,39
V_2O_5	0,01	0,04	0,05	0,01	0,01	*<0,01*
Cr_2O_3	*<0,01*	0,01	0,01	*<0,01*	0,01	*<0,01*
NiO	0,01	0,01	0,01	*<0,01*	*<0,01*	*<0,01*
ZrO_2	0,08	0,16	0,16	0,11	0,08	0,09
S	*<0,01*	0,08	0,09	*<0,01*	*<0,01*	*<0,01*
ZnO	0,01	0,02	0,01	*<0,01*	*<0,01*	*<0,01*
SrO	0,09	0,06	0,04	0,07	0,09	0,09
Y_2O_3	0,02	0,04	0,02	0,01	0,01	0,01
LOI	78,74	72,17	57,27	64,59	80,03	76,57
TOTAL	**99,97**	**99,98**	**99,95**	**99,96**	**99,95**	**99,96**

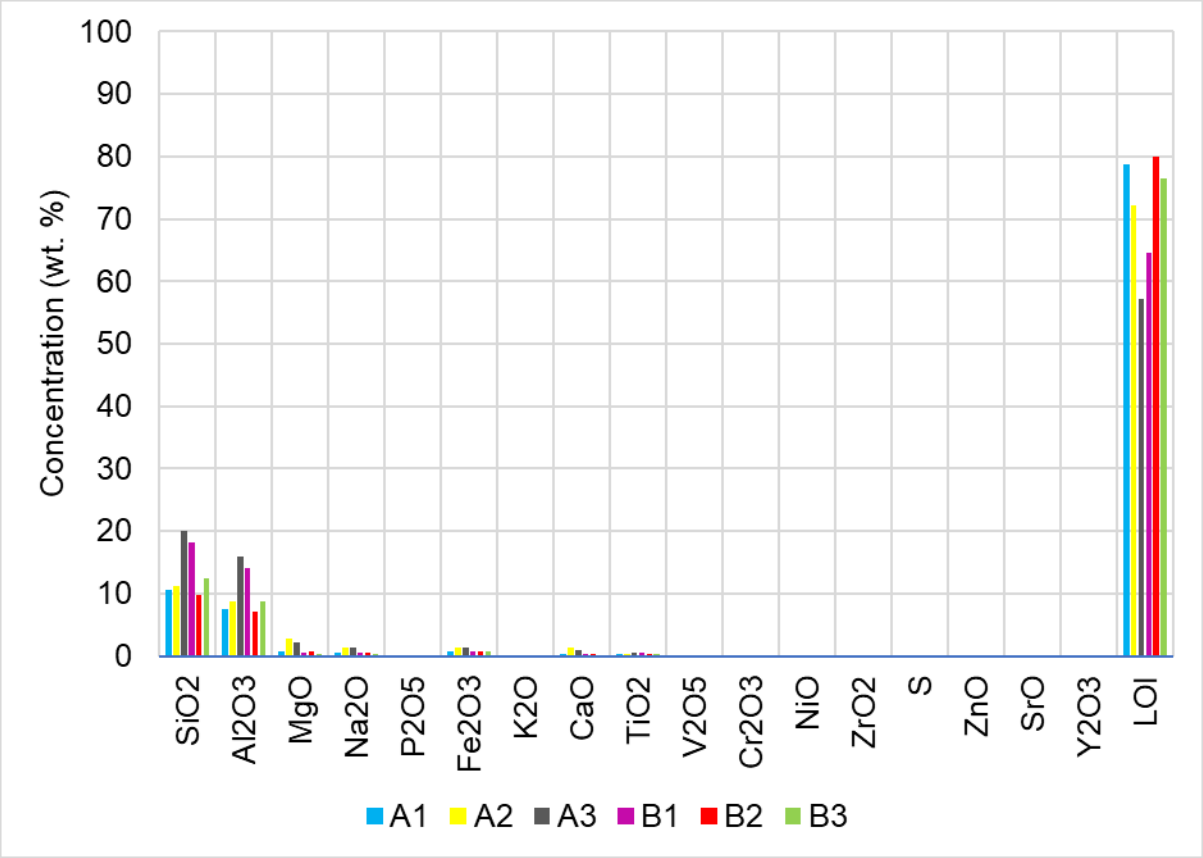

Figure 4.51: Composition of Mushithe coal ash.

4.6 Depositional Environments

The environments of deposition were inferred using petrographic indices. V/I (Vitrinite to Inertinite ratio) (Diessel, 1992) and facies diagram proposed by Singh and Singh (1996) were used to reconstruct the depositional environments.

Vitrinite to Inertinite ratio of coal from Mushithe ranges between 0.57 and 9.64 with majority of samples having V/I of greater than 1. Vitrinite to Inertinite of Ply A samples ranges between 3.63 and 9.64 with an available of 5.94. The V/I >1, represents a shallow water covered environment. Vitrinite to Inertinite of Ply B samples ranges between 0.57 and 1.17 with an average of 0.85. V/I <1, which represents a relatively dry terrigenous environment. High vitrinite content (65.77 vol %) within Mushithe coals is indicative of wet forest swamp depositional environment. The findings align with those of Malaza (2013), who observed that the coalfields in the Limpopo Province were formed through deposition in a fluvial setting.

Singh and Singh (1996) proposed a facies diagram in which the maceral content and mineral matter content are combined to represent the depositional environment (Fig.

4.52). Ply A samples experienced wet conditions within the moor with intermittent moderate to high flooding events and Ply B samples experienced alternate oxic and anoxic moor condition. The exposed coal at Mushithe is classified as low-grade coal with an average ash percentage of 25.20 wt % (Fig. 4.53). Based on petrographic composition, Ply A samples are generally vitrinite rich (85.60 vol. %) and Ply B samples are generally inertinite rich (54,07 vol. %). Although the Ply B samples contain the highest vitrinite vol%, they also contain a higher average ash content (30.0 wt %) than Ply B samples (20.40 wt %) due to the influence of inorganic material from intermittent moderate to high flooding events.

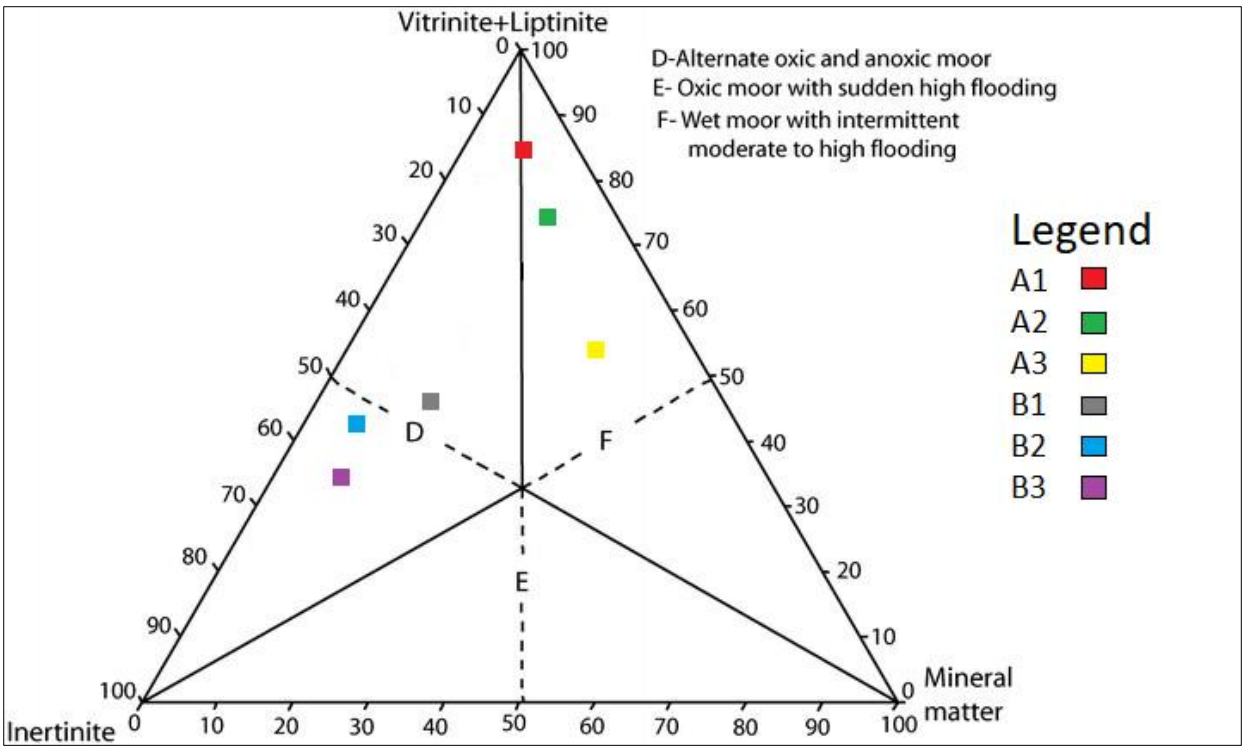

Figure 4.52: Ternary diagram illustrating conditions for deposition of coal (Singh and Singh, 1996).

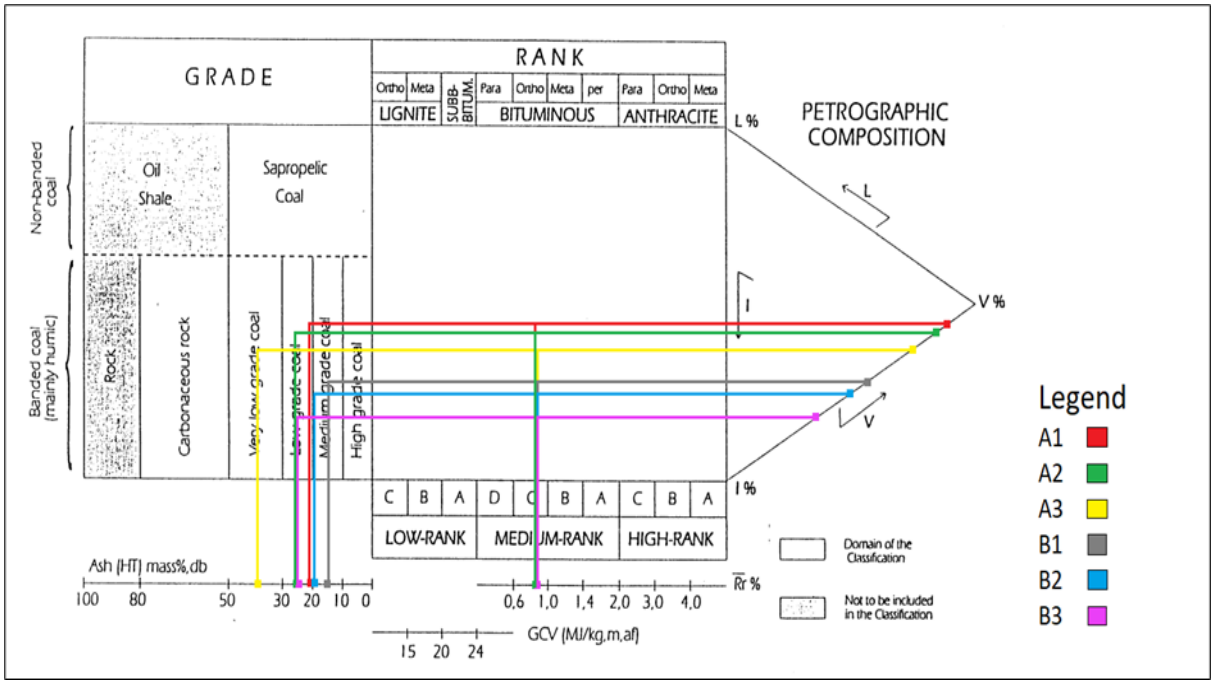

Figure 4.53: Classification of Mushithe coal based on UNECE (1998) classification.

CHAPTER 5 : CONCLUSIONS AND RECOMMENDATIONS

5.1 Conclusions

The current study came up with several conclusions and recommendations that are presented below:

- Coal at Mushithe is associated with various rock formations, including Wyllie's Poort, Nzhelele, Musekwa, Madzaringwe, and Mikambeni. Pink quartzite belongs to Wyllie's Poort Formation, red quartzite and mudstone are part of the Nzhelele Formation, basalt and quartz veins belong to Musekwa Formation, while sandstone, shale, and carbonaceous shale are associated with the Madzaringwe and Mikambeni Formations.
- Coal bearing rocks at Mushithe coal occurrence are occurring as a valley isolated from the Pafuri Basin by quartzites of the Nzhelele formation. The seam at Mushithe is exposed along Tshamatsha fault.
- Coal Measures consist of four to seven coal seams, with varying thicknesses ranging from 0.35 m to 11.38 m.
- The coal found at Mushithe has Vitrinite reflectance values ranging from 0.80 to 0.82%, with an average of 0.81%. According to UNECE (1998) classification, this places it within the Bituminous Medium-Rank C category.
- The maceral analysis revealed that Mushithe coal are dominated by vitrinite (65.77 vol%) followed by inertinite (34.23 vol%). Liptinite was not detected. Coal exhibited weathering features including cracks, fissures, and oxidation rims.
- The high vitrinite content of 65.77 wt % in Mushithe coals shows it was formed in a wet swamp environment. This supports the findings by Malaza (2013) that the Soutpansberg and Limpopo Coalfields were formed in a fluvial environment.
- Based on the proximate analysis, coal quality in the area is characterised by high fixed carbon (42.48 wt %), moisture content (8.73 wt %), ash yield (25.20 wt %), and volatile matter (32.33 wt %).
- The coal found in the Mushithe has a calorific value ranging from 12.97 MJ/kg to 23.35 MJ/kg, with an average of 19.52 MJ/kg. In comparison to Tshikondeni coal, the calorific value of Mushithe coal is lower, but higher than Makhado and Vele collieries, which have calorific values of 18.17 MJ/kg and 17.53 MJ/kg, respectively.

- Sulphur ranges from 0.23 wt. – 0.38 wt % with an average of 0.30 wt % indicating low sulphur coal type (Chou, 2012), indicating sulphur was derived from the original plant material during peat accumulation.
- Based on the reported ash contents and calorific value, Mushithe coal can be categorised as below grade D. Sparrow (2012), indicated that Soutpansberg coals can be upgraded with careful processing, according to plant trials.

5.2 Recommendations

- The coal studied at Mushithe was identified as Medium-Rank Bituminous C coal and was deemed to have economic significance. As a result, it was suggested that the Mushithe coal could be utilised for profitable activities like producing electricity.
- It is recommended to conduct additional research to explore the possibility of extracting coalbed methane at the Mushithe area from deep coal seams that cannot be economically mined through conventional mining methods.
- Further studies should be conducted on fresh samples to investigate the swelling properties of coal at Mushithe, as coal weathering can significantly impact important technological aspects of coals such as calorific value and coking properties.

REFERENCES

Bordy, E. and Head, H. (2018). Lithostratigraphy of the Clarens Formation (Stormberg Group, Karoo Supergroup), South Africa. *South African Journal of Geology*, Volume 121, Issue1, pp.119-130.

Bordy, E. and Paiva, F. (2021). Stratigraphic Architecture of the Karoo River Channels at the End-Capitanian. *Frontiers in Earth Science*, Volume 8, pp.1-22.

Bumby, A., Eriksson, P., Van Der Merwe, R. and Steyn, G. (2002). A Half-graben Setting for the Proterozoic Soutpansberg Group (South Africa): Evidence from the Blouberg area. *Sedimentary Geology*, Volume 147, Issues 1-2, pp.37-56.

Brandl, G. (1981). The Geology of the Messina area. Explanation, sheet 2230, Messina, Geological Survey of South Africa, 35 pp.

Bristow, J. (1986). An Overview of the Soutpansberg Sedimentary and Volcanic Rocks. *Koedoe*, Volume 29, Issue 1, pp.59-67.

Brouwer, N.P. (2010). Theory of XRF: Getting Acquainted with the Principles. 3rd Edition. PANalytical, Almelo, 59 pp.

Campbell, S., Lenhardt, N., Dippenaar, M. and Götz, A. (2016). Geothermal Energy from the Main Karoo Basin (South Africa): An Outcrop Analogue Study of Permian Sandstone Reservoir Formations. *Energy Procedia*, Volume 97, pp.186-193.

Cairncross, B. (2001). An Overview of the Permian (Karoo) Coal Deposits of southern Africa. *Journal of African Earth Sciences*, Volume 33, Issues 3-4, pp.529-562.

Catuneanu, O., Wopfner, H., Eriksson, P., Cairncross, B., Rubidge, B., Smith, R. and Hancox, P. (2005). The Karoo basins of South-central Africa. *Journal of African Earth Sciences*, Volume 43, Issues1-3, pp.211-253.

Chabedi, C. K. (2013). Analysis of Technical Factors for Underground Mining of Deep Waterberg Coal Resources. Unpublished PhD Thesis, University of Witwatersrand, 163 pp.

Chima, P., Baiyegunhi, C., Liu, K. and Gwavava, O. (2018). Petrography, Modal Composition and Tectonic Provenance of Some Selected Sandstones from the Molteno, Elliot and Clarens Formations, Karoo Supergroup, in the Eastern Cape Province, South Africa. *Open Geosciences*, Volume 10, Issue 1, pp.821-833.

Chou, C. L. (2012). Sulfur in Coals: A Review of Geochemistry and Origins. *International Journal of Coal Geology*, Volume 100, pp. 1–13.

Council for Geoscience. (2020). CGS Geological Maps. Council for Geoscience. Available at: https://www.geoscience.org.za/index.php/publication/306-geological-maps [Accessed 13 June 2021].

Council for Geoscience. (2021). Council for Geoscience Interactive Web Portal, Maps.geoscience.org.za. Available at: https://maps.geoscience.org.za/portal/apps/ [Accessed: February 14, 2022].

Diessel C.F.K. (1992). Coal-bearing Depositional Systems. Springer-Verlag, Berlin, 721 pp.

Environmental Systems Research Institute. (2019). ArcGIS Release 10.1. Redlands, CA.

Falcon, R. (2013). Coal petrography. In Osborne, D.G. (Ed.). The Coal Handbook: Towards Cleaner Production, Woodhead Publishing, Oxford, pp.53-79.

Faure, K., Willis, J. and Claris Dreyer, J. (1996). The Grootegeluk Formation in the Waterberg Coalfield, South Africa: Facies, Palaeoenvironment and Thermal History — Evidence from Organic and Clastic Matter. *International Journal of Coal Geology*, Volume 29, Issues1-3, pp.147-186.

Finkelman, R. (1999). Trace elements in coal. *Biological Trace Element Research*, Volume 67, Issue 3, pp.197-204.

Finkelman, R., Dai, S. and French, D. (2019). The Importance of Minerals in Coal as the Hosts of Chemical Elements: A review. *International Journal of Coal Geology*, Volume 212, pp.103-251.

Flores, R.M. (2014). Coalification, Gasification, and Gas Storage. In Flores, R.M. (Ed.). Coal and Coalbed Gas: Fueling the Future, Elsevier, Amsterdam, pp.167-233.

Geng, H., Brandl, G., Sun, M., Wong, J. and Kröner, A. (2014). Zircon Ages Defining Deposition of the Palaeoproterozoic Soutpansberg Group and Further Evidence for Eoarchaean Crust in South Africa. *Precambrian Research*, Volume 249, pp.247-262.

Hancox, P. (2016). The Coalfields of South-Central Africa: A Current Perspective. *Episodes*, Volume 39, Issue 2, pp.407-428.

Hancox, P. and Götz, A. (2014). South Africa's coalfields — A 2014 Perspective. *International Journal of Coal Geology*, Volume 132, pp.170-254.

Herbert, C. and Compton, J. (2007). Depositional Environments of the Lower Permian Dwyka Diamictite and Prince Albert Shale Inferred from the Geochemistry of Early Diagenetic Concretions, Southwest Karoo Basin, South Africa. *Sedimentary Geology*, Volume 194, Issue 3-4, pp.263-277.

Holder, C.F. and Schaak, R.E. (2019). “Tutorial on powder X-ray diffraction for characterizing Nanoscale Materials,” *ACS Nano*, Volume 13, Issue 7, pp. 7359–7365.

International Trade Administration (2023). South Africa - Energy. Available at: https://www.trade.gov/country-commercial-guides/south-africa (Accessed: 12 January 2023).

Jeffrey, L. S. (2005). Characterization of the Coal Resources of South Africa. *The South African Institute of Mining and Metallurgy*, pp.95-102.

Johnson, M., Van Vuuren, C., Hegenberger, W., Key, R. and Show, U. (1996). Stratigraphy of the Karoo Supergroup in southern Africa: an overview. *Journal of African Earth Sciences*, Volume 23, Issue 1, pp.3-15.

Kabanda, T. A. (2004). Climatology of Long-term Drought in the Northern Region of the Limpopo Province of South Africa. Unpublished PhD Thesis, University of Venda, 340 pp.

Kruszewska, K.J. (2003). Fluorescing Macerals in South African coals, *International Journal of Coal Geology*, Volume 54, Issues 1-2, pp. 79–94.

Malaza, N. (2014). Basin Analysis of the Soutpansberg and Tuli Coalfields, Limpopo Province of South Africa. Unpublished PhD Thesis, University of Fort Hare, 270 pp.

Malaza, N., Liu, K. and Zhao, B. (2013). Facies Analysis and Depositional Environments of the Late Palaeozoic Coal-Bearing Madzaringwe Formation in the Tshipise-Pafuri Basin, South Africa. *ISRN Geology*, pp.1-11.

Malaza, N., Liu, K. and Zhao, B. (2016). Petrology and Geochemistry of Clastic Sedimentary Rocks as Evidences for Provenance of the Late Palaeozoic Madzaringwe Formation, Tshipise-Pafuri Basin, South Africa. *Science China Earth Sciences*, Volume 59, Issue 12, pp.2411-2426.

McCourt, S., Brandl, G. (1980). A Lithostratigraphic Subdivision of the Karoo Sequence in the North-eastern Transvaal. Ann. *Geological Survey South Africa*. Volume 14, pp.51–56.

Miller, B.G. (2005). Coal Energy Systems. Elsevier Academic Press, London, 526 pp.

O'Keefe, J., Bechtel, A., Christanis, K., Dai, S., DiMichele, W., Eble, C., Esterle, J., Mastalerz, M., Raymond, A., Valentim, B., Wagner, N., Ward, C. and Hower, J. (2013). On the fundamental difference between coal rank and coal type. *International Journal of Coal Geology*, Volume 118, pp.58-87.

Pickel, W., Kus, J., Flores, D., Kalaitzidis, S., Christanis, K., Cardott, B., Misz-Kennan, M., Rodrigues, S., Hentschel, A., Hamor-Vido, M., Crosdale, P. and Wagner, N. (2017). Classification of liptinite – ICCP System 1994. *International Journal of Coal Geology*, Volume 169, pp.40-61.

Phokele, M. and Sylvester, M. (2015). Climate Change Status in the Mutale Local Municipality: A Case Study of the Smallholder Farmers in Vhembe District, Limpopo Province. *Journal of Human Ecology*, Vol. 52, Issues 1-2, pp.1-8.

Rubiera, F., Ivatt, S. and Miles, N.J. (1995). Coal Characterisation Strategy for Physical Desulphurisation Processes. Coal Science, *proceedings of the eighth international conference on coal science*, Volume 24, pp. 1545-1548.

Suárez-Ruiz, I., Diez, M. and Rubiera, F. (2019). Coal. In Suárez-Ruiz, I., Diez, M. and Rubiera. (Eds.). New Trends in Coal Conversion: Combustion, Gasification, Emissions, and Coking, Elsevier, Massachusetts, pp.1-30.

Suárez-Ruiz, I. and Ward, C. (2008). Basic Factors Controlling Coal Quality and Technological Behaviour of Coal. *Applied Coal Petrology*, pp.19-59.

Schweinfurth, S.P. (2009). An introduction to coal quality. In: Pierce, B.S., and Dennen, K.O. (Eds.), The National Coal Resource Assessment Overview: U.S. Geological Survey Professional Paper 1625–F, Chapter C, pp.1-16.

South African Committee for Stratigraphy. (1980). Stratigraphy of South Africa. Part 1. Lithostratigraphy of the Republic of South Africa, South West Africa/Namibia and the republics of Bophuthatswana, Transkei and Venda. Pretoria: *Geological Survey*, pp.1-690.

Sparrow, J. (2012). The Soutpansberg Coalfield “The Forgotten Basin”. Presentation at the Inaugural FFF Limpopo Conference, October 2012.

Singh, M.P., Singh, G.P. (1995). Petrographic Characterization and Evolution of the Permian Coal Deposits of the Rajmahal Basin, Bihar, India. *International Journal of Coal Geology*, Volume 29, pp.93-118.

Speight, J. (2005). Handbook of Coal Analysis. John Wiley & Sons, New Jersey, 227 pp.

Speight, J. (2013). The Chemistry and Technology of Coal. 3rd Edition. CRC Press, Boca Raton, 779 pp.

Stach, E., Chandra, D., Mackowsky, M., Taylor, G. H., Teichmuller, M., Teichmuller, R. (1982). Stach’s Textbook of Coal Petrology. Gebruder Borntraeger, Berlin, 533 pp.

Steyn, M., Minnitt, R.C.A. (2010). Thermal Coal Products in South Africa. *Journal of Southern African Institute of Mining and Metallurgy*, Volume 110, pp.593-559.

Scott, A. (2002). Coal Petrology and The Origin of Coal Macerals: A Way Ahead?. *International Journal of Coal Geology*, Volume 50, Issues 1-4, pp.119-13.

Singer, J.G. (1991). Combustion - Fossil Power: A Reference Book on Fuel Burning and Steam Generation. 4th Edition. Combustion Engineering, Inc., Windsor, 140 pp.

Spackman, W. (1958). Section of Geology and Mineralogy: The Maceral Concept and The Study of Modern Environments as a Means of Understanding the Nature of Coal. *Transactions of The New York Academy of Sciences*, Volume 20, pp.411-423.

Speight, J. (2013). The Chemistry and Technology of Coal. Taylor & Francis Group, New York, 807 pp.

Stopes, M.C. (1935). On the Petrology of Banded Bituminous Coals. *Fuel,* Volume 14, pp.4-13.

Taylor S. R. and McLennan S. M. (1985). The Continental Crust: Its Composition and Evolution. Blackwell, Oxford, 312 pp.

Thomas, L. (2012). Coal Geology. 2nd Edition. John Wiley & Sons, Chichester, 444 pp.

UNECE (1998). International classification of in-seam coals. Economic Commission for Europe, Committee on Sustainable Energy United Nations, New York. Document ENERGY/1998/19, 41 pp.

Van der Berg, H.J. (1980). Die Sedimentologie van Die Soutpansberg-steenkoolveld Met Spesiale Verwysing na Steenkoolvorming. Unpublished MSc Thesis, University of Orange Free State, Bloemfontein, 127 pp.

Van Der Walt, B. (2012). The Petrology, Petrography and Geochemistry of Anomalous Borehole Core Sequences: A Case Study of Diatreme Activity, University of Johannesburg, Johannesburg, Unpublished dissertation, 319 pp.

Von Brunn, V. (1996). The Dwyka Group in the Northern Part of Kwazulu/Natal, South Africa: Sedimentation During Late Palaeozoic Deglaciation. *Palaeogeography, Palaeoclimatology, Palaeoecology*, Volume 125, Issues 1-4, pp.141-163.

Ward, C. (2002). Analysis and Significance of Mineral Matter in Coal Seams. *International Journal of Coal Geology*, Volume 50, Issues1-4, pp.135-168.

Ward, C. (2016). Analysis, Origin and Significance of Mineral Matter in Coal: An Updated Review. *International Journal of Coal Geology*, Volume 165, pp.1–27.

Ward, C., Taylor, J., Matulis, C. and Dale, L. (2001). Quantification of Mineral Matter in the Argonne Premium Coals using Interactive Rietveld-based X-ray Diffraction. *International Journal of Coal Geology*, Volume 46, Issues 2-4, pp.67-82.

World Coal Association (2019). Coal in the energy mix of South Africa. [online] World Coal Association. Available at: https://www.worldcoal.org/coal-energy-mix-south-africa [Accessed 6 Jul. 2019].

Wagner, N. (2021). Geology of Coal. In Elias S. A. and Alderton D. H. M. (Eds.). Encyclopaedia of geology. 2nd Edition, Academic Press, London, pp.745-761.

Wagner, N., Eble, C., Hower, J. and Falcon, R. (2019). Petrology and Palynology of Select Coal Samples from the Permian Waterberg Coalfield, South Africa. *International Journal of Coal Geology*, Volume 204, pp.85-101.

Wagner, N. and Hlatshwayo, B. (2005). The Occurrence of Potentially Hazardous Trace Elements in Five Highveld Coals, South Africa. *International Journal of Coal Geology*, Volume 63, Issues 3-4, pp.228-246.

Wagner, N., Malumbazo, N. and Falcon, R. (2018). Southern African Coals and Carbons: Definitions and Applications of Organic Petrology. Struik Nature, Cape Town, 248 pp.

Xie, K. (2015). Structure and Reactivity of Coal. Springer-Verlag, Berlin, 413 pp.

APPENDICES

APPENDIX A: Drillhole Data

Appendix A1: Borehole 1901191 showing lithological variations.

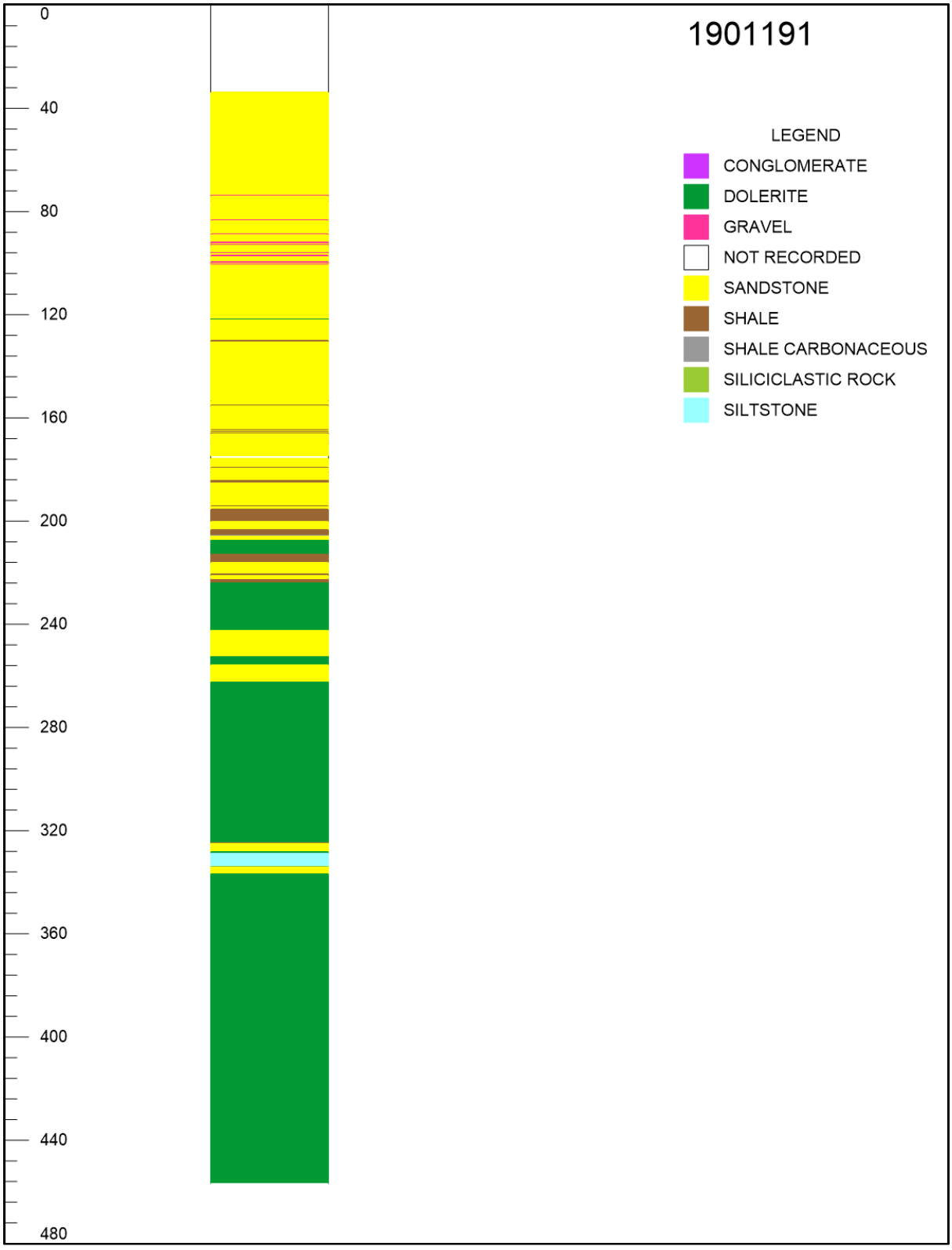

Appendix A2: Borehole 1900219 showing lithological variations.

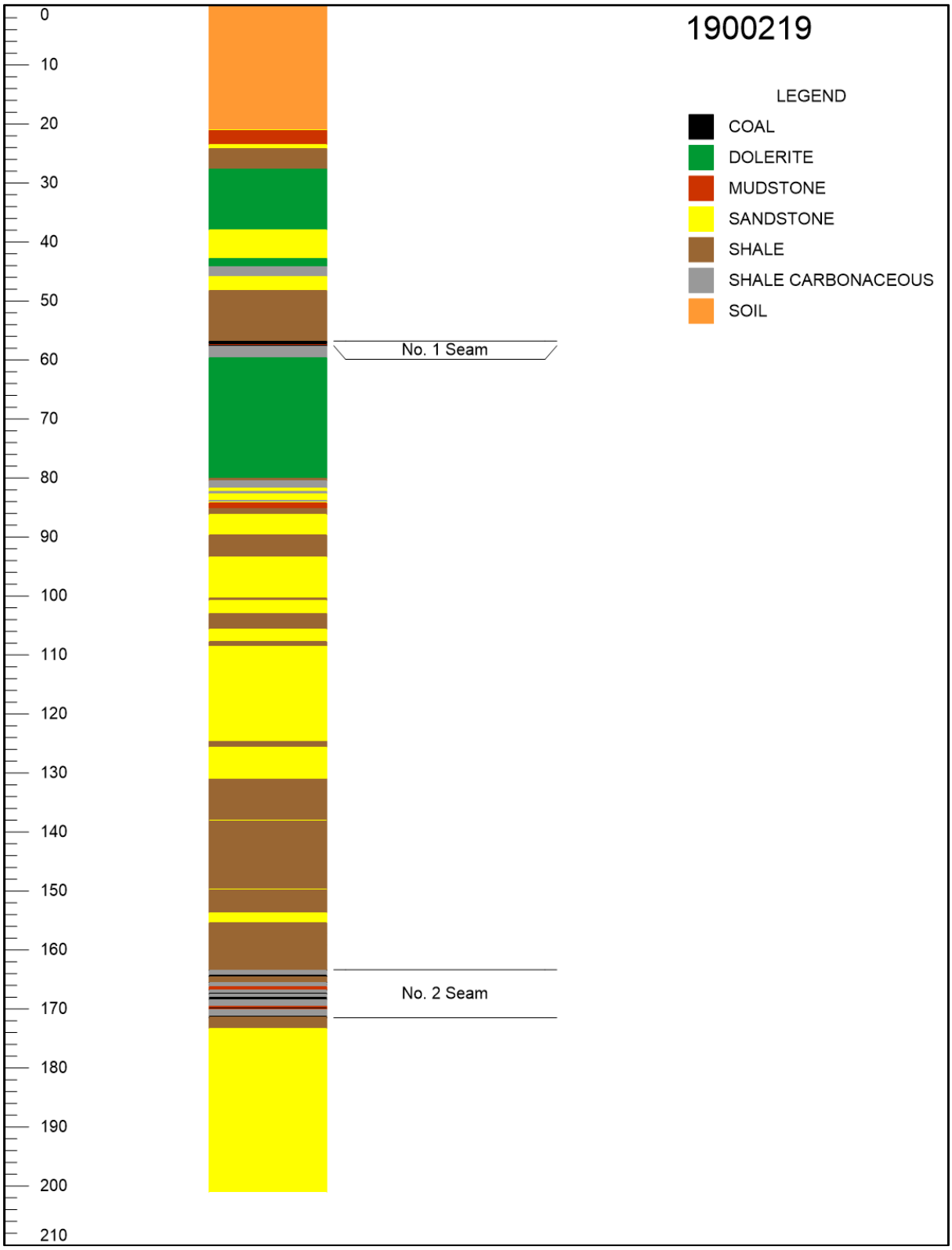

Appendix A3: Borehole 1901162 showing lithological variations.

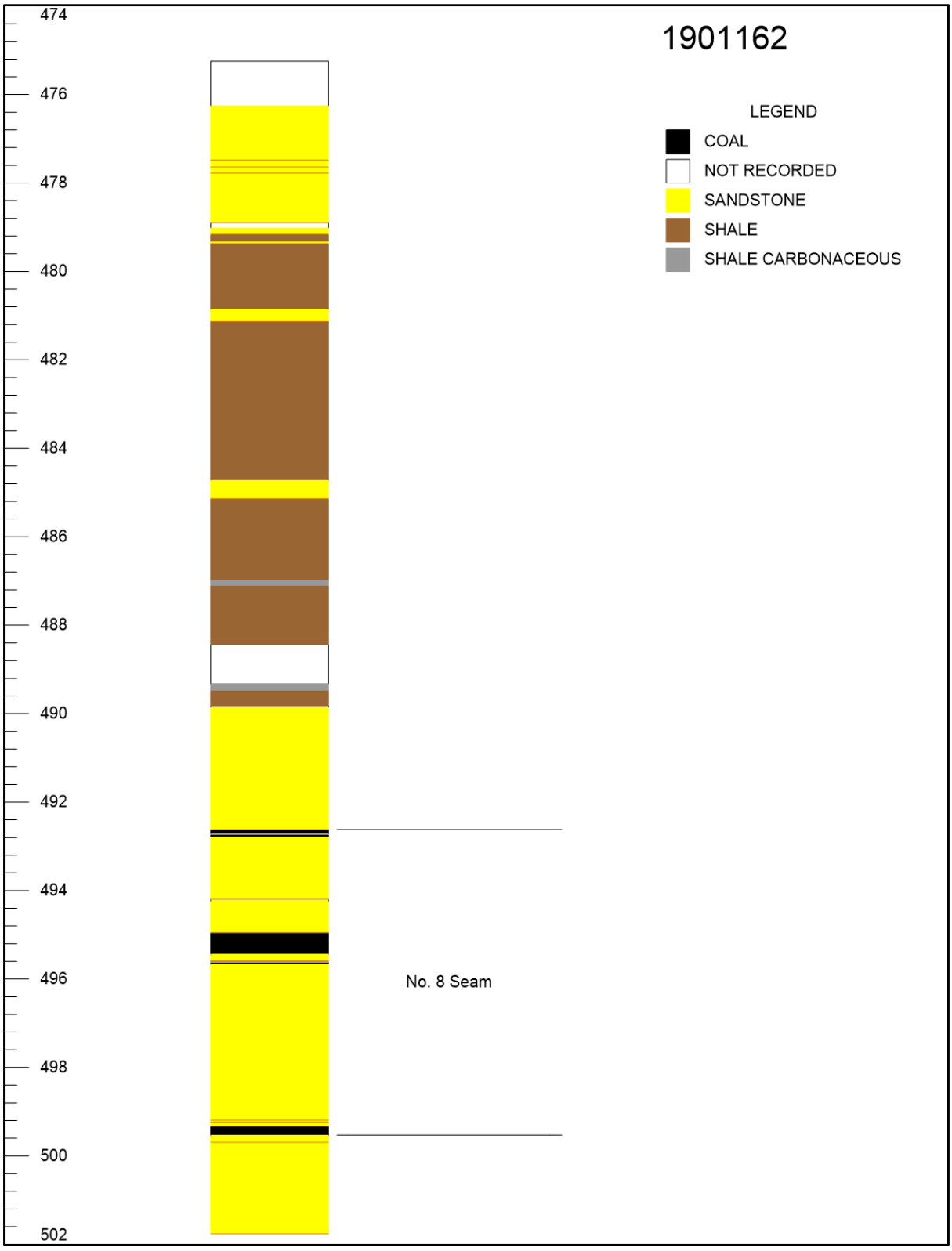

Appendix A4: Borehole 1901211 showing lithological variations.

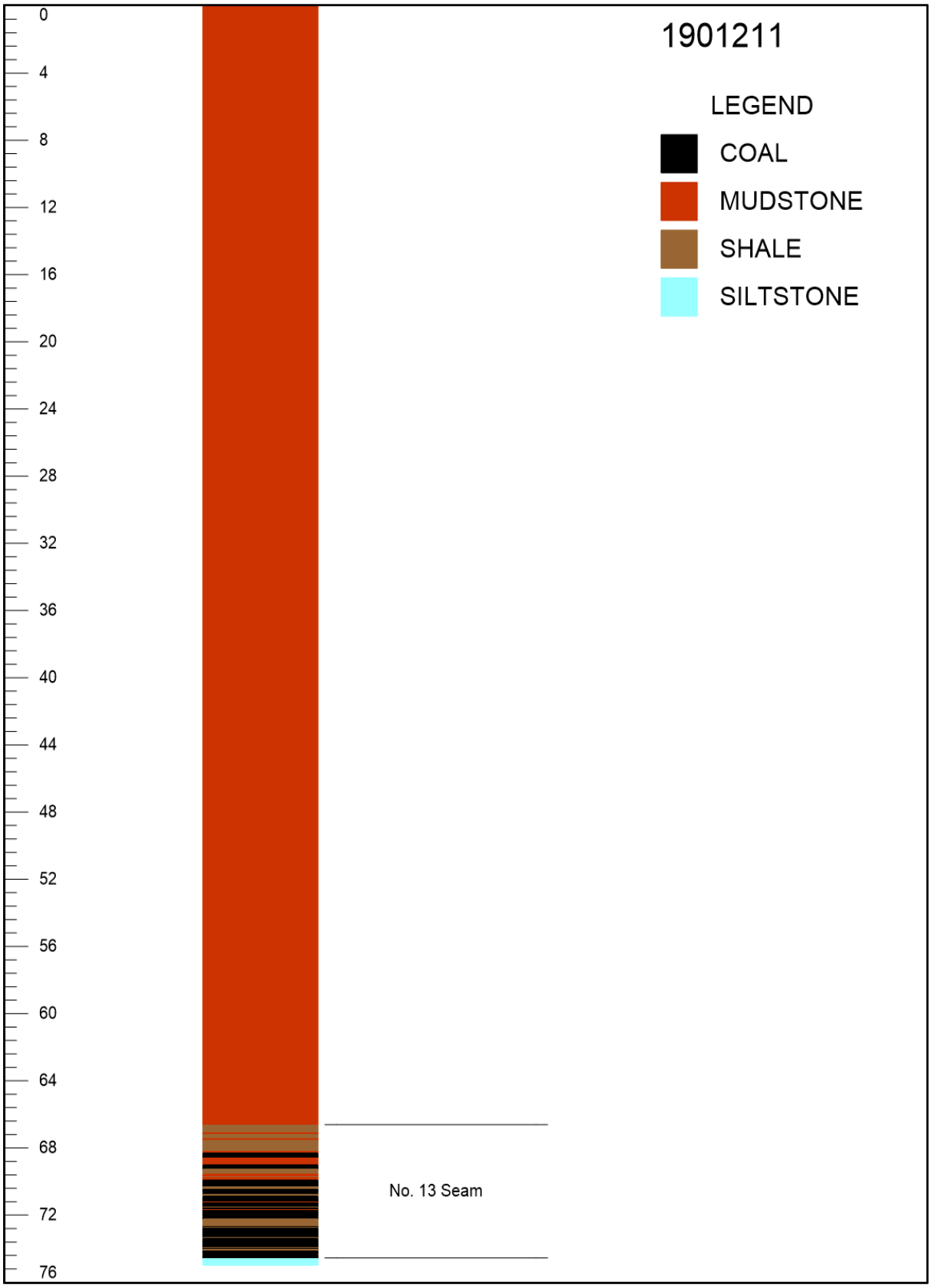

Appendix A5: Borehole 1900146 showing lithological variations.

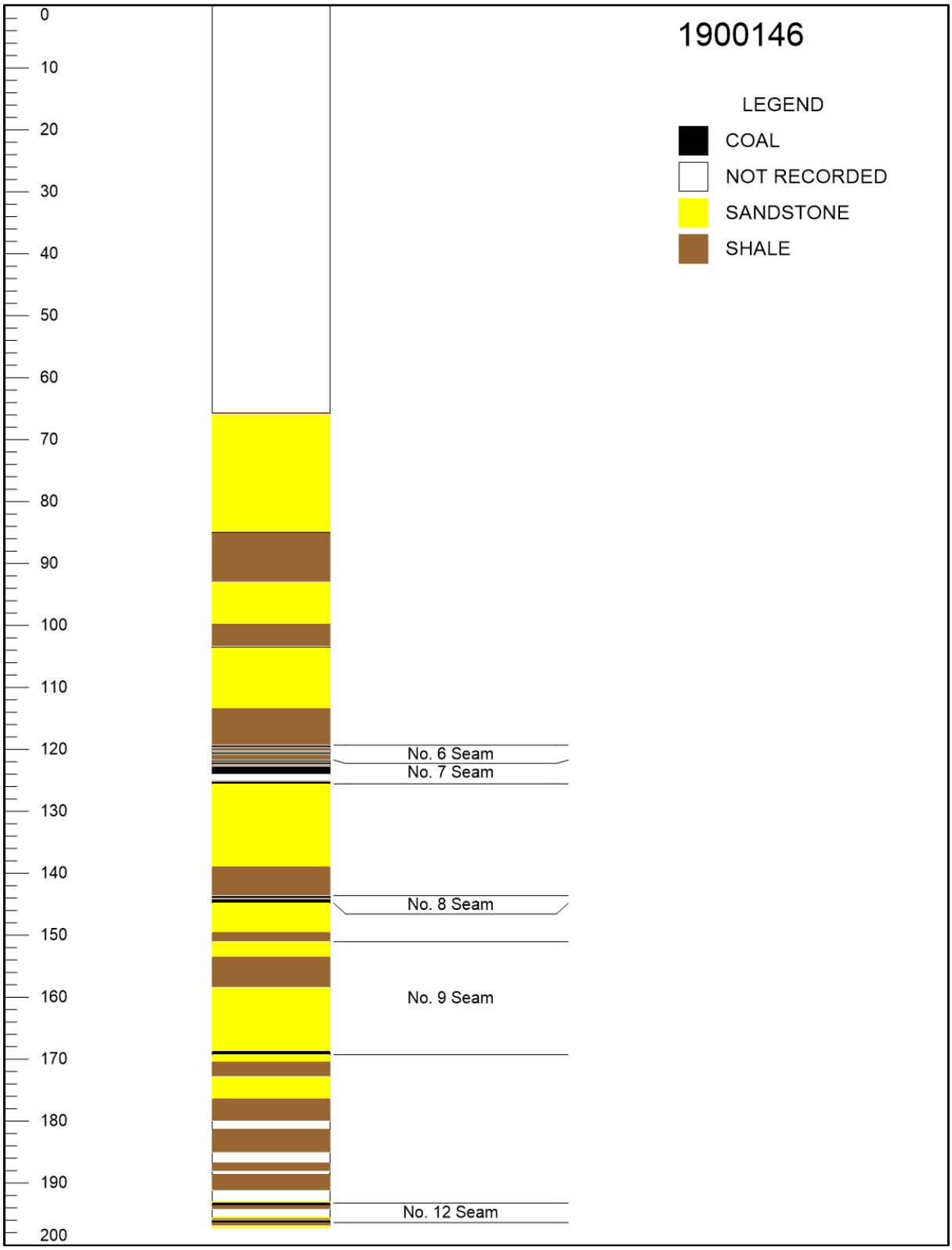

Appendix A6: Borehole 1900085 showing lithological variations.

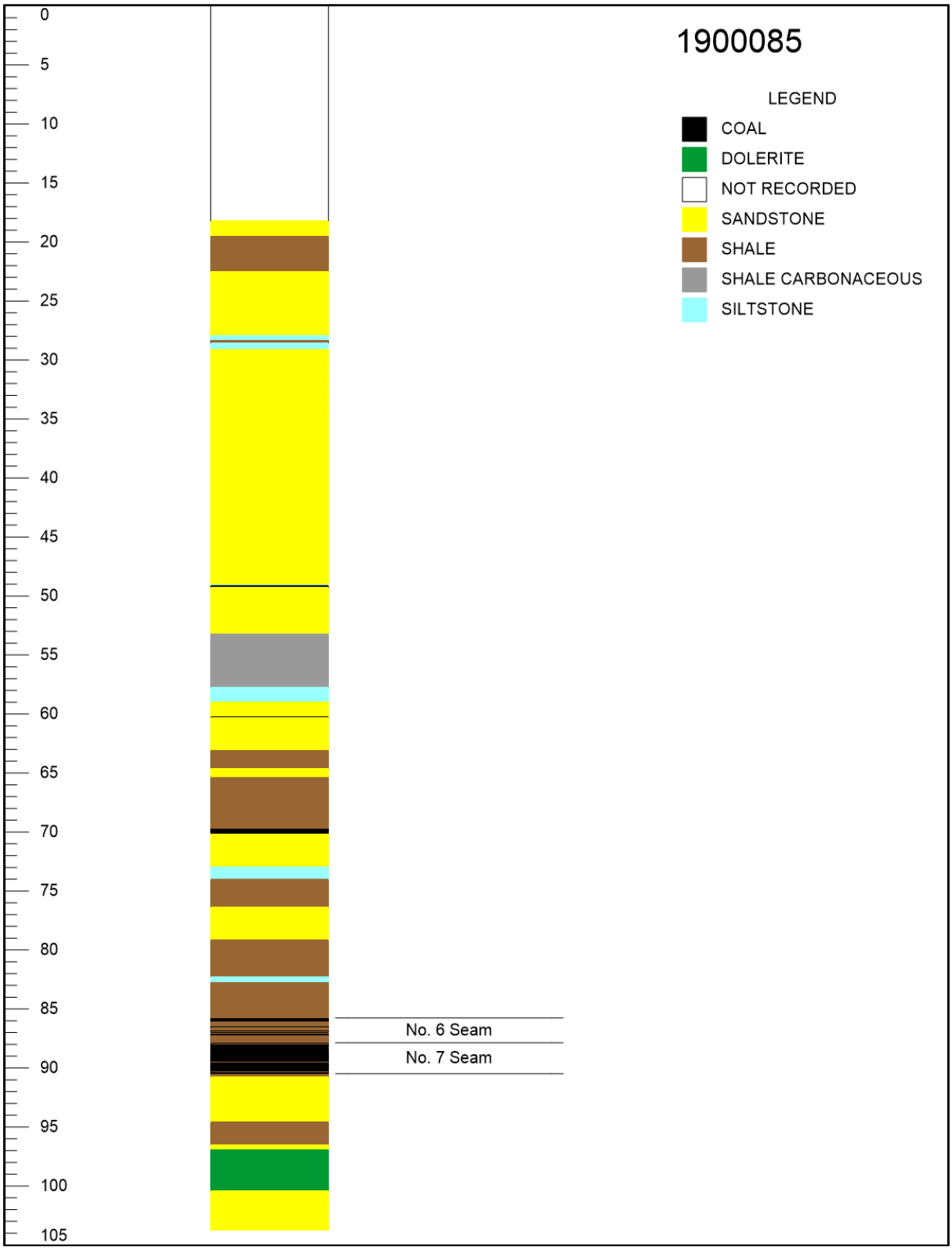

Appendix A7: Borehole 1900364 showing lithological variations.

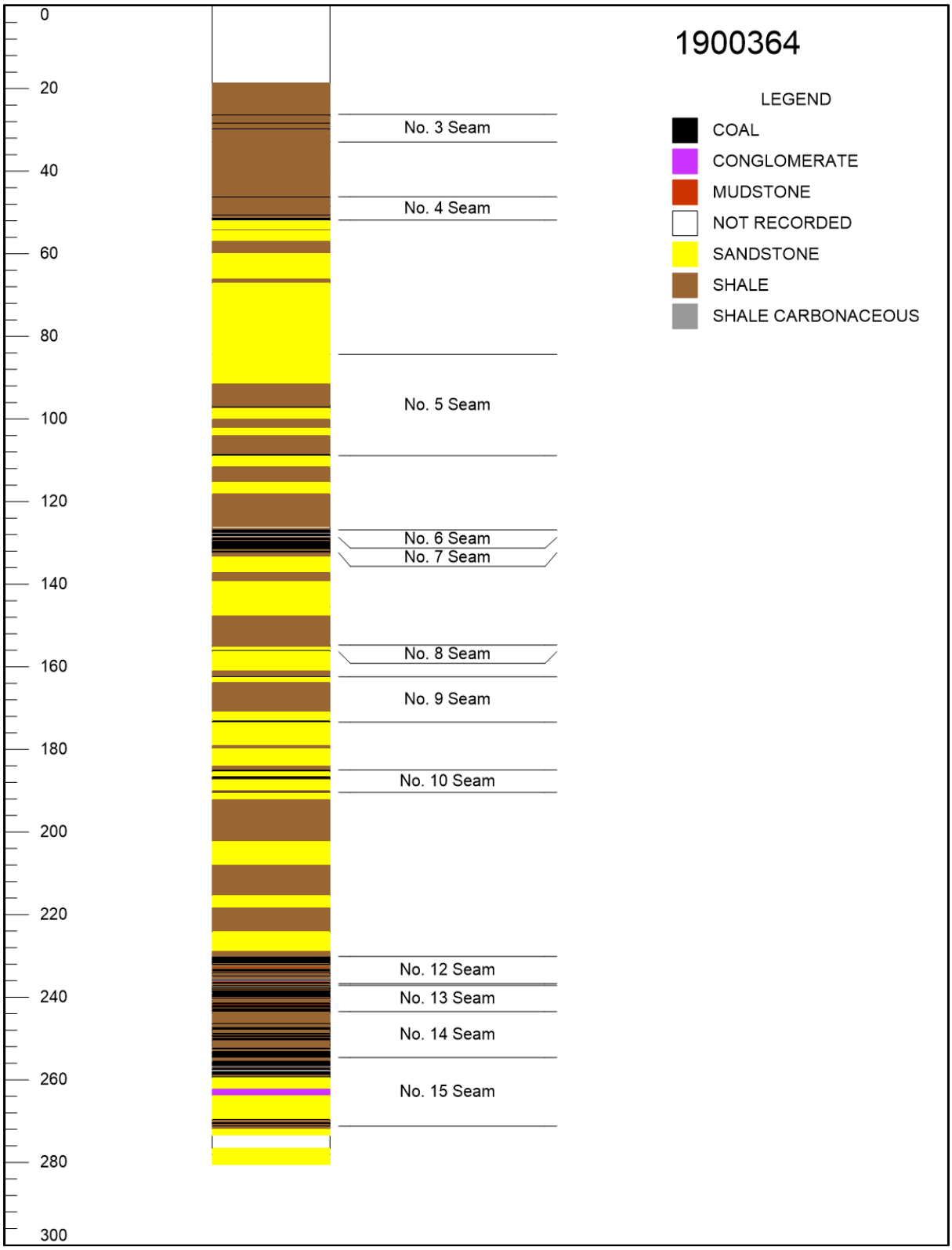

APPENDIX B: Rock Description

Appendix B1: Outcrop location, elevation, and attitude data

Sample ID	Coordinates		Elevation	Strike Direction	Dip direction	Dip Angle
	Longitude	Latitude				
TA1	30°48'55.70"E	22°30'00.90"S	370 m	N70°E	N340°W	24°
TA2	30°48'47.10"E	22°30'18.10"S	387 m	S95°E	N5°E	24°
TA3	30°48'45.85"E	22°30'22.80"S	384 m	S94°E	N4°E	24°
TA4	30°48'40.30"E	22°30'42.50"S	369 m	N/A	N/A	N/A
TA5	30°48'41.60"E	22°30'47.90"S	385 m	S110°E	N20°E	19°
TA6	30°48'43.40"E	22°30'51.40"S	381 m	N/A	N/A	N/A
TA7	30°48'57.60"E	22°31'11.30"S	367 m	N/A	N/A	N/A
TA8	30°48'38.00"E	22°31'23.90"S	421 m	S132°E	N42°E	24°
TB1	30°48'14.08"E	22°31'03.60"S	387 m	N74°E	N344°W	25°
TB2	30°48'07.30"E	22°30'51.53"S	401 m	N/A	N/A	N/A
TB3	30°48'07.30"E	22°30'42.44"S	408 m	S107°E	N17°E	18°
TB4	30°48'08.30"E	22°30'37.50"S	410 m	N/A	N/A	N/A
TB5	30°48'24.10"E	22°30'18.00"S	413 m	N/A	N/A	N/A
TC1	30°47'43.46"E	22°30'02.44"S	364 m	S106°E	N16°E	11°

Appendix B1: Continued…

Sample ID	Coordinates		Elevation	Strike Direction	Dip Direction	Dip Angle
	Longitude	Latitude				
TC2	30°47'45.70"E	22°30'11.40"S	378 m	N86°E	N356°W	24°
TC3	30°47'50.90"E	22°30'31.40"S	402 m	N/A	N/A	N/A
TC4	30°47'43.50"E	22°30'49.90"S	395 m	N73°E	N343°W	32°
TC5	30°47'45.70"E	22°31'00.10"S	392 m	N/A	N/A	N/A
TC6	30°47'48.90"E	22°31'04.50"S	373 m	N42°E	N312°W	16°
TC7	30°47'34.40"E	22°31'26.10"S	402 m	S96°E	N06°E	34°
TD1	30°47'12.20"E	22°31'04.30"S	385 m	N74°E	N344°W	21°
TD2	30°47'12.00"E	22°30'33.90"S	399 m	N81°E	N351°W	24°
TD3	30°47'08.29"E	22°30'15.65"S	384 m	S106°E	N16°E	43°
TD4	30°47'19.86"E	22°30'03.12"S	381 m	N/A	N/A	N/A
TE1	30°46'45.40"E	22°30'22.60"S	380 m	S103°E	N13°E	43°
TE2	30°46'43.90"E	22°30'36.40"S	398 m	N/A	N/A	N/A
TE3	30°46'43.70"E	22°31'02.30"S	418 m	N/A	N/A	N/A
TE4	30°46'51.70"E	22°31'20.20"S	393 m	N69°E	N339°W	25°
TF1	30°46'10.70"E	22°31'23.80"S	411 m	N/A	N/A	N/A
TF2	30°46'10.30"E	22°31'01.00"S	428 m	N41°E	N311°W	31°

Appendix B1: Continued…

Sample ID	Coordinates		Elevation	Strike Direction	Dip Direction	Dip Angle
	Longitude	Latitude				
TF3	30°46'08.90"E	22°30'53.60"S	416 m	N/A	N/A	N/A
TF4	30°46'13.00"E	22°30'33.90"S	384 m	N87°E	N357°W	08°
TF5	30°46'14.30"E	22°30'25.50"S	387 m	N81°E	N351°W	15°
TF6	30°46'12.80"E	22°30'22.00"S	420 m	N80°E	N350°W	15°

Appendix B2: Rock Description

ID	Mineral Composition	Colour and Texture	Description	Rock Name
TA1	Quartz, Mica	Pinkish, interlocking crystalline structure		Pink Quartzite
TA2	Quartz, Mica	Reddish, interlocking crystalline structure		Red Quartzite
TA3	Clay Minerals	Reddish, fine texture		Mudstone
TA4	Mafic Minerals	Greenish, aphanitic		Basalt
TA5	Quartz, Mica	Brownish, Interlocking crystalline structure		Pink Quartzite
TA6	Mafic Minerals	Greenish, aphanitic	Outcrop localised	Basalt
TA7	Quartz	Whitish		Quartz Vein
TA8	Quartz, Mica	Pinkish, interlocking crystalline structure	Presence of quartz veinlets	Pink Quartzite
TB1	Quartz, feldspars, and mica minerals	Whitish, sand sized grains		Quartz Arenite
TB2	Mafic Minerals	Greenish, aphanitic		Basalt
TB3	Quartz, Mica	Reddish, Interlocking crystalline structure		Red Quartzite

Appendix B2: Continued…

ID	Mineral Composition	Colour and Texture	Description	Rock Name
TB4	Mafic Minerals	Greenish, aphanitic	Presence of quartz veinlets	Basalt
TB5	Quartz	White		Quartz Vein
TC1	Clay minerals	Dark brown, very fine texture, exhibiting fissility	Outcrop highly fractured and weathered	Carbonaceous Shale
TC2	Quartz, Mica	Pinkish, Interlocking crystalline structure		Pink Quartzite
TC3	Quartz	White		Quartz Vein
TC4	Quartz, Mica	Pinkish, Interlocking crystalline structure		Pink Quartzite
TC5	Mafic minerals	Greenish, aphanitic		Basalt
TC6	Clay minerals	Grey, very fine texture, exhibiting fissility	Outcropping along Mbodi River	Shale

Appendix B2: Continued…

ID	Mineral Composition	Colour and Texture	Description	Rock Name
TC7	Quartz, feldspar, and mica minerals	Brown, sand sized grains		Quartz Arenite
TD1	Clay minerals	Dark brown, very fine texture, exhibiting fissility	Outcrop highly fractured	Carbonaceous Shale
TD2	Quartz, Mica	Brownish, Interlocking crystalline structure		Pink Quartzite
TD3	Quartz, Mica Minerals	Brown, sand sized grains		Quartz Arenite
TD4	Quartz	White		Quartz Vein
TC7	Quartz, feldspar and mica minerals	Brown, sand sized grains		Quartz Arenite
TD1	Clay minerals	Dark brown, very fine texture, exhibiting fissility	Outcrop highly fractured	Carbonaceous Shale
TD2	Quartz, Mica	Brownish, Interlocking crystalline structure		Pink Quartzite

Appendix B2: Continued…

ID	Mineral Composition	Colour and Textures	Description	Rock Name
TD3	Quartz, Mica Minerals	Brown, sand sized grains		Quartz Arenite
TD4	Quartz	White		Quartz Vein
TE1	Quartz, Mica	Brownish, Interlocking crystalline structure		Pink Quartzite
TE2	Quartz	White		Quartz Vein
E3	Carbonate minerals	Whitish	Sample reacts with diluted hydrochloric acid	Calcrete
E4	Quartz	White, sand sized grains		Quartz Arenite
F1	Carbonate minerals	Whitish	Sample reacts with diluted hydrochloric acid	Calcrete
F2	Quartz, Mica	Pinkish, Interlocking crystalline structure		Pink Quartzite

Appendix B2: Continued…

ID	Mineral Composition	Colour and Textures	Description	Rock Name
F3	Quartz	White		Quartz Vein
F4	Clay minerals	Dark brown, very fine texture	Outcrop highly fractured	Shale
F5	Quartz, feldspar and mica minerals	Light brown, sand sized grains	Outcrop exhibits bedding planes	Quartz Arenite
F6	Quartz	Whitish, sand sized grains	Outcrop exhibits bedding planes	Quartz Arenite

Appendix C: XRF Results for analysed rock samples

Table C1: Results for major oxides

	SiO_2	TiO_2	Al_2O_3	Fe_2O_3	MnO	MgO	CaO	Na_2O	K_2O	P_2O_5
TA3	66.26	0.69	14.96	7.28	0.15	3.21	1.48	1.32	4.36	0.10
TB4	60.07	0.805	15.76	7.69	0.104	4.0692	3.53	1.719	5.25	0.119
TA4	50.06	1.39	13.52	14.48	0.19	6.59	10.15	2.51	0.61	0.16
TA6	50.96	1.58	11.75	15.24	0.30	5.99	9.75	3.31	0.57	0.25
TB5	99.03	0.00	0.00	0.81	0.01	0.00	0.04	0.00	0.09	0.01
TF3	99.05	0.01	0.00	0.81	0.01	0.00	0.03	0.00	0.08	0.01
TE3	17.85	0.06	0.00	0.42	0.09	21.14	46.30	12.61	0.68	0.76
TF1	16.46	0.07	0.00	0.52	0.03	3.86	64.91	12.50	0.64	0.93
TF6	95.53	0.07	2.43	0.75	0.01	0.28	0.07	0.00	0.79	0.02
TE4	94.50	0.09	3.92	0.87	0.01	0.01	0.10	0.00	0.41	0.05
TC6	60.31	1.30	34.72	0.95	0.00	0.59	0.39	0.00	1.21	0.16
TC1	62.92	1.72	16.80	14.42	0.13	0.56	0.34	0.17	2.51	0.08
TC2	91.87	0.10	3.28	1.20	0.19	0.34	1.80	0.19	0.89	0.05
TA2	91.44	0.20	2.46	3.09	0.07	0.49	1.88	0.18	0.04	0.05

Table C2: Trace elements associated with host rocks

	TA3	TB4	TA4	TA6	TB5	TF3	TE3	TF1	TF6	TE4	TC6	TC1	TC2	TA2
Sc	<3	<3	<3	<3	<3	<3	4.2	5.9	<3	<3	<3	<3	<3	<3
V	173.0	199.7	341.3	378.8	<1	<1	10.9	15.9	17.3	15.2	269.7	379.3	25.3	56.3
Cr	43.6	50.6	99.5	79.5	43.9	9.0	4.0	6.3	17.0	19.6	68.1	90.0	5.1	18.9
Co	18.6	17.4	36.0	37.4	2.0	2.1	1.0	1.2	1.9	2.2	2.5	35.6	3.8	8.4
Ni	122.5	111.9	134.9	94.6	8.6	2.7	40.2	126.6	4.8	27.4	66.5	<1	217.0	43.8
Cu	5.0	<2	274.4	222.8	15.2	10.5	2.8	3.5	12.7	20.7	204.1	64.1	39.6	27.2
Zn	111.5	125.8	151.5	147.9	2.7	<2	116.7	10.4	4.5	22.1	42.8	97.2	31.7	34.7
Ga	16.3	17.6	15.2	16.9	2.4	3.0	2.5	2.2	4.5	4.4	58.2	17.7	5.2	6.2
Ge	1.2	1.5	1.2	1.2	1.2	1.2	1.2	1.2	1.4	1.3	1.7	1.5	1.2	1.3
As	<4	<4	<4	<4	<4	<4	<4	<4	<4	<4	13.1	4.7	1.2	2.4
Rb	107.9	126.6	18.9	15.7	<2	2.8	9.1	5.2	25.8	23.1	89.6	74.5	29.8	<2
Sr	79.6	64.9	182.7	88.5	4.4	7.6	455.6	163.6	26.9	36.6	507.0	69.4	55.7	428.1
Y	32.1	35.1	16.9	16.9	<1	1.0	12.4	4.3	9.6	6.4	55.5	31.4	18.3	10.3
Zr	135.6	154.5	108.6	110.5	<3	6.4	84.1	51.8	254.4	76.8	408.2	558.0	73.2	126.9
Nb	4.9	5.8	4.1	4.8	<1	<1	2.7	<1	2.2	3.1	27.1	13.8	2.0	2.9
Mo	<2	<2	<2	<2	<2	<2	<2	<2	<2	<2	<2	<2	<2	<2
Ag	0.4	0.2	0.2	0.6	0.5	0.4	0.5	0.3	0.6	0.5	0.6	0.3	0.5	0.5
Cd	0.1	0	0.1	0.1	0.1	0.1	0.1	0.0	0.1	0.1	0.1	0.1	0.1	0.1

Table C2: Continued…

	TA3	TB4	TA4	TA6	B5	F3	E3	F1	F6	E4	C6	C1	C2	A2
Sn	2.9	2.4	2.7	3.4	2.7	2.9	2.8	2.1	3.2	2.7	3.4	2.5	2.8	2.7
Sb	0.2	0.4	0.8	0.5	0.3	0.0	0.0	0.2	0.0	0.5	0.0	0.5	0.0	0.0
Cs	5.4	5.4	5.4	5.4	5.4	5.4	5.5	5.4	5.4	5.4	5.5	5.4	5.4	5.4
Ba	570.3	659.2	1097.9	1234.4	60.0	62.3	101.8	106.5	113.4	99.8	1027.4	1338.4	136.3	204.1
La	85.4	91.6	170.3	182.8	<10	<10	<10	<10	<10	<10	31.4	181.7	11.5	33.7
W	<3	12.6	<3	<3	<3	<3	<3	<3	<3	<3	<3	<3	<3	<3
Ta	<2	<2	3.3	2.7	<2	<2	<2	<2	<2	<2	2.5	<2	<2	<2
Hf	4.1	<3	30.1	27.5	5.3	<3	<3	<3	10.4	4.6	37.9	4.3	9.2	7.4
Tl	<3	<3	3.0	<3	<3	<3	<3	<3	<3	<3	<3	<3	<3	<3
Pb	28.6	17	4.2	3.5	2.5	5.0	15.6	4.1	14.9	19.7	121.6	44.6	10.8	22.4
Bi	<3	<3	<3	<3	<3	<3	<3	<3	<3	<3	<3	<3	<3	<3
Ce	152.2	140.5	174.2	135.8	<10	<10	<10	11.5	<10	<10	550.2	254.7	31.1	<10
Sm	<10	<10	33.4	20.8	<10	<10	<10	<10	<10	<10	<10	39.2	<10	<10
Eu	1.5	1.1	2.0	3.0	0.1	0.1	0.9	0.3	0.1	0.1	0.0	1.3	1.9	0.7
Gd	22.2	21.9	50.4	49.9	0.4	0.0	2.6	0.4	0.0	0.0	0.0	49.5	5.2	9.0
Tb	2.5	2.3	5.0	5.2	0.3	0.3	0.1	0.2	0.3	0.3	0.4	4.9	0.5	1.2
Dy	23.1	24.4	46.0	48.4	2.6	2.6	1.3	1.7	2.4	2.8	3.0	45.8	3.8	9.8
Er	17.3	3.8	34.1	35.5	1.9	1.9	0.9	1.2	1.8	2.1	2.3	34.3	2.9	7.4
Yb	52.7	49.6	66.9	53.9	4.1	<3	14.6	44.9	<3	10.7	24.5	14.9	77.3	19.5
Th	22.1	7.2	70.3	61.8	<3	<3	<3	<3	<3	<3	25.2	13.3	<3	3.7
U	<2	3.2	<2	<2	<2	<2	<2	<2	<2	<2	6.5	4.1	<2	2.1
S	71.9	7.4	61.8	35.4	0.0	0.0	111.6	167.0	0.0	5.7	118.2	3.4	0.0	51.4

Appendix D: Coal Petrography

Apjendix D1: Histograms for Mushithe coal, showing the frequency distribution of vitrinite across various reflectance categories. These histograms demonstrate a single peak or unimodal distribution in all samples

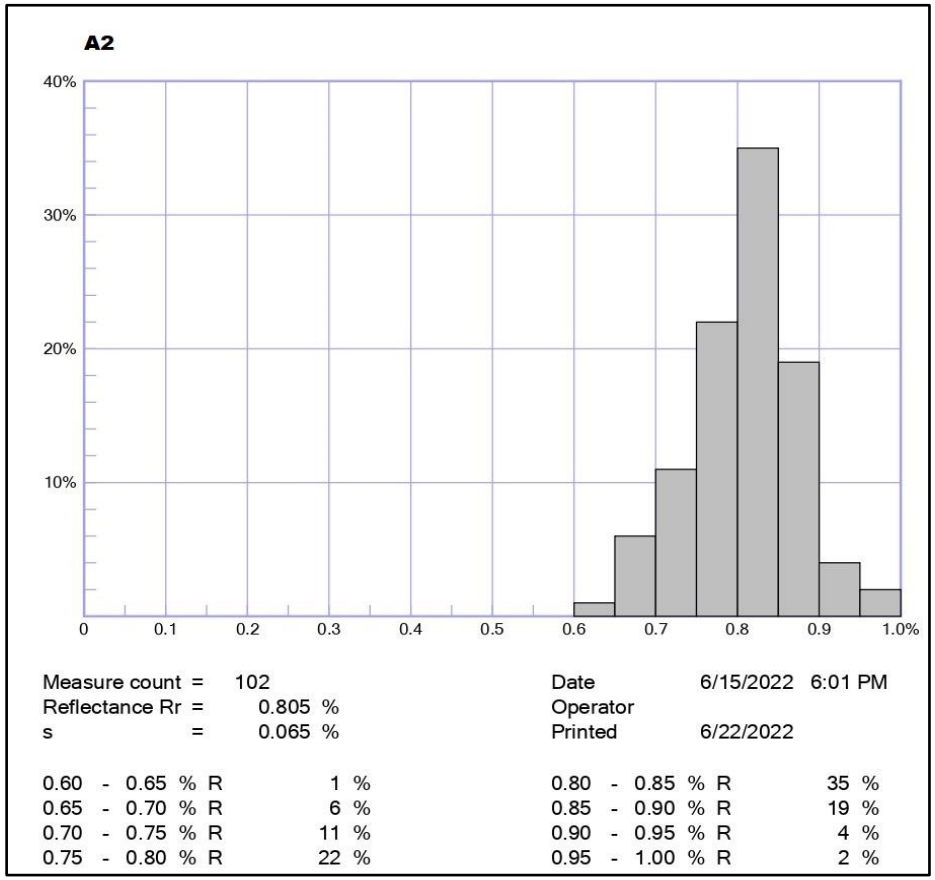

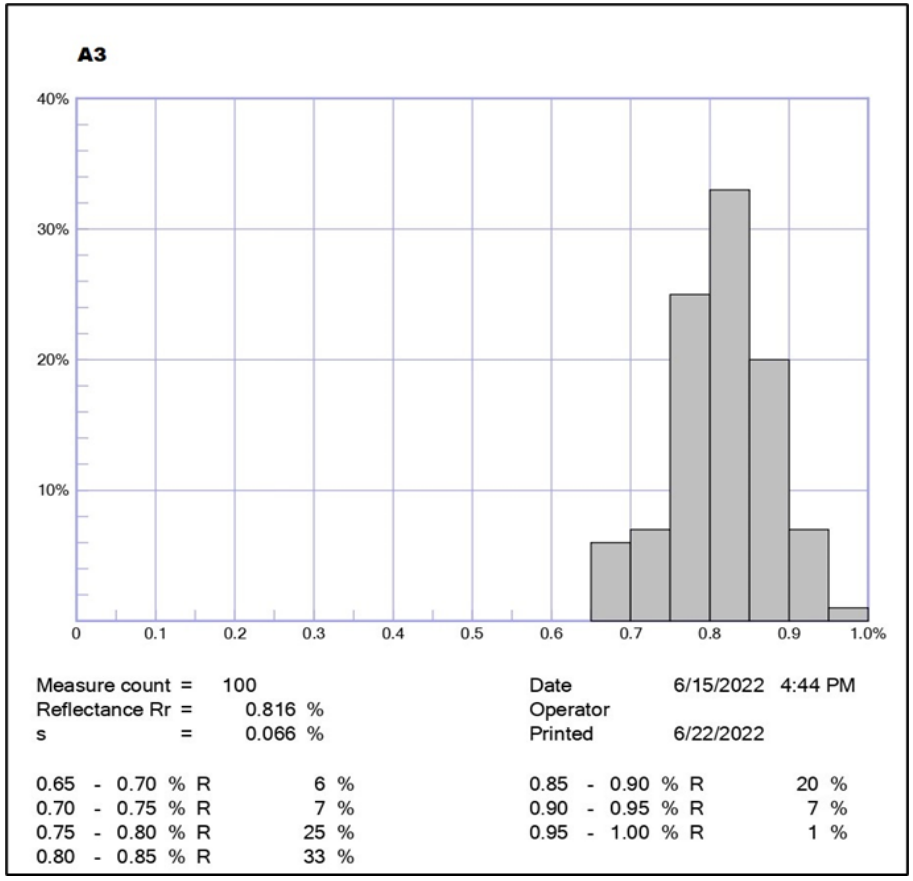

B1

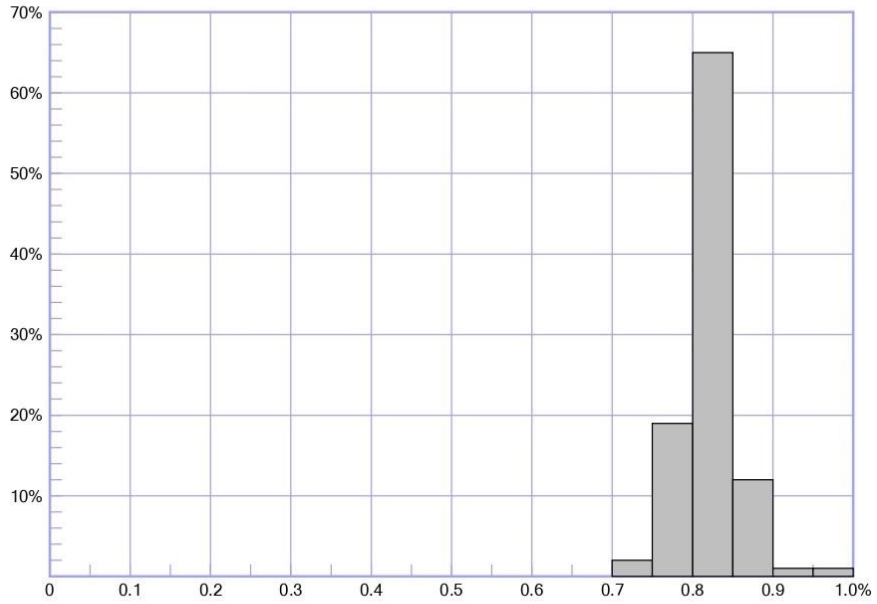

Measure count =	100	Date	6/14/2022 2:27 PM
Reflectance Rr =	0.817 %	Operator	
s =	0.034 %	Printed	6/22/2022

0.70 - 0.75 % R	2 %	0.85 - 0.90 % R	12 %
0.75 - 0.80 % R	19 %	0.90 - 0.95 % R	1 %
0.80 - 0.85 % R	65 %	0.95 - 1.00 % R	1 %

B2

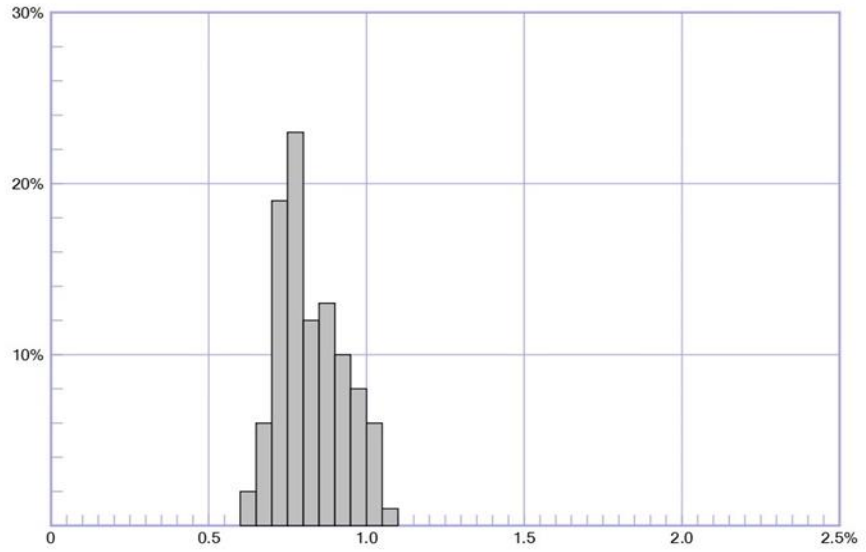

Measure count =	100	Date	6/15/2022 5:02 PM
Reflectance Rr =	0.818 %	Operator	
s =	0.102 %	Printed	6/22/2022

0.60 - 0.65 % R	2 %	0.85 - 0.90 % R	13 %
0.65 - 0.70 % R	6 %	0.90 - 0.95 % R	10 %
0.70 - 0.75 % R	19 %	0.95 - 1.00 % R	8 %
0.75 - 0.80 % R	23 %	1.00 - 1.05 % R	6 %
0.80 - 0.85 % R	12 %	1.05 - 1.10 % R	1 %

B3

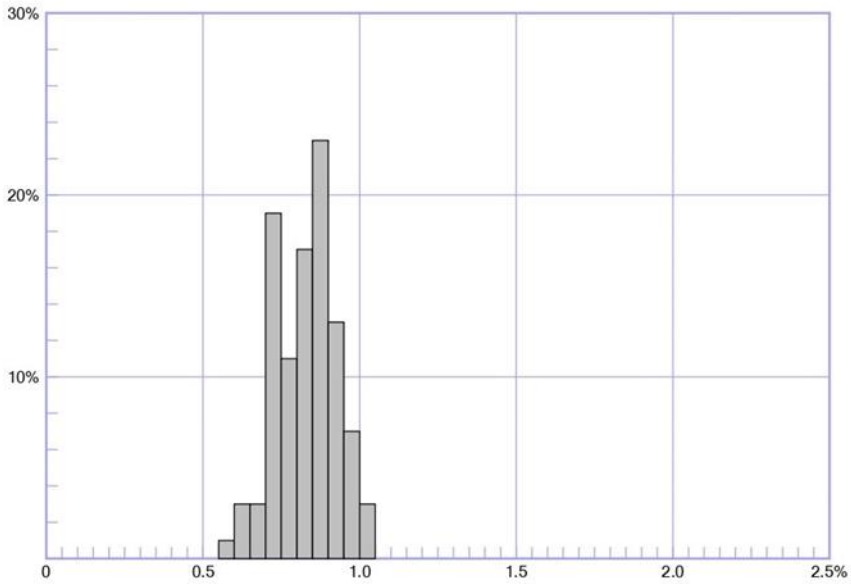

Measure count =	90	Date	6/15/2022 5:21 PM
Reflectance Rr =	0.821 %	Operator	
s =	0.096 %	Printed	6/22/2022

0.55 - 0.60 % R	1 %	0.80 - 0.85 % R	17 %
0.60 - 0.65 % R	3 %	0.85 - 0.90 % R	23 %
0.65 - 0.70 % R	3 %	0.90 - 0.95 % R	13 %
0.70 - 0.75 % R	19 %	0.95 - 1.00 % R	7 %
0.75 - 0.80 % R	11 %	1.00 - 1.05 % R	3 %

Appendix E: Host rock and coal samples XRD spectra

Coal A1 sample XRD spectra.

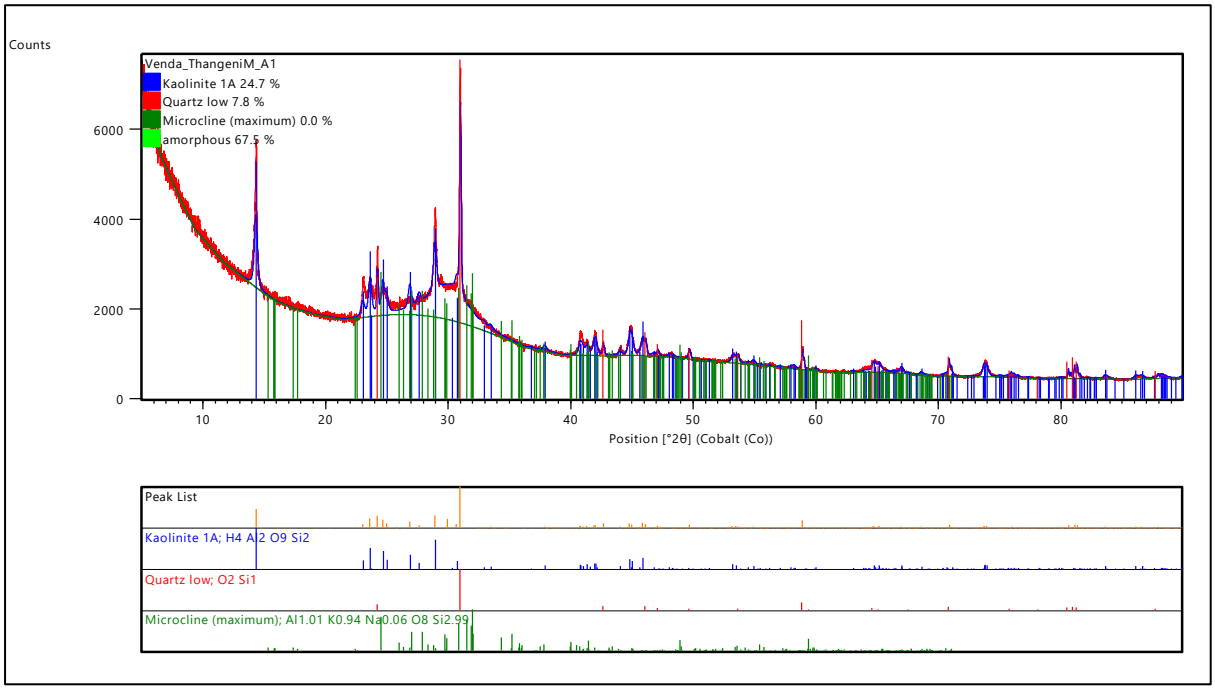

Coal A2 sample XRD spectra.

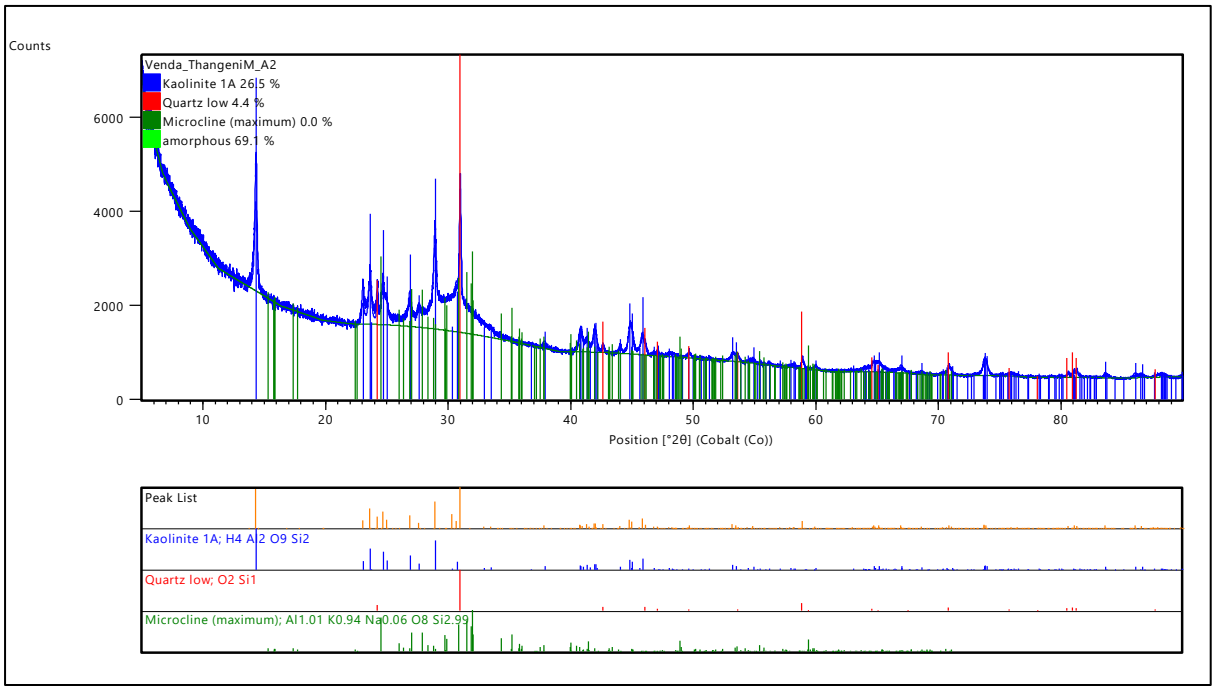

Coal A3 sample XRD spectra.

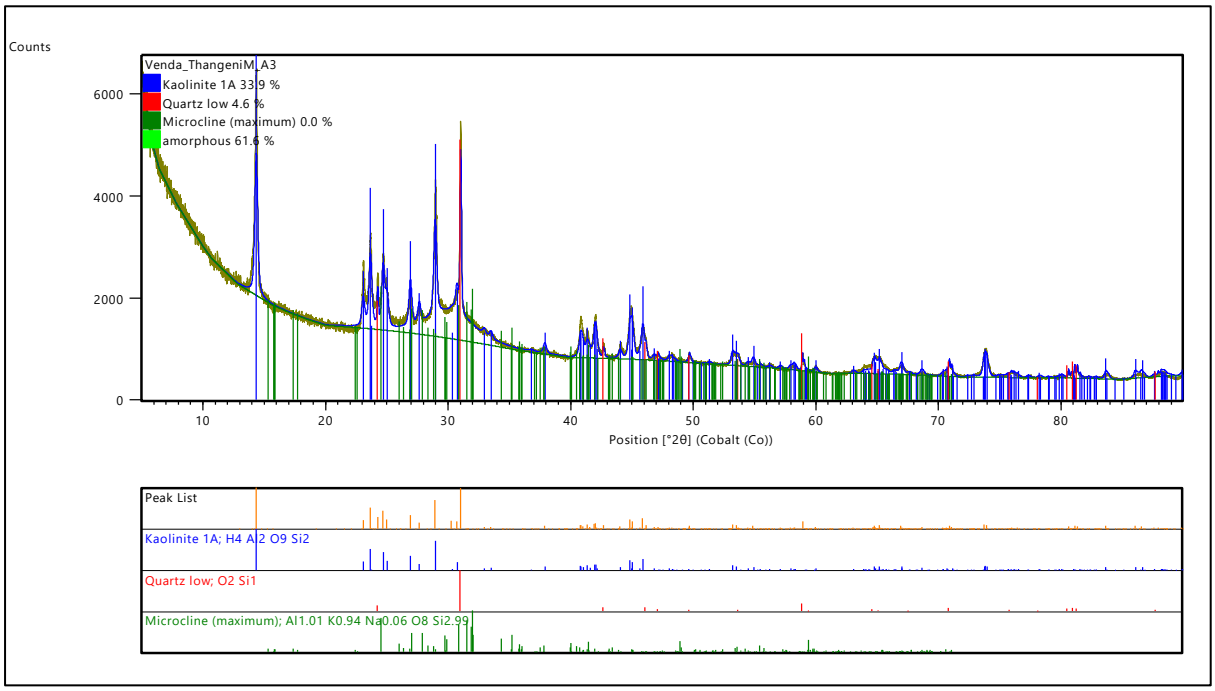

Coal B1 sample XRD spectra.

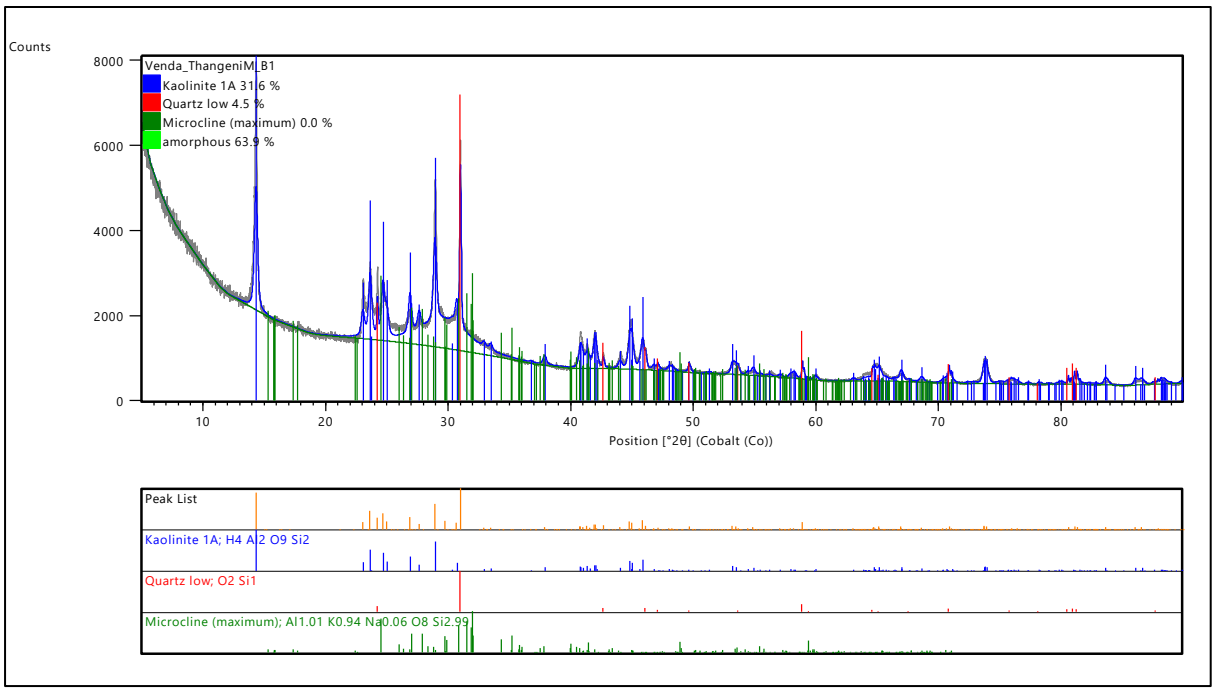

Coal B2 sample XRD spectra.

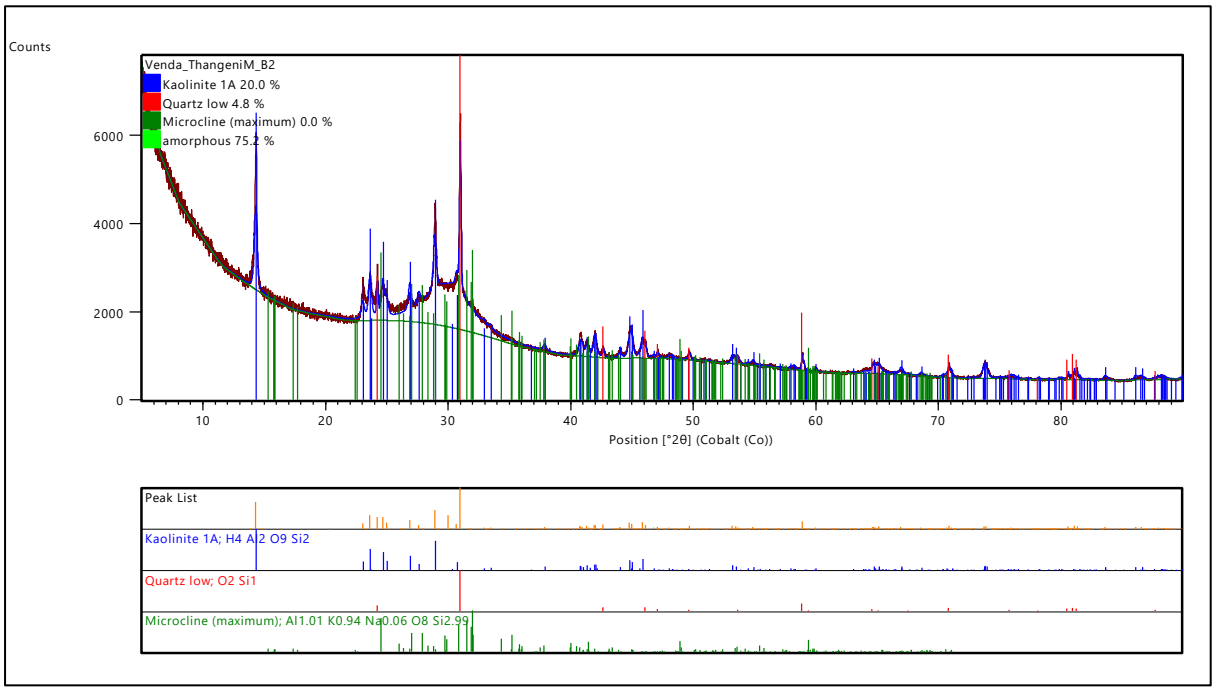

Coal B3 sample XRD spectra.

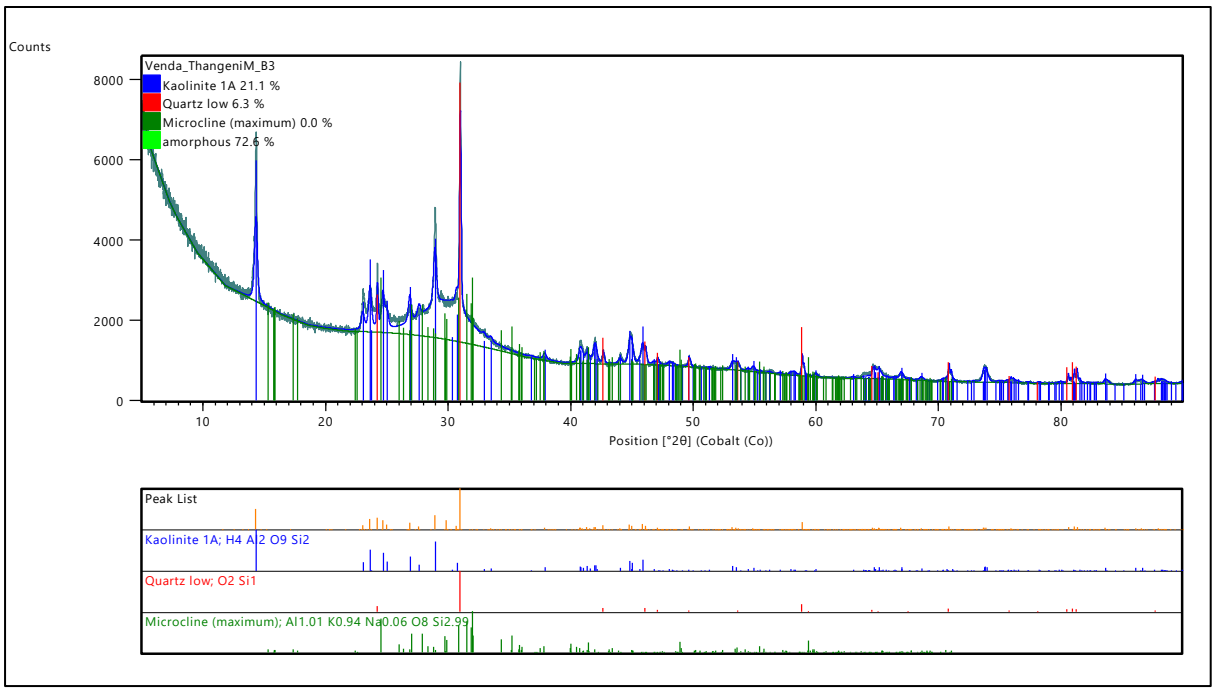

Sample TA3 XRD spectra.

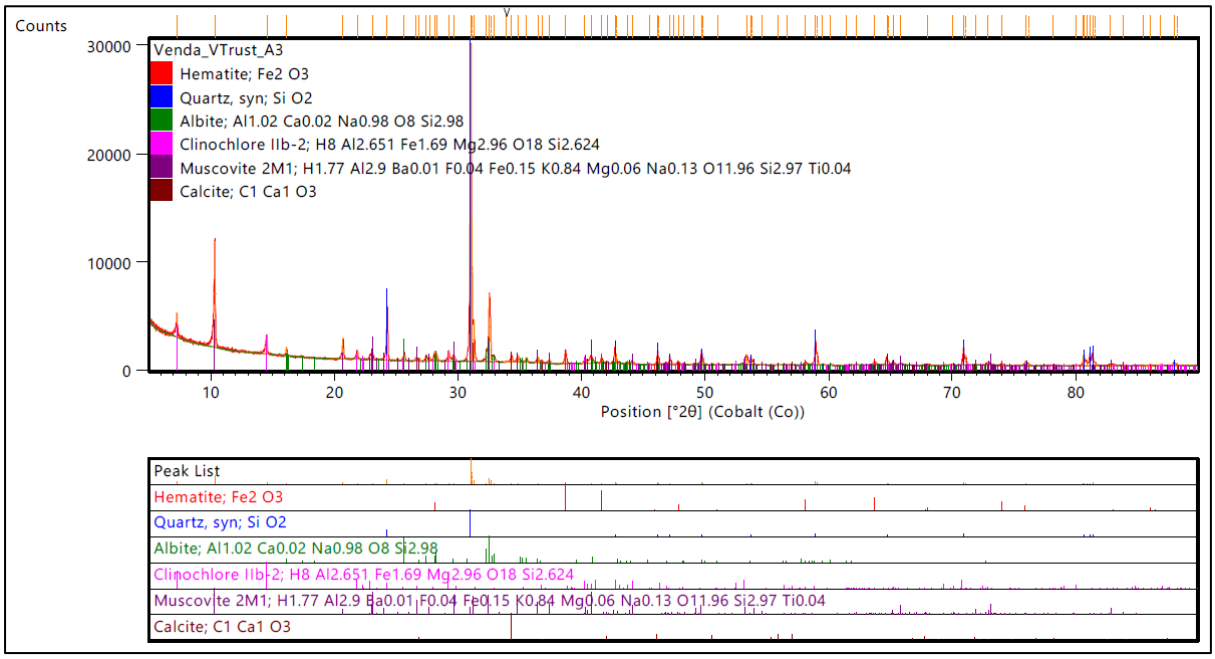

Sample TB4 XRD spectra.

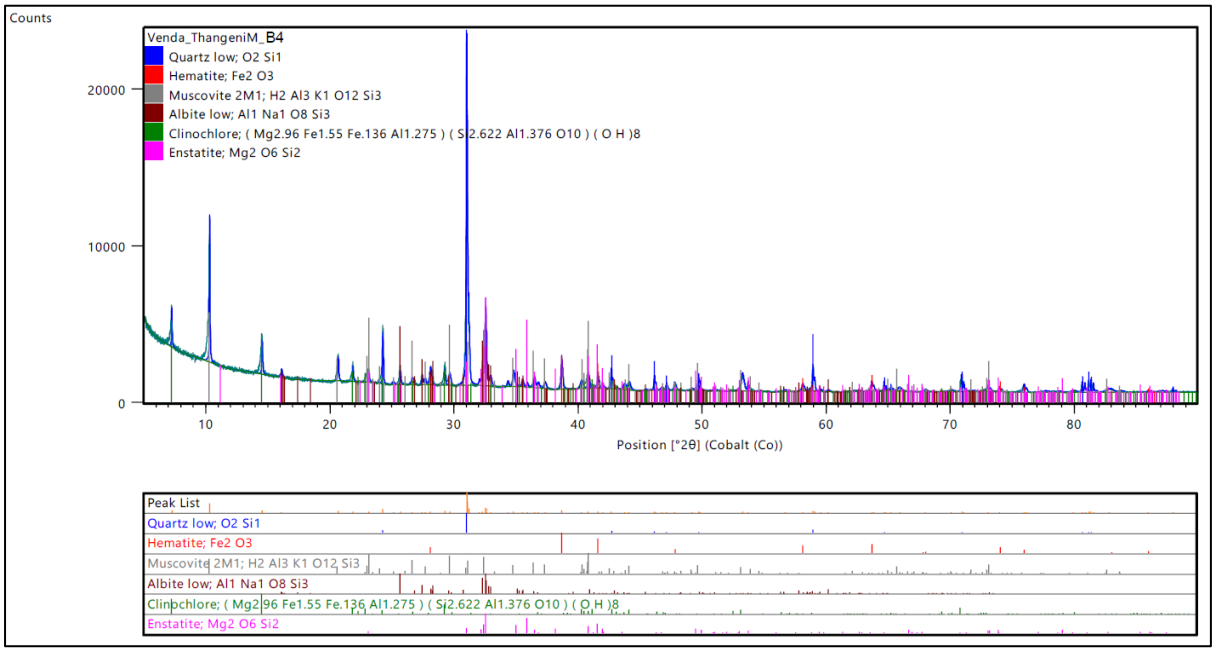

Sample TA4 XRD spectra.

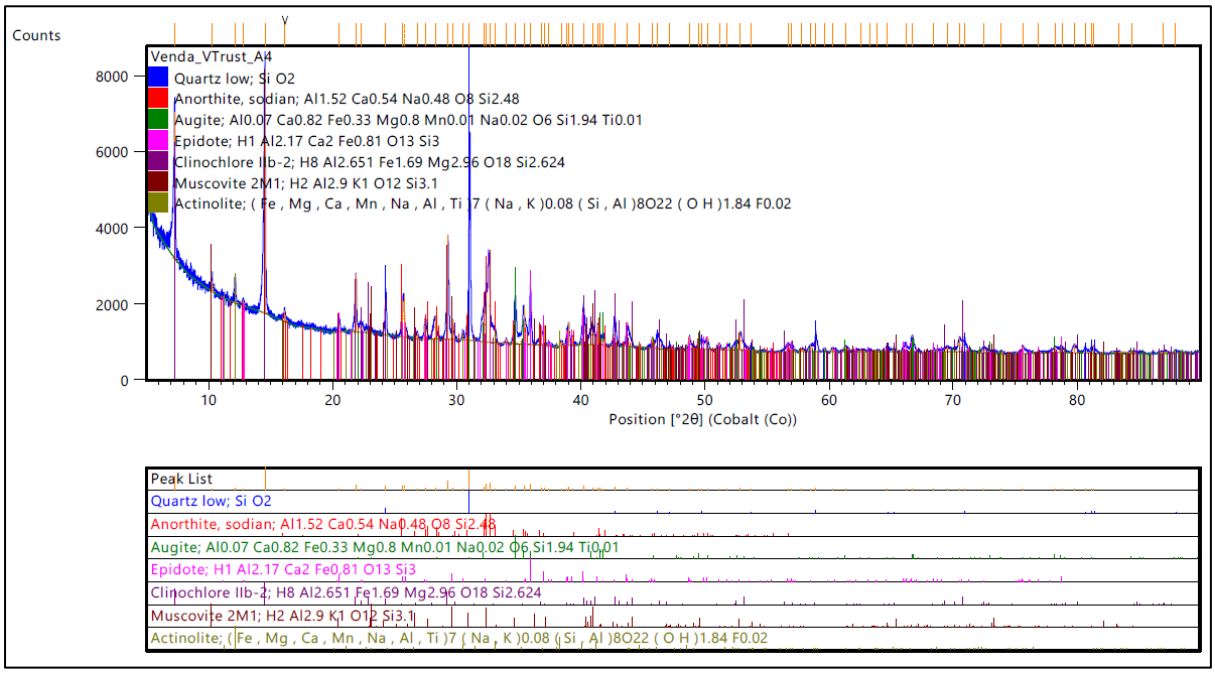

Sample TA6 XRD spectra.

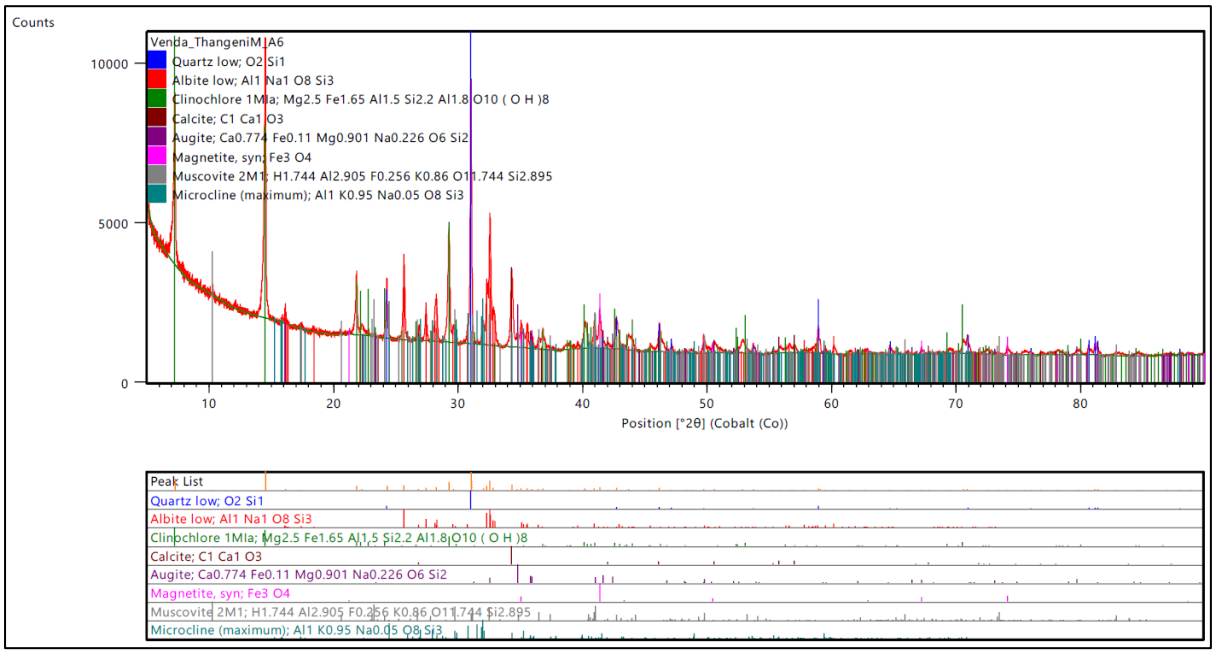

Sample TB5 XRD spectra.

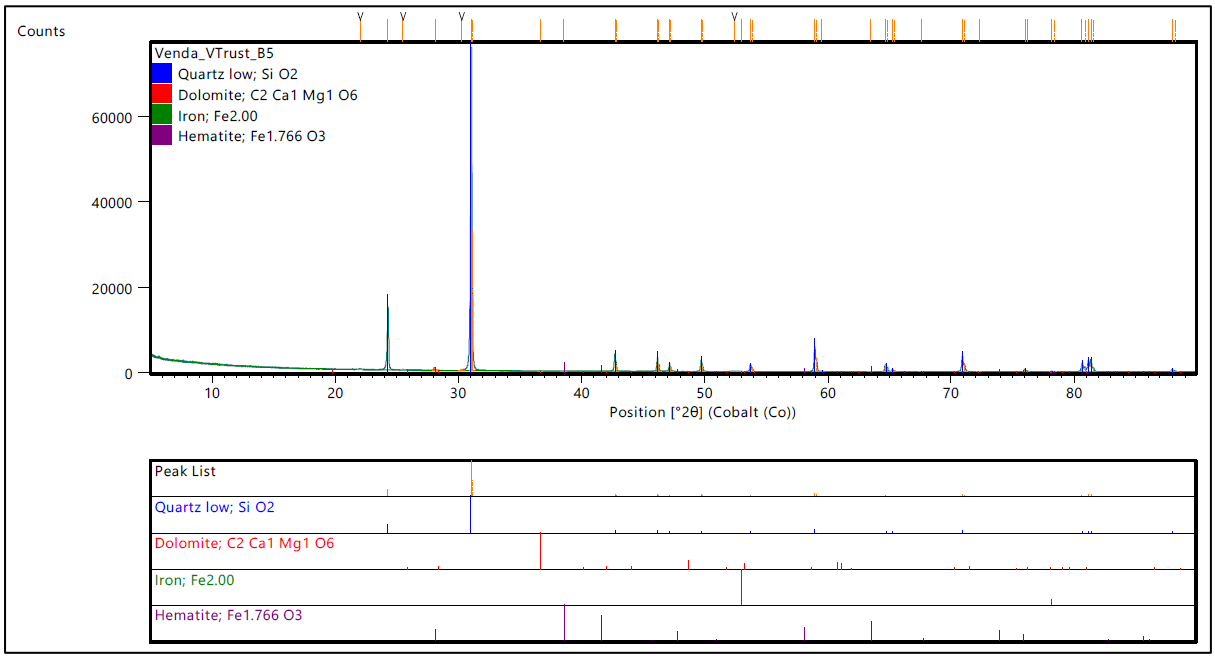

Sample TF3 XRD spectra.

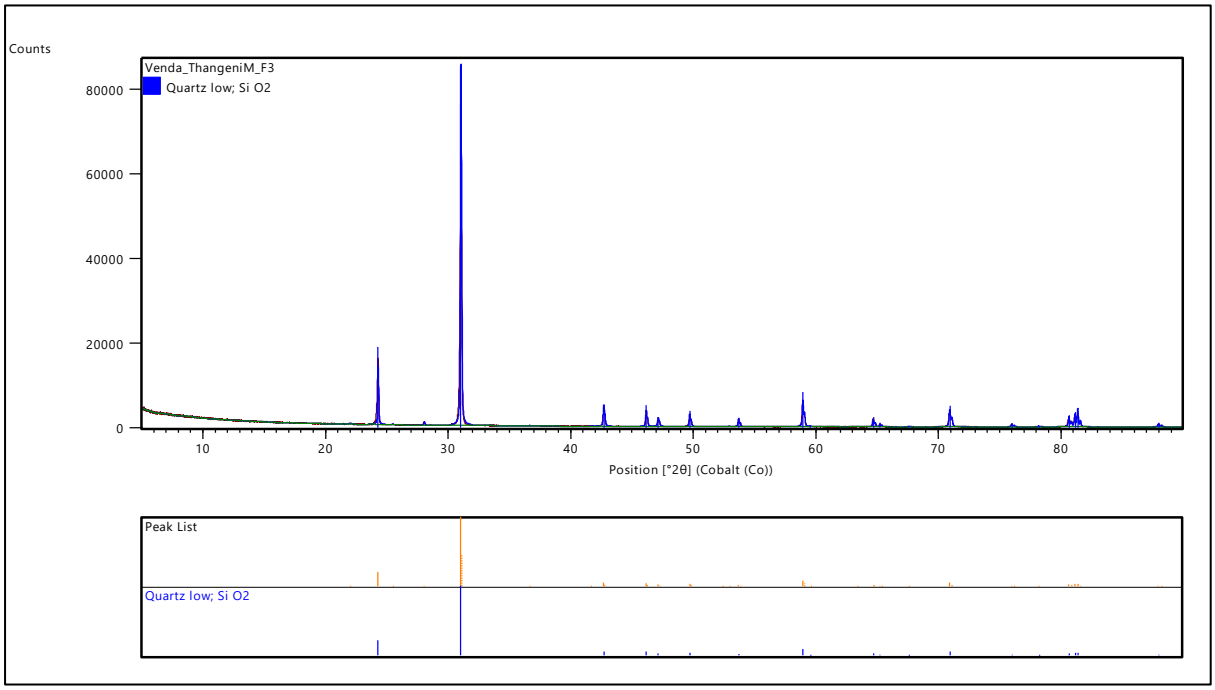

Sample TE3 XRD spectra.

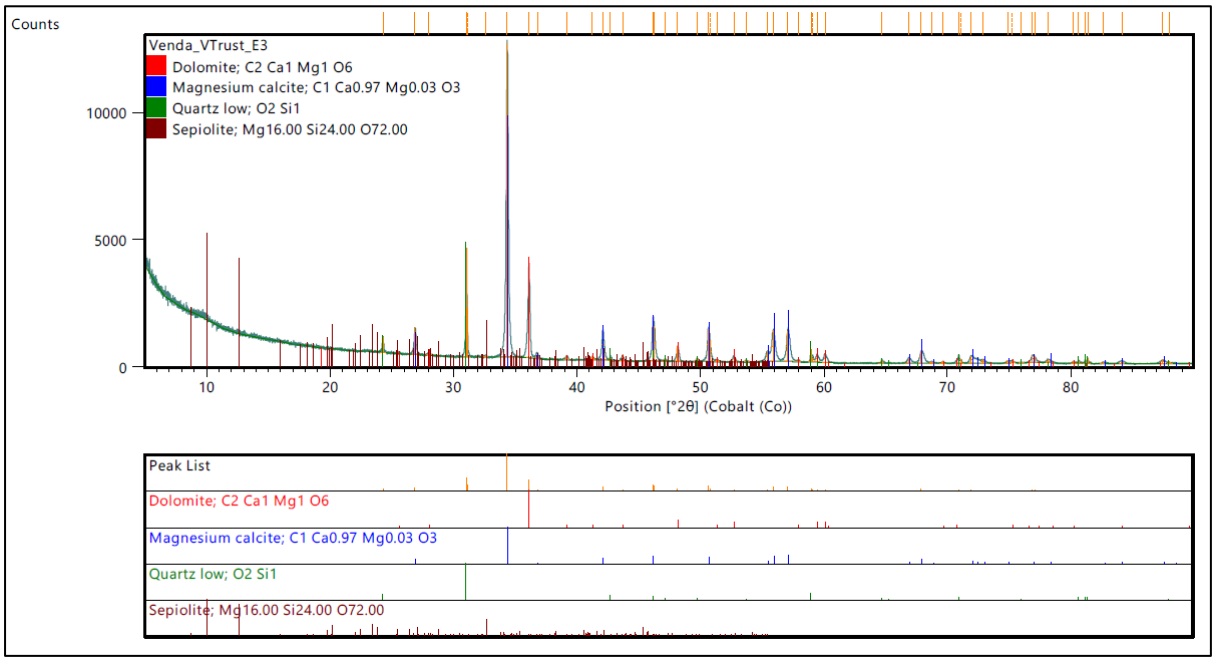

Sample TF1 XRD spectra.

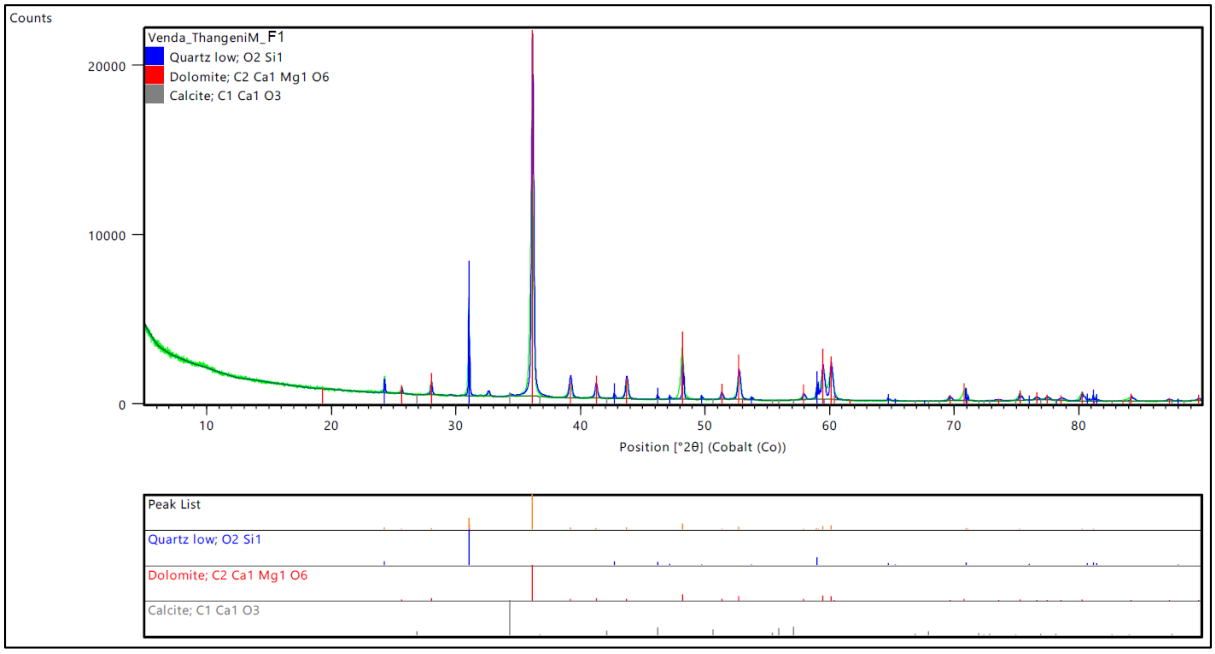

Sample TF6 XRD spectra.

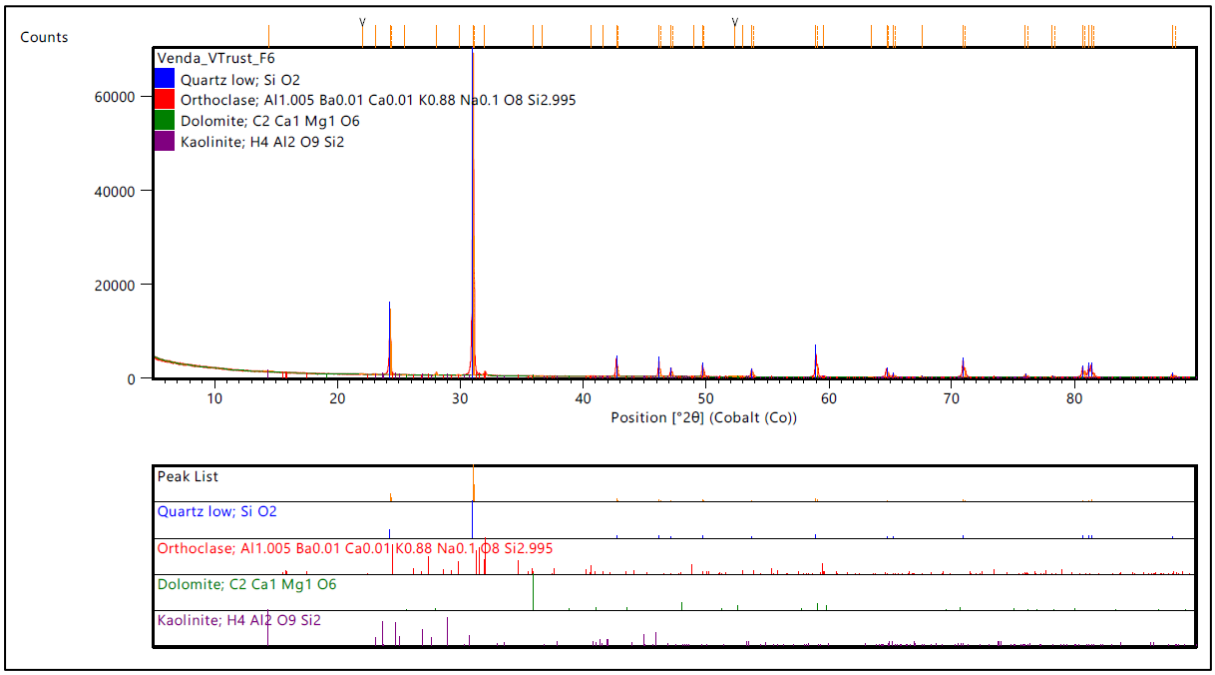

Sample TE4 XRD spectra.

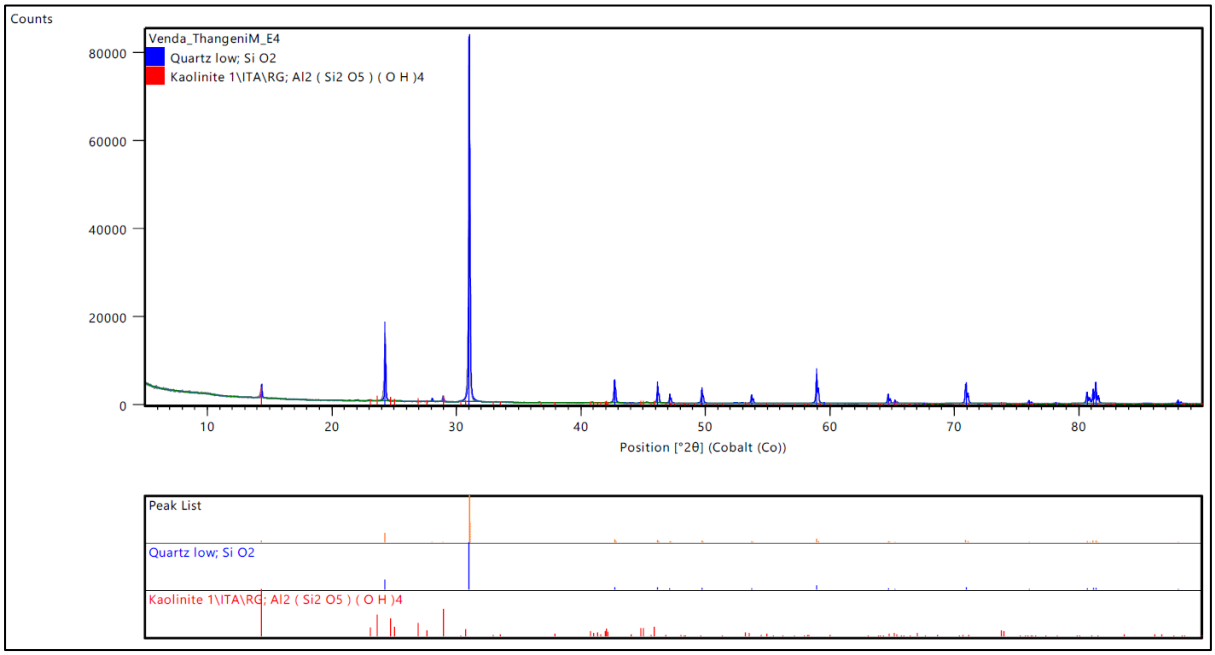

Sample TC6 XRD spectra.

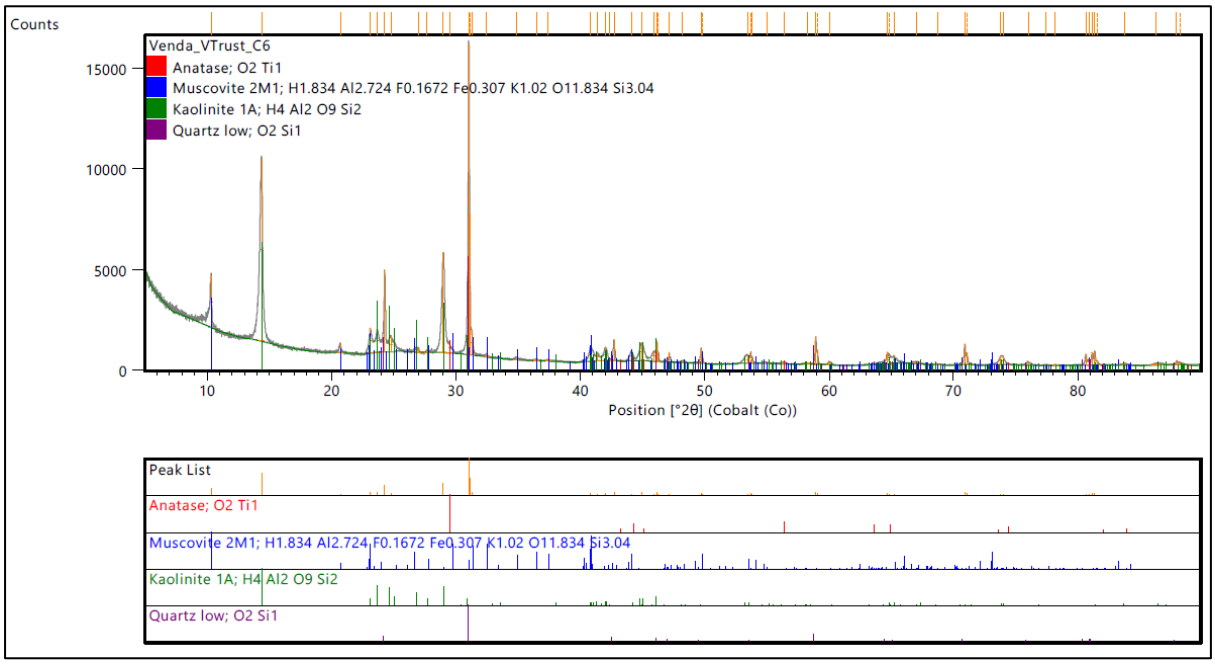

Sample TC1 XRD spectra.

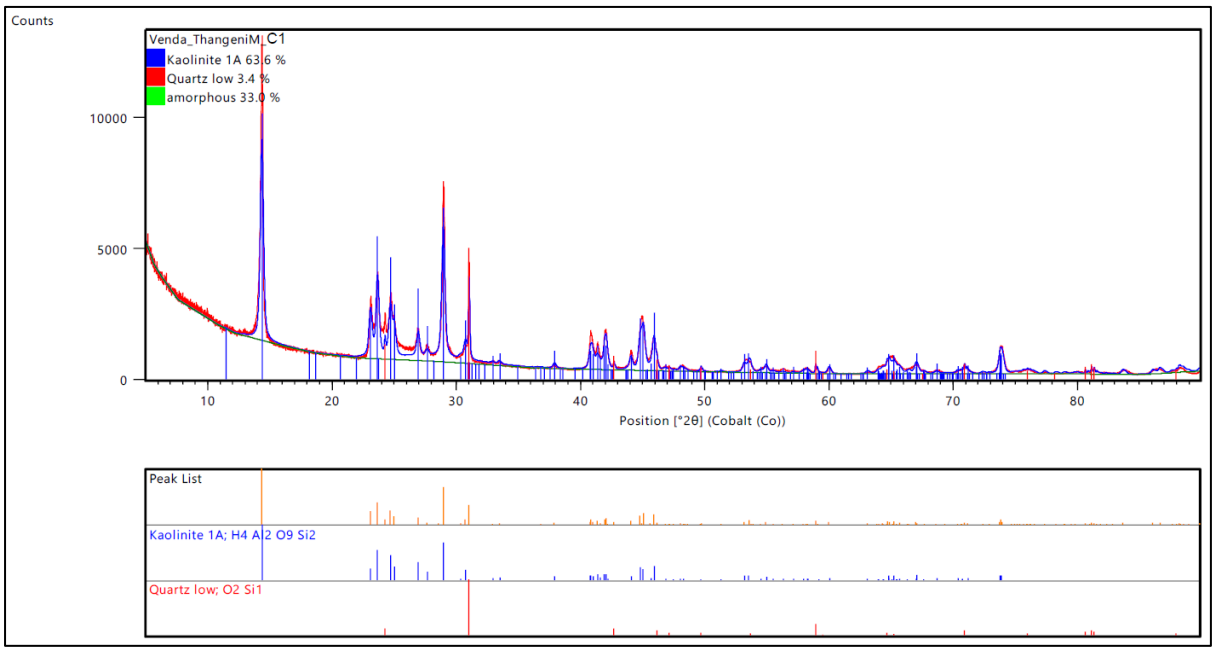

Sample TC2 XRD spectra.

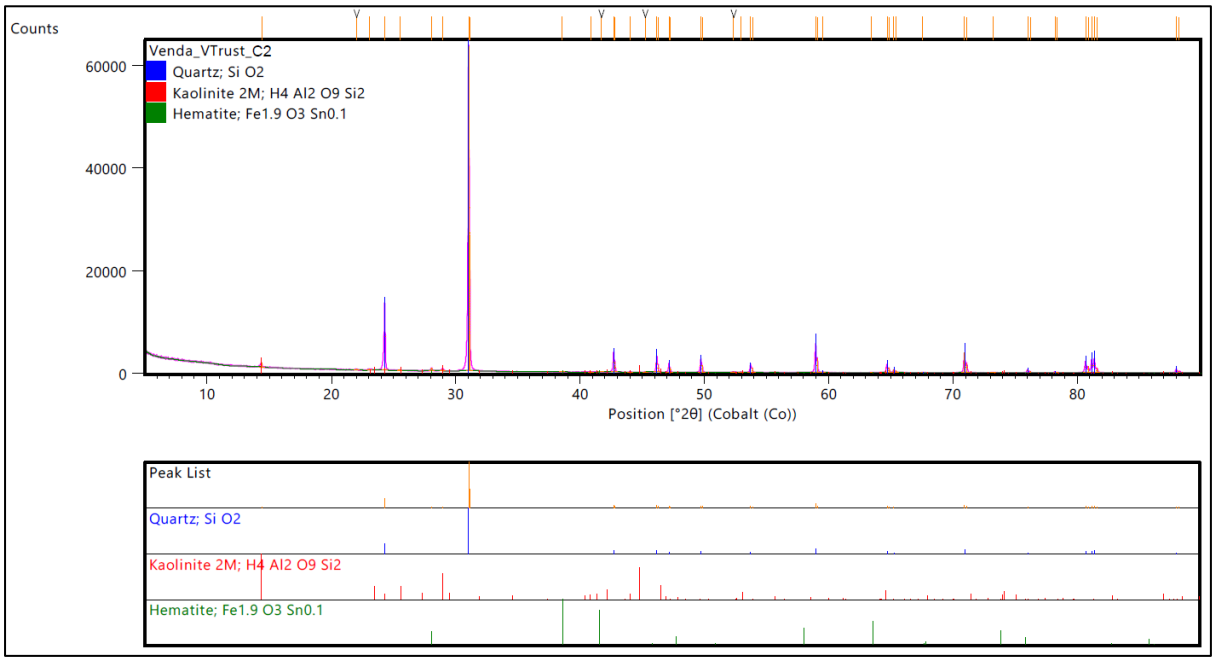

Sample TA2 XRD spectra.

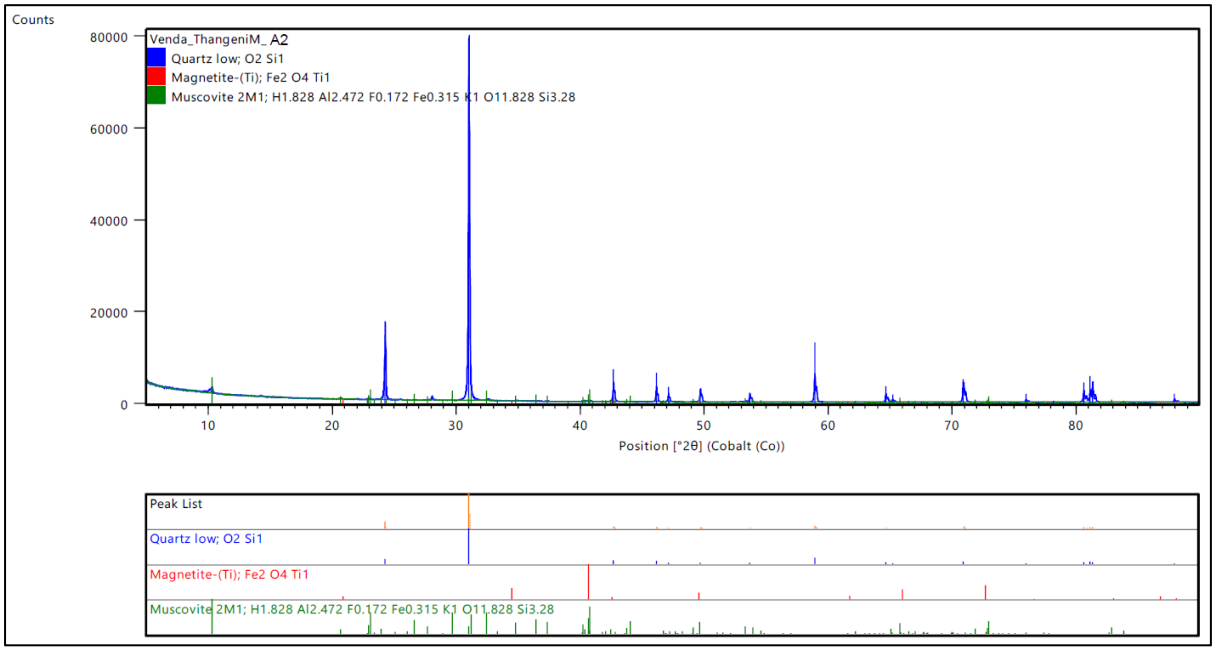

Appendix F: University of Venda research ethics certificate

ETHICS APPROVAL CERTIFICATE

ETHICS APPROVAL CERTIFICATE

FACULTY OF SCIENCE, ENGINEERING AND AGRICULTURE
RESEARCH ETHICS COMMITTEE

NAME OF RESEARCHER/INVESTIGATOR: MPHANAMA T

STAFF/STUDENT NO: 15001079

PROJECT TITLE: Investigation of Coal Occurrence and Quality at Mushithe Area, Soutpansberg Coalfield, Limpopo Province, South Africa

ETHICAL CLEARENCE NO: FSEA/21/ES/05/1707

SUPERVISORS/ CO-RESEARCHERS/ CO-INVESTIGATORS

NAME	INSTITUTION & DEPARTMENT	ROLE
Dr Mundalamo	University of Venda, Department of Earth Sciences	Supervisor

Type: **Student research**

Risk: **Minimal risk to humans, animals, or environment (Category 1)**

Approval Period: **June 2022-May 2023**

The Faculty Research Ethics Committee (FREC) of the Faculty of Science, Engineering and Agriculture hereby approves your project as indicated above.

General Conditions
While this ethics approval is subject to all declarations, undertakings and agreements incorporated and signed in the application form, please note the following.

- **The project leader (principal investigator) must report in the prescribed format to the REC:**
  - **Annually (or as otherwise requested) on the progress of the project, and upon completion of the project**

University of Venda

PRIVATE BAG X5050, THOHOYANDOU, 0950λ LIMPOPO PROVINCEλ SOUTH AFRICA
TELEPHONE (015) 962 8504/8313. FAX (015) 962 9060
"A quality driven financially sustainable, Comprehensive University"